

Automation and Robotic Control of a Multi-sensor Medical Device Platform



Robert Byrne B.Eng. (Hons)

School of Mechanical & Manufacturing Engineering

Dublin City University

Submitted for fulfilment of the qualification

MEng

September 2021

Dr Harold Esmonde

Dr Garrett McGuinness

Declaration

Name: Robert Byrne

Student number: 15331606

I hereby certify that this material, which I now submit for assessment on the programme of study leading to the award of Master of Engineering (MEng) is entirely my own work, that I have exercised reasonable care to ensure that the work is original and does not to the best of my knowledge breach any law of copyright and has not been taken from the work of others save and to the extent that such work has been cited and acknowledged within the text of my work.

Robert Byrne

Date:

Table of Contents

1.	Introduction	1
1.1	PANBioRa project overview	1
1.2	DCU work package	2
1.3	Objectives	2
2.	Background and Literature Review	3
2.1	Introduction	3
2.2	Driving mechanics	4
2.2.1	Linear drives	4
2.2.2	Lead-screw	4
2.2.3	Ball-screws	5
2.2.4	Belt drive	6
2.3	Mechanical Nonlinearities	8
2.3.1	Friction	8
2.3.2	Backlash	13
2.3.3	Belt Dynamics	15
2.4	Motor Review	16
2.4.1	Dc Motor Brushed and Brushless	17
2.4.2	Servo motor	18
2.4.3	Stepper motor	18
2.4.4	Back EMF	21
2.5	Control of positioning table	21
2.5.1	Position Homing	22
2.5.2	Micro Switches	23
2.5.3	Proximity sensors	23
2.5.4	Hybrid Options	27
2.6	Control design	27
2.6.1	Sensorless based control	29
2.6.2	Sensor-based control	29
2.6.3	Closed-loop control techniques	32
2.7	Microscope design for cell observation	35
2.7.1	Digital backplane	37
2.7.2	Magnification and Lens Selection	39
2.7.3	Objective Lens	40
2.7.4	Lighting opinions	42

2.7.5	Lighting Techniques	44
2.7.6	Autofocusing on an image.	49
2.7.7	Focusing algorithms and techniques	50
3.	System Development, Testing, and Optimization	52
3.1	Robotic Brief	52
3.2	XY Robotics Design.....	53
3.2.2	Control design.....	58
3.2.3	XY axis testing	59
3.2.4	Relative movement control	64
3.2.5	Designing a path for testing and testing that the operation is successful	68
3.2.6	Z-axis design, testing, and control	69
4.	Microscope Design and Testing.....	70
4.1	Lighting design	77
4.1.1	Resolution slide testing.....	93
4.1.2	Cost Analysis of Microscope	96
5.	Autofocusing of the microscope.....	101
5.1	Development of LabVIEW program	102
5.2	Dual focus technique	105
5.3	Investigation of Double peak in SD curve.....	110
6.	Conclusions.....	114
7.	Future Work.....	115
8.	References	116
9.	Appendix.....	127

List of figures

Figure 1: System overall block diagram	1
Figure 2: Lead Screw [11]	5
Figure 3: Ball Screw [11]	6
Figure 4: Belt drive system outlined [20].....	7
Figure 5: Static/Kinetic friction diagram [29].....	9
Figure 6: Friction model introducing viscous friction [36].....	10
Figure 7: Stribeck effect [39]	11
Figure 8: Mechanical Backlash [45]	13
Figure 9: Belt drive compliance [22].....	16
Figure 10: Servo vs Stepper motor Torque graph[60]	19
Figure 11: Optical sensor diagram [81].....	24
Figure 12: Open loop block Diagram	28
Figure 13: Closed loop block Diagram	29
Figure 14: Light path experienced in a common benchtop light microscope [123].....	36
Figure 15: CCD vs CMOS output measuring design [129].....	38
Figure 16: Lens Equation	39
Figure 17: Finite vs Infinite lenses[135].....	41
Figure 18: A apochromatic (left) vs. achromatic (right) objective design [132].....	41
Figure 19: Optical Path for Darkfield Illumination [147]	45
Figure 20: Rheinberg illumination [150].....	46
Figure 21: Comparison of illumination techniques [152]	46
Figure 22: Condenser Annulus [157]	48
Figure 23:Phase Plate [157].....	48
Figure 24:DIC Illumination Path [161]	49
Figure 25: Focusing microscope on cells	50
Figure 26:Image of XY robotics.....	53
Figure 27: T-frame XY Robotics.....	55
Figure 28: H-frame XY Robotics	56
Figure 29: Ustepper S-lite with encoder.....	57
Figure 30: Control Chart for Soft Stop Test	60
Figure 31: Control Chart for Hard Stop Test.....	61
Figure 32:Homing Test Fast Approach.....	62
Figure 33: Homing Hall Effect Fast approach	63
Figure 34: Homing Hall Effect Slow approach	63
Figure 35: Open-loop test.....	64
Figure 36: Proportional control large movement.....	65
Figure 37: Accuracy for proportional control	65
Figure 38:PI control chart for large movement	66
Figure 39: Error in measured vs calculated performance PI control.....	67
Figure 40:Accuracy for PI control following system adjustments and realignments	68
Figure 41: Nanotec actuator [167]	69
Figure 42: CMOS housing and objective lens	71
Figure 43: Magnification to lens relationship.....	72
Figure 44: Image at 22°C (room temperature).....	74
Figure 45: Image at 37°C human body temperature.....	74
Figure 46: Image at 50°C.....	75

Figure 47: CMOS base bracket.....	75
Figure 48: Image obtained without tubing lining	76
Figure 49: Image obtained with lining	76
Figure 50: Microscope design with actuator	77
Figure 51: Led array	79
Figure 52: cell image from Celine	79
Figure 53: Image with bare array as the light source	79
Figure 54: Diffuser Testing rig.....	80
Figure 55: Chosen Diffuser	83
Figure 56: Bare Led Array	84
Figure 57: Led Array + Aperture Diaphragm.....	84
Figure 58: Led array + Aperture diaphragm + Diffuser	84
Figure 59: No aperture present when imaging	85
Figure 60: aperture fully closed 0.5mm.....	85
Figure 61: aperture set at 4mm.....	86
Figure 62: aperture fully open 7mm.....	86
Figure 63: 2.5mm Aperture	87
Figure 64: 3.5mm aperture.....	87
Figure 65: 4.5mm aperture.....	87
Figure 66: 5.5mm aperture.....	88
Figure 67: Lighting testing Rig.....	89
Figure 68: shows from left to right images obtained with lenses of focal length 3.1mm, 6mm, 7.5mm respectively	89
Figure 69: No condenser lens present.....	90
Figure 70: Cell Chamber Precision Holder	91
Figure 71: Microscope model including a light source	92
Figure 72: USAF 1951 Target [168].....	93
Figure 73: Resolution image of USAF 1951 Slide	94
Figure 74: Image used to determine FOV.....	95
Figure 75: Dimensions Relationship of Line Pairs on USAF 1951 Slide [169]	96
Figure 76: Range of Images focus using USAF 1951	103
Figure 77: Manually obtained in focus Image	104
Figure 78: Image obtained from autofocusing VI	104
Figure 79: Coarse focus of cells	105
Figure 80: Fine focus of cells.....	106
Figure 81: A blurred image of cells due to vibrations.....	107
Figure 82: Image obtained without vibrations present.....	107
Figure 83: Manually focused	108
Figure 84: Autofocused image.....	108
Figure 85: USAF 1951 SD curve for autofocusing	109
Figure 86: Test cell slide SD curve for autofocusing	109
Figure 87: Cell chamber SD curve for autofocusing	109
Figure 88: Bright cell image	110
Figure 89: Dark cell image	111
Figure 90: Standard deviation curve for cell chamber	111
Figure 91: SD curve of finalised autofocus output	113
Figure 92: Example of the output image of autofocus algorithm following adjustments	113

List of tables

Table 1: Testing for diffuser arrangement.....	80
Table 2:Diffuser table	82
Table 3: Cost Breakdown of Microscope	98

Abbreviations

AI: Artificial Intelligence

ANN: Artificial neural networks

Back emf: Back electromotive force

CCD: Charge Coupled Device

CL : Closed Loop

CMM's : Coordinate Measuring Machines

CMOS: Complementary metal-oxide-semiconductor

CNC: Computerised Numerical Control

DIC: Differential Interference Contrast

EKF: Extended Kalman Filter

FMFs: Focus measure functions

GUI: graphical user interface

HFPI: High-frequency pulse injection

KF: Kalman Filter

LEDs: Light Emitting Diodes

LT: light transmission

NA: numerical aperture

PI: proportional integral

PID: Proportional integral derivative

VI: Virtual Instrument

WD: working distance

Thesis abstract

Robert Byrne

Automation and Robotic Control of a Multi-sensor Medical Device Platform.

Biocompatibility testing is a complex and time-consuming process that can create significant delays when new medical devices and systems are brought to market. This thesis summarises work performed when automating a platform that incorporates new technologies to speed up the test protocol. As part of the H2020 project PANBioRa, several partners within the consortium have developed sensing technologies for cytotoxicity and cytokine analysis which are intended for inclusion in a multi-test platform. This platform is designed for use in the medical device industry and for use in hospitals, where tests on individuals will provide personal biocompatibility results. Dublin City University has been tasked with integrating the novel sensing methods to determine cell health and to design the system so that it is contained in a user-friendly bench-top unit.

The thesis is focused on the design of an autofocusing microscope that will be used to identify cells, test for confluency within cell chambers, and determine cell health throughout the testing process by implementing image processing algorithms. The microscope is designed to obtain approximately 10x magnification and to have a physical size that allows it to move and operate as an end effector of a robotic system, meaning it can navigate to various cell locations. The objective of this project was therefore to design, construction, and validation of a high precision multi-axis robot to control the position and focus of the microscope, while in addition meeting the cost and size demands of the project.

With the system being capable of moving the microscope assembly into various positions where cells were present, while with the desired level of accuracy. Continuing to autofocus on cells and collect Images of cells to a level where the desired characteristics could be determined.

Acknowledgements

I would like to take this opportunity to make note of my deepest appreciation for the love and support I received from my family. Both in the decision to pursue this Masters, and also over the duration of which it took place. To Mam and Dad specifically, your kind words, encouraging phone calls, and everything else you both did to make the two years as pleasant as possible, thank you. To my siblings whom I feel very lucky to have, your reassurance and efforts in providing an escape from my work when I managed to get home, thank you for being ever the entertainers.

To my friends, I would like to apologise for having nothing to talk about other than writing this thesis for the last year. For your support, continued friendship, and advice I thank you, regardless of if it was taken on board at the time or not. To those kind enough to proofread and provide feedback on the various parts of this thesis both from technical, linguistic, and structural perspectives thank you.

To all the technical staff in the school of mechanical engineering that both worked with me and assisted me over the course of my six wonderful years in DCU, thank you. To Dean and Liam, I will be grateful for your support and friendship over the past two years. To my supervisors Garrett, and Harry I truly want to extend my gratitude to you both for giving me this opportunity to continue my studies in a research-based role.

Finally, I would like to say a particularly special thank you to Dr. Harry Esmonde whom I worked closely with for the course of this Master's. The level of support and interest shown was a huge factor in my maintaining perseverance with the project over the course of the two years. I genuinely can say I will miss our coffee breaks from research to discuss how we'd solve all the world's problems.

This thesis is dedicated to

Peig Wickham

Patsy Byrne

and *Paddy Wickham*

1. Introduction

1.1 PANBioRa project overview

The overall purpose of PANBioRa as a project is to reduce the time taken to assess biomaterials for their suitability to use with respect to how the patient's body reacts to the foreign material. To do this, improving upon the currently used techniques, while also using a format that makes the overall process more cost-effective is critical to producing actual value to this industry.

PANBioRa aims to develop a system that allows for both time and cost-effectiveness, evaluation of general testing on a novel biomaterial, and personally compatibility tests which can determine how an individual will respond to a biomaterial this can reduce the need for anti-rejection medication and reduce complications around implants.

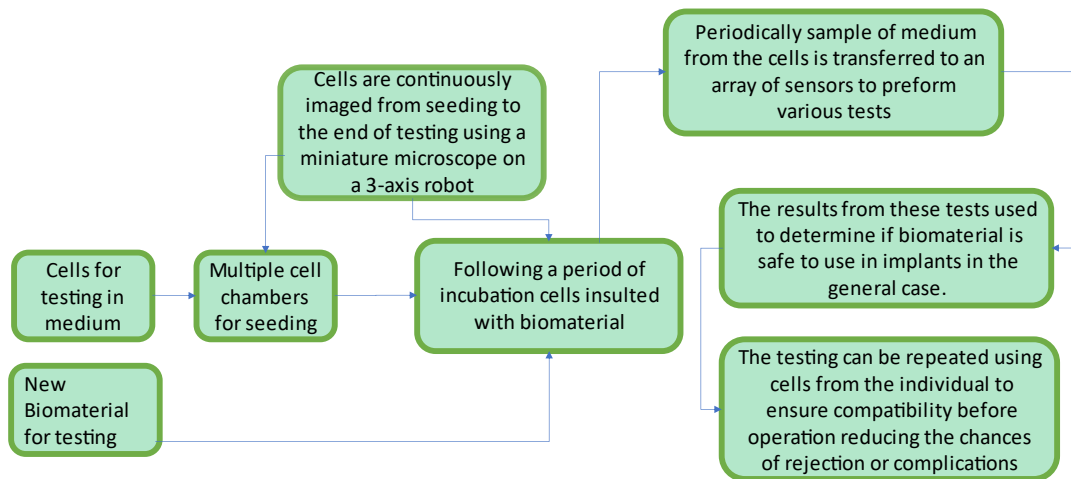


Figure 1: System overall block diagram

This will be achieved by creating a modular bench-top device that internally houses all consumables and equipment to perform a full biocompatibility test to determine the response of living cells to any given biomaterial. Once initially setup these tests would run autonomously

removing the chance for human error or contamination spoiling the test. This is done by introducing a common operating system between the different tests required to determine a full risk assessment of the tested bio-material. The system will integrate different technologies to be able to perform the necessary analyses on both cell and micro tissue levels.

1.2 DCU work package

As one of the consortium partners, the team assigned to this project in Dublin City University (DCU) was tasked with the design and control of both the robotics to position the microscope in this system and the microscope itself. Also, as part of the work undertaken by DCU, integration of all project partner's deliverables into the one functional prototype was required. Finally, the redesign with a fellow partner of the consortium to integrate the system into a commercial-grade, end user-tested enclosure was also required. Also as part of the integration work, A microfluidic system was taken and adapted to suit the system to deliver the various materials and cells to the different locations in the system automatically without human intervention.

1.3 Objectives

The objectives for this project as part of the work undertaken by DCU are as follows in no particular order:

- To Design a multi-axis robotic system that is capable of positioning its end-effector with an accuracy tolerance of 0.1mm for both the X and Y axis and of 0.01mm for the Z-axis.
- Manufacture, assemble and test robotic systems to prove operational capabilities.
- Design a compact lightweight microscope suitable to project demands. For this, the microscope must have a magnification of approximately 10x and produce images with a high contrast of cells to allow for image processing.
- Design a program to allow for autofocusing of the microscope on cells.

- Complete the above challenges within the project while doing so in the most cost-efficient manner.
- Assist with the Integration work carried out by DCU and develop using LabVIEW an automated sequence for collecting the necessary images of the cells in cell chambers.

2. Background and Literature Review

2.1 Introduction

This literature review includes an overview of dual-axis Cartesian robotics using motors and the different methods of transmitting the rotary power into linear movement. Pneumatic positioning systems were not investigated as per the brief for this project. With the long-term goal of PANBioRa to deliver a bench top device, which could be used in a various number of settings including hospital labourites. The addition of a pneumatic system would be an extra expense on the customer, that was deemed unnecessary by the consortium.

The literature review catalogues the different factors that affect these electro-mechanical systems causing them to be non-linear. Following this, the potential control techniques are analysed. As the system requires a high level of accuracy in terms of the robotic movement both open and closed-loop control methods will be investigated. The next section of this literature review looks at microscope design and how to obtain the required level magnification. Continuing from the microscope design the literature review investigates autofocusing images specifically images of cells and the different individual factors that affect the ability to focus.

2.2 Driving mechanics

2.2.1 Linear drives

This chapter aims to provide a brief technical overview of the core disciplines required for the solution of this project. It will define and investigate various types of driving mechanics. Today across a vast range of industry, robotics is becoming more and more vital. One subsection of robotics that is particularly well exploited is linear drives [1]. Linear drives are mechanical assemblies that provide linear motion, normally by converting the rotational movement of a motor. Linear drives are used in many applications, pick and place operations, Computerised Numerical Control (CNC) machining, Coordinate Measuring Machines (CMM's) and 3D printing to name a few [2][3]. These machines use motors combined with a method to transfer the rotary motion of the motor to linear translation [4]–[6]. The most popular methods for this conversion in linear drives are lead-screws, ball-screws, and belt drives. All have their respective advantages and disadvantages and depending on the application's requirements some are better suited than others. All of these systems are non-linear by design so it is important to account for this effect in each of the systems.

2.2.2 Lead-screw

A lead-screw is a driving mechanic that uses a threaded rod to translate its rotational motion into linear motion. The lead-screw example seen below in Figure 2 is most often found in situations where high precision is required over short distances [7][8]. Lead-screws have good axial stiffness making them good at moving large loads. To minimise hysteresis lead screws are pre-loaded with an axial load to keep permanent contact between screw and nut [9][10]. They produce low speed due to the pitch of the screw being small to obtain high precision positioning, meaning that even at high motor speeds the linear movement is relatively small [7].

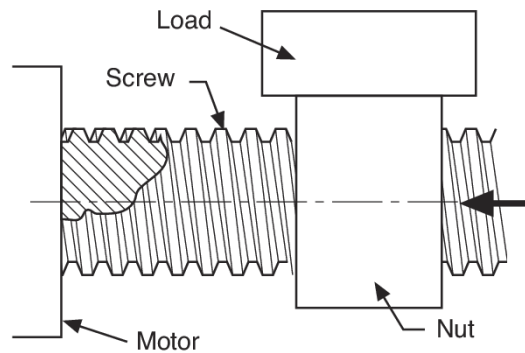


Figure 2: Lead Screw [11]

It is important to note that when the lead screw is long in the horizontal orientation, the screw may sag depending on the location of the load [9]. For when the mass is furthest from the screws supporting points, i.e. in the middle, sagging may occur. This therefore, adds another unknown to the system and may lead to unpredictable behaviour in the system. Both friction and stick-slipping, which is discussed later, are present in any lead-screw system. However, by using control methods with systems such as the one developed in this project, it is manageable to minimise their effect on the system [12]. Lead-screws can be easily designed to be self-locking in the vertical orientation which depending on the application can be very useful to maintain a desired location. This offers a secure solution to slippage under the effects of gravity [13][9][12].

2.2.3 Ball-screws

Ball-screws use a motor to turn a screw in order to move a special cartridge along its primary axis. This cartridge uses recirculating balls to provide a bearing effect, and minimise the effects of friction on the system [14]. However, due to the design of ball screws, they do not operate as well in vertical applications due to their requirement for braking mechanisms to eliminate back driving. They do however perform more efficiently and need less torque than lead-screws[10]. Ball-screws also have lower friction in the system and can effectively run at lower temperatures[13]. Ball-screws are more expensive than lead-screws but, once maintained need to be replaced less frequently. Another feature to consider is the noise

produced by ball-screws while lead-screws tend to be silent or close to it. In Figure 3 the internal structure of a ball screw is illustrated to show how the recirculating bearings lower friction.

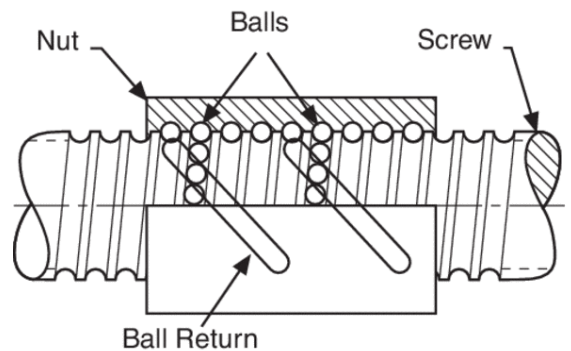


Figure 3: Ball Screw [11]

In relation to the accuracy, both lead screw and ball screw systems have to overcome the error introduced to the system from two areas, firstly the stepper motor itself slipping or missing a step which may be caused by static friction or the inertia load when accelerating the payload[8]. The second way inaccuracy arises is due to the characteristics of the mechanical system which, can be minimised by design but not eliminated. For example, the ball screw reduces the static friction so reduces the effect of the error by comparison to the lead screw [7]. However, both types of transmission systems will still be nonlinear systems and one must look at ways to compensate for these errors through control approaches [15]. One approach is to use feedback with a linear encoder which will be reviewed later.

2.2.4 Belt drive

The next mechanism reviewed for use in linear drives to convert the motor's rotary motion to linear motion in modern-day systems is the belt drive. This system detailed in Figure 4 comprises of; two pulleys, one the driver, attached to the motor shaft and the other the idler, attached at the other end of the linear drive and is free to rotate. These two pulleys are connected by a belt which is also connected to the stage of the linear drive[16]. There are multiple variations of belt drives. Variation often arises due to the design of the cross-section

of the belt, which then, in turn, dictates design. Some belts are flat, for example, a fan belt in cars, whereas others are toothed such as the belts in 3D printers. Round and v belts are often employed in robotic systems and general industrial machinery[17]. In respect to modern-day linear drives toothed belts make up the vast majority of linear drive systems that incorporate a belt[18][19].

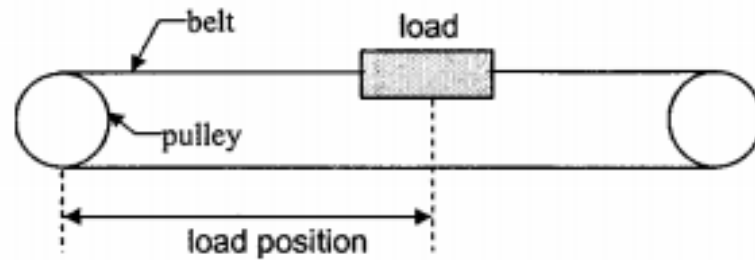


Figure 4: Belt drive system outlined [20]

The reasoning behind this is that the teeth on the belt interlock with the toothed pulley attached to the motor shaft which allows for greater power transmission than would be the case for a flat or V-shaped belt that relies solely on the friction between the pulley and belt [20]. Toothed belts are always used where a fixed relation must be maintained between the driving and the driven pulley such as in an automotive timing belt. [9]

Historically in industry where precision is required over short distances and where speed is not a priority, lead and ball screws are much more common than belt drives due to their ability to perform to higher accuracy [21] [22]. By contrast, belt drives exhibit nonlinear behaviour giving rise to small errors in position precision and accuracy. These nonlinearities are belt elasticity which can be dependent on temperature, belt slack which causes a dead space in movement, along with system friction and backlash[23]. However, in recent years due to the saving potential in using belt drives over leadscrews, a lot of research has been conducted on developing belt drives to obtain higher levels of accuracy and precision. [24]

2.3 Mechanical Nonlinearities

2.3.1 Friction

Friction is ever-present and robotics is no exception. It is a major cause of positioning errors in linear drives. To properly understand these errors, one needs to look at the various forms of friction that need to be taken into account for the particular system in question. For simple examples of two dry surfaces, it is commonly thought at school level that there is one coefficient of friction and that is all that is required to solve the question in terms of friction. This approach is fine for estimates or systems that don't require a level of accuracy in the range of mili, micro, or nanometers. However, If a system does require such performance the friction imposed on the system must be more carefully analysed, identified, and minimized through design. The remaining non-linearities can be compensated for through means of control algorithms. [21][20][9][25]

2.3.1.1 Static Friction

With respect to linear drives that require obtaining a sub-millimeter level of performance, friction is broken up into multiple parts and individually investigated before a sum of total friction is derived for the system[25] [26]. The first type of friction which is normally the friction used in the low-level calculations mentioned earlier is Static friction. Also referred to as Stiction this is the friction before the desired load is in motion. This friction is higher than that of the load once it is in motion, and hence introduces error to the system as the torque in a motor required to overcome static friction, is higher than the minimum torque required to move the system once the Coulomb friction is in effect. This causes an initial jump or launch in the system and thus introduces an element of non-linearity this can be seen in Figure 5. Static friction is labelled F_s and can be seen to have a higher magnitude in both directions to that of kinetic friction labelled F_c note that V is the velocity in either given direction. Depending on other factors in the system this non-linearity may not be a constant[27][28][18].

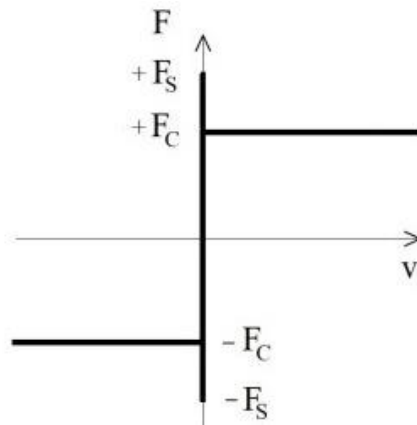


Figure 5: Static/Kinetic friction diagram [29]

2.3.1.2 Coulomb friction

The frictional force between two dry bodies in motion is known as Coulomb friction and a lot of research has gone into understanding this frictional force, through different experiments it was observed that the general Coulomb friction is constant once static friction was overcome [24], [30]. However, this was not always equal in opposing directions nor was the static friction. In many studies the static friction and Coulomb friction was asymmetrical. This introduced the need for different control parameters for each direction of motion in a linear system[31][32]. Coulomb friction is sometimes referred to as dynamic friction in basic models and can be seen in Figure 5 where F_c is the labelling for Coulomb friction, it is important to note that like static friction F_s , the magnitude in opposing directions is not necessarily equal and experimental data suggests both are more commonly asymmetrical. [32]

2.3.1.3 Viscous friction

With the development of robotics in industry and the increase of using lubricants in machinery due to the demand for high-speed operations. It became apparent that a speed dependant component of friction was present, known as viscous friction[26][33]. One study found that the friction caused by the lubricant between the two pieces was proportional to the square root of the velocity at any given time. [30]

Viscous friction is also present in linear drive systems and depending on the mechanical design of the system, can cause significant errors in high-level precision positioning if not accounted for correctly[26][34].

The viscosity of the liquid between the two surfaces will be fundamental in determining the frictional force created. This force is present in the ball-screw arrangement and also in any linear rails used for support on the systems. If either screw arrangements use lubrication this will also add viscous friction which needs to be taken into account. Like the previously mentioned frictional forces, viscous friction is asymmetrical. It has a linear relationship increasing proportionally to the increase in the system's relative velocity[35]. Below in Figure 6, the sum of static, Coulomb, and viscous friction displayed can be seen. As shown in Figure 6 the viscous friction is greater than that of the kinetic friction and hence is the force impeding the system greatest in terms of friction once static friction is overcome.

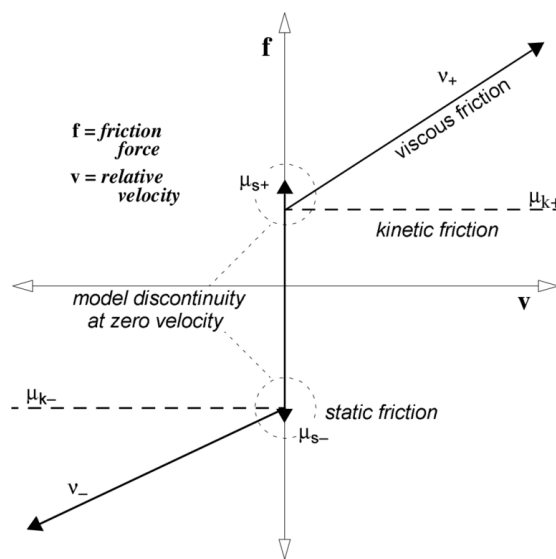


Figure 6: Friction model introducing viscous friction [36]

2.3.1.4 Stribeck effect

The above model for friction shows discontinuity upon the instant where static friction is overcome as the static friction is larger than the dynamic friction at this instance. The Stribeck effect when added to the above model is a more accurate model for friction and is continuous,

an example is shown below in Figure 7. R. Stribeck made the discovery accredited to him while studying lubricated bearings on machines [26].

This effect is in two parts, the first being the *velocity dependant* Stribeck effect this is the more applied of the two, and the majority of papers refer to this and just the Stribeck effect[37]. It states that once a layer of fluid completely separates two bodies from contact, it is observed that friction force decreases with the increase of the sliding speed at extremely small velocities this is displayed below[38][15][27].

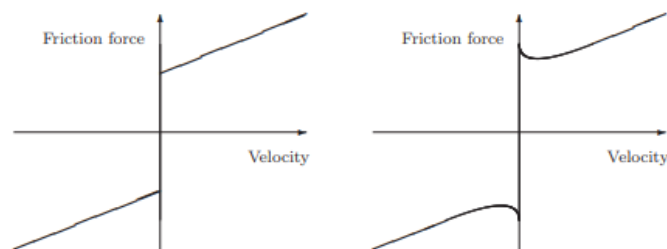


Figure 7: Stribeck effect [39]

The second part of R. Stribeck's research led him to identify the temporal Stribeck effect this showed that during the period the lubricant underwent warming the frictional force is greater than during steady operation. However, the time for this warming to occur was hours of operation at continuous high velocities[25][26]. Therefore, this effect is not as well researched or commonly applied. The reasoning for this is simple, there is not a large demand for high precision machines to operate at the required capacities that would cause this heating to occur, and so the effect does not warrant inclusion in the control design for the majority of linear drives or other robotics[26].

Moving forward from this point, when referring to the Stribeck effect it is regarding the velocity dependant effect. Which occurs at the point where stiction is overcome and movement

starts to occur. This is common practice amongst many research papers in this field[40][33][25][27][8].

The benefits of adding the Stribeck effect to the friction model are great with respect to obtaining high precision and accuracy in robotics. This is because one can use the Stribeck effect to model for stick-slip in a system[33]. In modern linear drives, the stick-slip phenomena is still something which is considered spontaneous and difficult to correct. Machines exhibit this phenomenon as they overcome static friction i.e. the immediate instant in which they start moving[41][14]. Certain research proposes that a well design PD controller is capable enough to counteract this movement in the system. Others propose a more complex control design and even look at ways to feedback stage position as well as the motor position[42].

With stick-slipping a motor rotary encoder is capable in relaying back to the control system where the device is in terms of a number of motor rotations this is very useful information and with simple control techniques and a good method for predicting friction allows one to minimise the errors introduced to the system due to stick-slipping [38][33][41].

2.3.1.5 Dahl Model

Similar to how the Stribeck effect targets the behaviour of friction pre displacement Dahl developed the Dahl model in 1968 which also offers an alternative to how friction behaves pre displacement to that suggested of the Coulomb friction model. While studying the behaviour of ball bearings he noticed that for small input forces where displacement did not occur there were small elastic restoring forces [43]. From this observation, his theory was that the behaviour between two surfaces under frictional force has mechanical bonds and that the transition from static to kinetic friction can be best analogised by the stress-strain behaviour of a material which shows elastic and plastic regions where the deformation is compared to the displacement in a friction model. Once the elastic limit is reached, i.e when displacement is first seen, the Dahl model is now the same as coulomb model.

2.3.1.6 LuGre Model

The next friction model investigated was the LuGre Model. The Dahl model is the base for LuGre however, like many other models LuGre disputes that frictional force is only dependant on displacement, whereas previous models of dahl and coulomb agree with this ideal[43]. Instead, the LuGre model emphasizes the importance of velocity particularly in the case where there is a lubricant between the two contact surfaces. Effectively the LuGre model looks to incorporate this into what was previously the dahl model to create a more suitable model for the entire range of activates for friction[39]. The LuGre model also integrates Stribeck effect which the Dahl model does not include. This model, therefore, is the sum of the previously mentioned friction components.

2.3.2 Backlash

The following mechanical non-linearity has been heavily researched for years as it has proved to inflict errors in power transitions within robotics and machinery for centuries[5][44]. This phenomenon is known as backlash, defined as “the play between adjacent moveable parts” in the Webster dictionary, backlash will exist in every mechanical system where a driver, for example, a motor shaft, is not directly connected to the load for example a CNC stage. Therefore, it is a major ever-present factor in most robotic systems[21][20]. Below in Figure 8 is an example where meshing gears experience backlash.

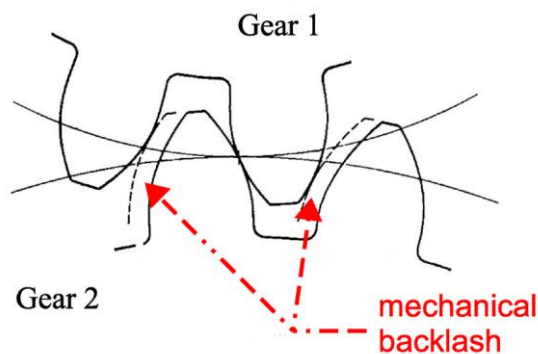


Figure 8: Mechanical Backlash [45]

This is particularly a nuisance when high precision is required in a system. In 2002 a group collected a survey on previous research on backlash and summarised their findings from 96 different references[44]. It looked at the different control techniques applied and analysed for minimizing the effect of backlash. It covered things from PI, PID controllers as well as fuzzy logic it also covered the idea of preloading both in systems of open-loop and adaptive techniques[5][41][42][26]. Depending on the number of points where backlash occurs in a given system it may be possible through modelling and experimentation work to find a value to add to the control to compensate for backlash in either direction of operation[8][10][7]. This is known as preloading. But, many factors must be considered with each specific system before it can be determined if this value would be accurate in correcting the offset caused by backlash. However, backlash does tend towards being repeatable in systems and thus can regularly be compensated for in the majority of systems effectively[9][26].

The survey paper previously mentioned along with other sources illustrates some of the results of the different approaches that various researchers take in trying to compensate for backlash in their individual systems. From the examination of all these collective works, one can conclude that there is a difference of opinion on how to act within the region of backlash to minimise its effect on the overall system [44]. The vast majority of conclusions from individual works can be split into two arguments. The first being that strong quick action should be used to minimise the time occupied by the gap and thus returning the system to an in contact state as quickly as possible thus limiting the time for the offset to introduce error to the system. However, the other side to this argument is something of the opposite in that other researchers argued that weak action in the gap would prevail in minimising the effects, they argued against the idea that inverse compensation with strong action in the gap of backlash would be effective. A list of references supporting each side of the debate can be found in the conclusions of this paper[44].

2.3.3 Belt Dynamics

It was previously stated that traditionally when high repeatability and precision was required in linear drives, a screw-type power transmission was preferred to a belt drive system due to its performance capabilities over belt-style systems. This was due to the fact that they were made from rigid components where in contrast the belt systems had elastic elements which added non-linearities to the overall system[20]. With the development of control methods and research into the different varying parameters of toothed belts, they are now seen as a viable alternative for high precision movements[46]. This along with higher operational speeds as well as being much more cost-effective than screw-type systems has seen the rapid growth in popularity for belt drives. Depending on the literature reviewed the potential cost saving ranges from 20-70%[20][24][22]. With such a large return in potential savings, the understanding of the extra nonlinearities became a very popular area of research.

The vast majority of non-linearities specific to belt drives were asymmetrical in direction which meant there was a need for experimental work to obtain adequate data to design a control system[34]. By optimizing the tension of the belt in the system one can reduce the majority of negative effects caused for repeatability and accuracy[47]. If the belt tension is not optimised the belt may loop upright before the stage starts to move. This would be likely to occur if initial acceleration is too fast which, in turn may cause the belt to slip on the pulleys[48]. As discussed above backlash in a system can be a big contributing factor to a lack of accuracy for a system.

With a toothed belt, drive system backlash will be present however, with the correct tension on the belt it should be possible to calculate a suitable compensator for each movement in each direction [49]. Following the end of the dead-band from backlash, there is an additional nonlinearity due to the belt elasticity which can be minimised through correct tension but not completely irradiated. This dead-band or non-linearity is created by the belts stretching when initially put in contact with the driver pulley following backlash and is referred to as compliance.

It is dependent on things like load weight and distance of the load from the driver pulley and the specific belt material and thickness[20][26]. Also, depending on temperature atmospherically and heat generated for long periods of operation, the compliance will be susceptible to variance.

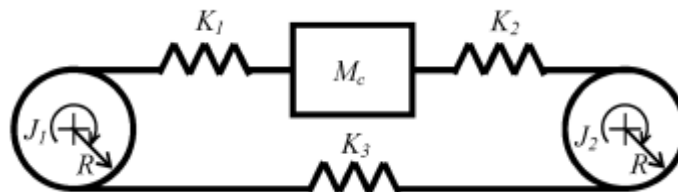


Figure 9: Belt drive compliance [22]

Figure 9 shows a simple model of the belt drive where there are three values for belt tension. K_1 and K_2 will be in tension as they move the load M_c . Whereas K_3 is not under tension. As the belt and driver pulley are toothed to mesh into each other slipping is prevented once the belt is tensioned correctly[46]. Depending on the absolute position of the load with respect to the driver pulley these values for K_1 and K_2 may change, this may result in the need for a more complex controls system to compensate and obtain precision with the system [20]. Similarly, belt vibrations if significant could reduce the reliability of the system[48][3][49]. Other elements which require investigation in terms of potential nonlinearities include pulley stiffness and belt meshing angle with the pulleys[50][51].

2.4 Motor Review

For each of the power transmissions previously discussed, a motor of some description is needed to drive the system. When choosing a motor for any application it is important to highlight the requirements of the system in order to select the most suitable motor.

The different requirements that one must consider for this project are that for all axes due to the size of the proposed system and the lack of time constraints, high speed and acceleration is not a requirement. However, given the end-effector positional accuracy is of the

highest importance maximizing the precision and repeatability of the system is the principal goal. As well as position accuracy it is important that the XYZ robot can hold its end-effector in place at zero velocity without vibration and therefore a sufficient hold torque or locking mechanism is required.

While AC motors have various advantages over DC motors when it comes to power demanding applications where motor power and efficiency is of high importance for example a washing machine. Their ability to supply precision in terms of positioning is very poor, also AC motors tend to be used in operation where there is a large tolerance on its running speed. In contrast to that, the advantages to DC motors, in general, is the ability to control the speed at which the motor runs. Also for use with other sensitive electrical equipment, DC motors are better than AC motors due to their low electromagnetic interference. Based on this and the scale of the project only DC motors were considered.

2.4.1 Dc Motor Brushed and Brushless

The Brushed DC motor has been around for centuries and are still used to date due to their low cost and reasonable efficiency. This motor often now used by hobbyists or teachers for small low budget projects can be controlled through a simple switch. As the voltage increases the speed also increases proportionally and when the current direction is reversed the direction of rotation too changes. However, these motors require maintenance as the brushes wear and damage easily, also overheating can be a common issue [52]–[55].

Therefore, the development of the brushless motor soon followed, and today due to their lower maintenance requirements and low noise production compared with the brushed motor, are the more popular of the two motors for simple low precision tasks [56], [57]. They are, however, more expensive than their brushed counterparts but depending on the application the initial extra cost may be warranted due to its many advantages over its counterpart. It's important to note that high precision is not something that is easily obtained

with standard DC brushless motors, they also have poor torque at low speeds and hence would not be suitable. [58]

2.4.2 Servo motor

A servo motor differs from the above due to its ability to move to a precise position as it incorporates an encoder to feedback its desired position to its actual and can thus continuously correct its position. They are particularly useful for high-speed high torque applications. However, a servo motor tends to jitter at its end position as it searches for its final position and also continuously corrects for drift in position as servos do not have a zero velocity holding torque. Due to the characteristics of servo motors having their best performance at high speeds, gearboxes are often required to obtain desired performance at lower speeds and thus this adds complexity and expense[59].

If a Servo motor is used in an application one must also include a safety circuit as servos will continuously accelerate to top speed when something breaks, this is referred to in literature as run away and in a sensitive application is far from desirable [60], [61]. Servo motors are efficient motors as they will only draw the current required relative to the load they are under hence they can be substantially more efficient than stepper motors which constantly regardless of load, draw maximum current available when in use. Servos, therefore, are a potential motor to consider for the requirements of this project. Unless an alternative option was deemed more suitable for a lower total cost, keeping in mind the additional extras it would require to obtain high torque at low speeds and also a holding torque at the final position when using Servo motors [63].

2.4.3 Stepper motor

Stepper motors are the last of our investigated motor types. The biggest difference to the working principles of a stepper motor compared with those other DC motors previously discussed is the number of poles present. Most typically modern stepper motors contain

between 50-100 poles this allows for precise open-loop movement, in contrast, a servo motor has between 2-8 poles [53], [64]. Given the high quantity of poles, precise speed and position control are possible and hence stepper motors are commonly found in 3d printers, CNC's, and camera platforms.

Stepper motors may also perform what is known as half-stepping and micro-stepping, this is where by using multiple poles the one revolution can be divided further than to whole poles. For example, 1/16th micro-stepping in a standard hybrid stepper motor means one revolution is now 3200 micro steps meaning more precise control on positioning is possible [65]. Another feature of stepper motors to mention is their ability to produce high torque at low speeds, this can prove very useful in applications such as in robotic manipulators or driving a CNC as previously stated. The trade-off to this, however, is that as the speed in a stepper motor increases the torque falls off and thus its effective torque is only at lower speeds. This is where their torque to speed profile is very interesting between servos and steppers depending on the application which can be seen below in Figure 10[66].

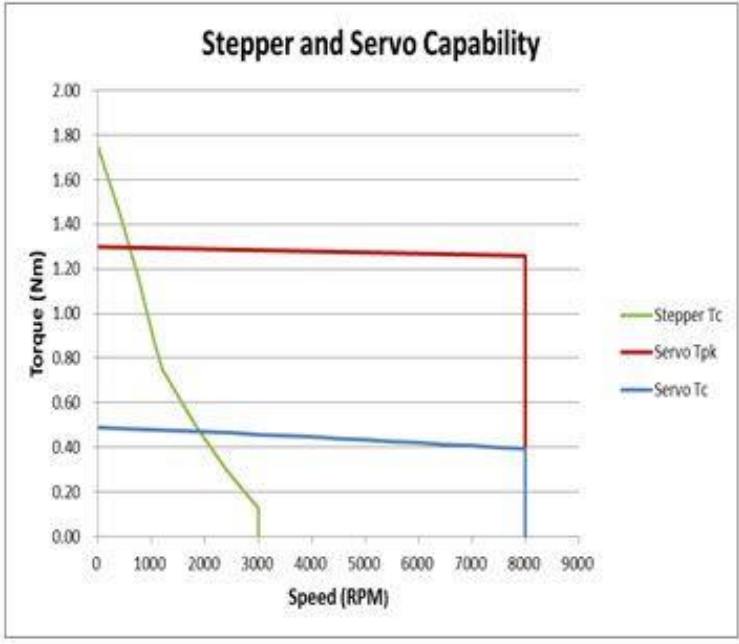


Figure 10: Servo vs Stepper motor Torque graph[60]

Stepper motors also produce a higher holding torque when stationary compared to servo motors which to be fixed in a zero-velocity scenario often need extra components. In Figure 9 the blue line plots the continuous torque for a servo where the red shows the plot if running at peak capacity, however in the majority of cases this cannot be done for prolonged periods. Therefore, stepper motors are particularly useful in applications where maintaining position is crucial to functionality. For micro-stepping as the number of micro-steps per revolution increases the effective torque per micro-step decreases so it is important to ensure that the effective torque still can cope with the load of the system to ensure step skipping does not occur [67], [68]. Initially, a large torque relative to the load must be overcome due to static friction and other counteracting forces to the motor. Multiple micro-steps may be needed to initialize movement thus depending on the level of precision required it may be necessary to incorporate an encoder with the stepper motor. Therefore, for low-speed but high-precision demanding applications stepper motors are the more popular choice [65].

In many applications, the use of stepper motors in open-loop systems is popular to save on the additional cost of encoders and work on designing a controller, however, given the level of accuracy required in this project and the need to perform sub-millimeter precise movements a review of suitable encoders and control methods will be carried out.

Finally, many internal effects occur in a motor causing it to not behave in an ideal manner. Some of these are the focus for much research as they have been reviewed in depth through various works. However, seeing as it is not the focus of this project only those effects that will affect the design of this system will be included in the literature review. Back EMF or Counter-electromotive force is one example being of interest due to the possibility to use it to provide feedback to the motor controller.

2.4.4 Back EMF

Back electromotive force (emf) or also known as Counter electromotive force is the force that is created in a motor relevant to the speed at which the motor moves as the motor velocity increases so does the back EMF. As its names suggests the force produced is counterproductive to that of the voltage supplied to the motor[69]. This explains in turn how motors and generators are essentially the same device as the shaft is turned by whatever means the back EMF created is thus the output of the generator in the form of electricity[70]. The reason one must consider this phenomenon in relation to the nonlinearities in our robotic system is if not accounted for back EMF can lead to an error in stopping accuracy. However, the back EMF is both measurable and through system modelling predictable, therefore, it can be accounted for through control techniques[71]. In an attempt to reduce cost in systems that required closed-loop control back emf was investigated as a potential method of a sensorless feedback option that would not require any extra components[72]–[74].

Below is the equation showing the relationship it has to input voltage, the armature current, and resistance where E_b = Back EMF, V = voltage, I_a = armature current and R_a = armature resistance. Note as the motor speeds up, the back emf increases.

$$E_b = V - I_a R_a$$

Equation 1

2.5 Control of positioning table

In any robotic system with moving parts, identifying the different nonlinear elements within the system is crucial in minimizing their effects. With careful design some may even be removed but, for those that remain control techniques and algorithms can be designed and tuned to minimize the remaining error in a system.

There are two types of system nonlinearities to consider, the first being that of the motor. If the output of the motor matches that of the input command then the motor is said to

be ideal and non-linearities do not exist in the system. However, this does not exist in reality both characteristics of the motor and internal errors as well as overcoming load torque due to previously discussed mechanical nonlinearities will incur error to the system. Secondly, as well as the nonlinearities with the motor there also nonlinearities within the power transmission setup, which have been discussed in detail previously.

In modern systems used to control linear robotic drives, it is common to use a collaboration of micro-controllers, motor controller boards, rotary encoders, and where these are still not capable of obtaining desired accuracy and precision a linear encoder is incorporated also. However, the introduction of each encoder and control component will cause the cost of the system to increase substantially and also increase the complexity of the system. Given the scope of this project and the desire to create a finalized profitable product, maximizing performance with the minimal cost incurred is desirable.

2.5.1 Position Homing

It is important to investigate the different potential components and look at the literature to justify their inclusion in the design of the control system. The first thing to consider when designing a linear drive system is to have an absolute home position from which all movements can be referenced, this is critical in achieving precision[75]. If this point is not a constant, the error will transmit to the position of the end effector.

With the addition of every component, there are hidden costs as well as upfront ones and thus it is important to investigate options that may exist without introducing additional equipment. When it comes to creating a zero position for linear drives one method used to do this is to simply return the drive in one direction until a certain stalling torque is met and then the motor is either set to hold this position or powered off awaiting its next command. However, there are many disadvantages to this approach, for one example the noise production from vibrations caused by this method. Also following the initial impact from driving the motor in one

direction to the end position can allow error into the system as the motor can recoil when either powered off or set to hold its position following impact, this is very hard to measure or predict and thus not suitable for a system requiring the level of accuracy and precision as ours. Similarly, the vibrations that occur from his method can introduce changes in the system, and so for multiple reasons, this method was not desirable.

2.5.2 Micro Switches

The most commonly used solution to homing linear drives in Cartesian robotics is using micro switches which when triggered sends a signal to the motor controller for the motor to hold its position with correct placement of these switches repeatable homing can be possible for many functions. Some CNC machines use micro switches for all of their end-stops as do extrusion style 3D printers[76]. Given their minimal price and relatively long lifespan the use of micro switches should be investigated for the use of this project. This mechanical solution requires physical contact with a moving part and so may be difficult to incorporate without thoughtful design, also the repeatable accuracy for micro switches varies depending on several factors like manufacturer type and additional features like an arm or roller attachment[77], [78]. Given the interest in highly accurate and repeatable micro switches, a lot of development has occurred in this area with products claiming repeatability of sub-micron order, whereas a standard micro switch for the minimal expense can produce repeatability to within 25-100 μm [79]. However, with the gain in performance, costs tend to increase, therefore it is necessary to investigate other means of homing the linear axis's to determine the most cost-effective solution.

2.5.3 Proximity sensors

Having discussed the mechanical contact option in the micro switch and thus, examination into a contactless approach is undertaken. A proximity sensor is a contactless method where a sensor detects a nearby material, they can use a variety of different methods

to do so. The most common methods relative to the application of this project are optical sensors, infrared sensors, and electromagnetic sensors. Each has their respective advantages and disadvantages which have been examined to determine if any of the options could provide a suitable solution for homing the linear drives while remaining aware of the required level of accuracy and also to minimise the cost incurred.

Optical sensors use a light emitter and a phototransistor to determine the location of a material which is referred to as the target. A phototransistor is a transistor that will change the current it allows to pass through it based on the light it detects. Optical sensors use two different alignments of these parts the first being that the light source is opposite that of the sensor (phototransistor) in this arrangement the target breaks this path and thus triggers the sensor to feedback that the linear drive is homed in the case of our proposed project [80]. The second method is to use a reflective surface to redirect the light emitted to the sensor as they are orientated inline but not opposite both of these designs can be seen in Figure 11 [81].

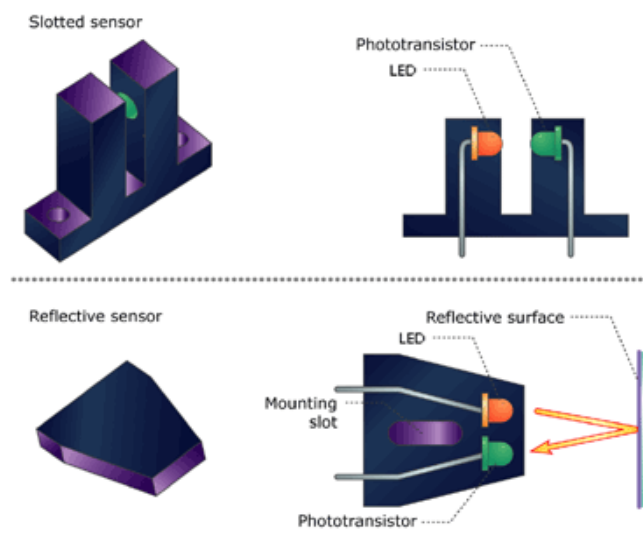


Figure 11: Optical sensor diagram [82]

The issues which can be prevalent with these types of sensors are as follows. Changes in ambient light can affect the repeatability and therefore in applications where this cannot be

controlled or kept a constant it will lead to a drop in performance similarly small changes in position will affect the sensor's performance. While vibrations also tend to affect performance. Also, when one considers the reflective approach the target material will affect the repeatability as how the light is reflected may cause inconsistencies over time with oxidation or dust settling[83], [84]. It also worth noting that upon impact optical sensors are not typically durable so should there be an error in the system and the stage of the linear drive collides with the sensor maintenance may be required[85]. Should these mentioned concerns not be of concern then there is literature to support the use of optical sensors when trying to obtain a highly precise homing position however even for lower-end components optical sensors seem to be considerably more expensive.

Next is an infrared sensor which operates in the same manner as the optical sensor however, it only uses light from the IR part of the light spectrum and thus reduces the effects of changes in ambient light from the system significantly[86]. Otherwise, the majority of the same pros and cons apply to that of the optical sensor, again it is worth noting that the sensor does have the advantage of being non-contact by design. With this said, optical and infrared sensors tend to be the least common approach for end stops in the likes of CNC's and 3d printers as the level of repeatability and accuracy required can be mostly be achieved by less expensive options which are easier to install and less affected by system conditions and material debris which may be produced[84].

The final type of proximity sensor is the electromagnetic sensor this sensor type is split into two subcategories, the first being the inductive proximity sensor and the second being the hall effect sensor. Both have been chosen to perform tasks throughout robotics in the industry for example the inductive proximity sensor is commonly used as a bed levelling sensor in 3D printers while Hall effect sensors have been used as an end stop in multiaxial machines as well as being developed further to act as rotary encoders for motor shafts and ventilators and other

medical devices[84]. When considering these components for inclusion it is important to look at how they operate and if that is suitable for this project moving forward.

Induction proximity sensors although more expensive than a standard microswitch have multiple advantages in industry and are more regularly used in systems where accuracy and precision requirements increase, however typically the price of these sensors also increases. An induction sensor works by passing a current through a coil inside the sensor from this a magnetic field is created, when metal interacts with this magnetic field it produces its own Eddie currents which experience resistance and thus a drop in the magnetic field is experienced this drop is what the sensor uses to determine the presence of metal entering the magnetic field and thus located the object in question[84], [87], [88]. While the proximity sensors have high repeatability and accuracy they are relatively expensive in comparison to micro switches.

Next focus turns to Hall effect sensors. These sensors are another type of sensor which is also a popular choice when it comes to linear end stops as they are relatively cheap and do not require much extra design consideration for inclusion[89]. A hall effect sensor works with a small magnet that is positioned on the target and as the two come close to contact the sensor detects the magnetic field produced by the magnet and sends a signal to the motor control board to stop[89]–[91]. Where proximity sensors can be used over a range to detect and give back an analogue response, hall effect sensors are either on or off in terms of their output which makes them suitable for end stops the triggering point for these sensors can be altered with the use of a potentiometer. Given their low price point hall effect sensors are very repeatable with an accuracy of within 10microns for under €1 approximately per axis. From a price point when compared with the other options micro-switches and hall effect sensors should be prioritised as end stops.

2.5.4 Hybrid Options

Finally having reviewed the options for positioning homing it was considered that perhaps a team of components might be a suitable alternative if suitable accuracy is not obtained with one solution. Given the average price of a simple micro-switch and a hall effect sensor, it would be worthwhile to test the pair in a configuration that allowed the magnet to approach the sensor at minimal speed to ensure that the maximum accuracy is availed of and the motor does not have a chance to rotate further before signalled to stop[92]. It is worthwhile to also note that the maximum accuracy will be affected by the smallest step size available however using micro-stepping should not be an issue. Another consideration in axis position homing is that if there is backlash in the system can be preloaded to remove the effects of such backlash and thus this should be considered in the design and positioning of any sensors used for homing [10], [44].

2.6 Control design

By using stepper motors as driving mechanism it allows for the motor to be driven in terms of steps. This is done by sending pulses from the controller board to the motor causing it to rotate in a defined direction for a specific number of steps. However, the pulses sent out do not always result in the correct number of steps taken, this is due to several reasons for example step skipping due to overcoming a sticking point or the initial load being greater than the available torque of each micro-step. The most basic and inexpensive control option for any system is an open-loop system seen in Figure 12 below. This incorporates no feedback and thus uses a simple command to the motor without any encoders or sensors obtaining information and relaying it back to the system[76], [93]. This means that any errors that enter the system will not be compensated for. Optimizing open-loop systems entails trial and error testing with max velocities, acceleration, and motor current supplied[67]. Depending on the task of a system

this can be sufficient, but for high precision operations like the one this project is focused on, it is not adequate as the position accuracy tolerance is of the order of microns[93].

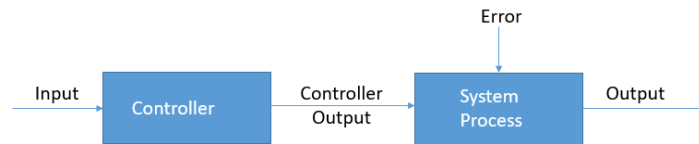


Figure 12: Open loop block Diagram

The alternative to open-loop design is closed-loop system design which a simple block diagram illustrates in Figure 13. Closed-loop(CL) control uses feedback from either the motor or the end effector to the control system.[2], [22], [94] There are two ways in which one can feedback information to the motor controller. The first being sensorless methods whereby the position is estimated through a means of calculating the likes of back emf or the use of high-frequency pulse injection method(HFPI). The second through means of additional sensors which are added to the system [72], [95]. With respect to Back emf as a sensorless method of CL control, research shows that it has more success in the medium to high-speed operations of motors and that it is less effective in low-speed operation[72], [74], [94]. The reason for this is the back emf created at low speed is minimal and therefore is very hard to identify, thus this method of control is not suitable for this project.

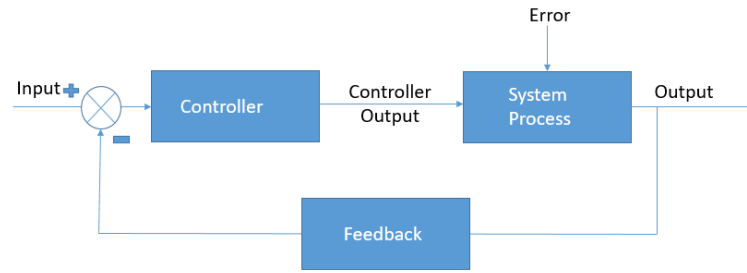


Figure 13: Closed loop block Diagram

2.6.1 Sensorless based control

When it comes to High-frequency pulse injection (HFPI) methods for sensorless control there is more promise for low-speed applications as it does not depend on a speed dependant created voltage the same way back-emf sensing methods do [95], [96]. This method sends a high-frequency voltage into the motor and the corresponding high-frequency current is then analysed to estimate rotary position. While a lot of the research done on HFPI focuses on speed control and not position control there is literature on its use in position control. These papers discuss the estimation of rotary position and speed response and while they do show improvements in performance at low and zero speeds when compared with open-loop control and back emf style control, the experimental results do not yet indicate that this approach would be sufficient for the requirements of the project this thesis focuses [73], [91], [95]. Also, given the complexity of the implementation of HFPI, next attention focuses on sensor-based solutions for closed-loop control.

2.6.2 Sensor-based control

2.6.2.1 Rotary encoders

The second way in which closed-loop motor control is applied is through the use of external sensors and encoders. Regardless of the encoder type, the principal is the same, the actual position is returned to the micro-controller and then this data is manipulated to alter the

pulses sent out to the motor, with the use of some control technique or algorithm until the desired outcome is achieved. To obtain the most precise and accurate movement the selection of control type applied is crucial to the optimization of the overall system performance.

Encoders can be broken up into two main groups, rotary encoders, and linear encoders. Rotary encoders as their name suggest focus on the rotor of the motor and precisely identifies the actual position of the motor. This allows the system to remove errors in the system due to the motor's nonlinearities. There are multiple classes of the rotary encoder from the simplest tachometer such as a bike speedometer[97]. Then there are different variations of incremental motors and finally, an absolute encoder that uses internal sensing to know the absolute position. Given the application at hand, whatever type of encoder is selected must be a multi-turn encoder as the motors will have to rotate multiple times to reach their desired destinations. The sensing method for these encoders are similar to the methods for the earlier discussed end stops. With regards to encoders two designs are possible these are incremental and absolute, incremental are relatively cheap but require a method to set a datum point, which is simply a reference point from which to take all measurements. Whereas absolute encoders have a natural datum that is constant, this is the encoder type normally employed by linear encoders and hence they are usually expensive when compared with rotary encoders.

Previously it was mentioned that hall effect sensors were used in rotary sensors this is achieved by placing a magnet on the back of the motor shaft and using an array of hall effect sensors to accurately compute the change in motor shaft position by investigating the change in orientation of the magnets' poles, this is the design behind magnetic rotary encoders [91], [98]. Another common type of rotary encoder is an optical encoder which pulses light from LEDs to a photodiode detector, similar to end stops optical encoders are susceptible to error induced from dust and change in temperatures where magnetic equivalents are not.

The final type of rotary encoder is the capacitive encoder and is the newest in a technology sense, while this type shows good promise in achieving the requirements it is still expensive in comparison to older equivalent technologies such as the magnetic encoder[70], [99]. Size is another important factor when choosing components as there is an obligation to minimize the system to the needs of the overall project, optical encoders are traditionally bulky, while the other types of encoders are available in configurations to merely look like thick leads attaching to the back of the motor. Regardless of whether it be optical, magnetic, or capacitive, the important thing is that the encoder satisfies the need of the project in terms of resolution and reliability.

2.6.2.2 Linear Encoders

The other type of encoder is the linear encoder which focuses on the position of the end effector as opposed to the position of the motor. This allows for the system to remove the error that would exist in the system due to mechanical nonlinearities beyond the motor, for example, belt tension or backlash[22], [100]. Thus linear encoders are more effective in obtaining high precision in robotics. Similar to rotary encoders they use magnetic and optical technologies to sense a distance travelled and are available in both incremental and absolute configurations[101]. When selecting a linear encoder, it is important to identify which of these are suitable, if it is required for the system to retain its position even when power is off or interrupted then an absolute encoder is needed regardless if it is rotary or linear however if it is suitable to home the system and continue from that point upon each loss of power then incremental encoders are suitable and regularly available at a lower cost[87], [102]. For all uses of optical sensing, whether it be simple to end stops of absolute linear encoders, the technology is susceptible to induced errors due to dirt, dust, and vibrations. The constant air gap is also required to remain constant and thus if this is not maintained it may also lead to errors infiltrating the system [101], [102].

Magnetic linear encoders however like their rotary counterparts are not susceptible to these things and for the most part, are robust to shocks and vibrations. They do however experience interference from other electromagnetic fields and therefore should not be used in close proximity to iron and steel[91], [103]. However linear encoders are considerably more expensive in comparison to rotary encoders and so the latter should be used in the system if possible to reduce cost once the desired precision is attainable.

2.6.3 Closed-loop control techniques

Whether the system is operated with the addition of a physical sensor such as the options mentioned above or the system operated using sensorless approaches, some control algorithm must be used to process the new information being fed back from the sensor to drive the motor. There are many types of intelligent controllers today which can operate independently of a system model and use adaptive techniques to counteract unaccounted-for variables in real-time. However, these systems have their strengths and weaknesses. In this section, the different options for control are reviewed for use concerning the demands of this project, as there is a hope for future commercialisation the simplest and most cost-effective approach that delivers the required performance is desired.

Firstly, focus is on the conventional PID controller, which will also include our review of commonly used PI control. PID is still the most commonly applied control used across industry today. Proportional, integral, and derivative (PID) control uses functions of the error to reach a targeted position. Proportional is used to give a gain to the response and thus is the basis of this style controller. Integral integrates the error signal to the effect of removing steady-state error in the system and thus tends to be a desirable part in most controllers. Finally, the derivative element in a controller uses the error signal to increase the response speed of the controller, this allows for the other elements to be increased without the system becoming unstable and where there is a time constraint on the response of the system PID control would be used.

Three individual parameters are used to implement the control K_p , K_i , and K_D if one of these parameters is set to zero that part of the controller is said to not exist[94]. This explains the difference between PID control and PI control as for the latter the derivative control parameter K_D or derivative parameter is set to zero. PI and PID are the most commonly used techniques as both, due to the integral component of the controller, can get rid of steady-state error[21], [94].

The methods used to set the PID parameters have been widely explored with PID controllers designed using many control techniques such as the Ziegler-Nichols and Cohen-Coon methods to name two classical tuning techniques[104]–[107]. In terms of high-level precision, some research suggests this type of control outdated, and ineffective when obtaining accuracy, precision, and repeatability[20], [22]. One reason for this is its non-adaptive design which means if there is a change in the nonlinearities affecting the system, parameters for the controller must be manually re-optimized. However, other researchers state that under well-modelled systems the PID and PI controllers are capable of achieving the level of accuracy required for position control[108]–[110].

It is also important to note that those who disregard PID as an adequate option are proving the performance of more advanced AI type controllers which require much larger computational and processing power which in turn makes the system expensive in comparison to PID and PI control. Given that for this project the final position of each movement is all that requires a high-level accuracy and not the speed of operations or run time, the PID controller, given its simple design and popularity in industry should be considered initially for this project[96], [111].

Next, attention to Fuzzy Logic control which similar to PID and PI control is relatively simplistic in its design and cheap to construct[105]. However, one highlighted disadvantage is the need for expertise to set the parameters via a trial and error approach which reduces its application in industry[20]. Fuzzy logic is a type of computer logic used that allows for

intermediate states as opposed to say Boolean logic which has only on and off or 1 and 0 values. This in turn allows for a rule basis to be designed which is used to dictate the response to the feedback in a system.

Many papers compare the use of PID controllers and fuzzy logic controllers[105], [112], [113]. While many point at the latter as higher-performing due to a reduction of overshoot and the lowering of settling time. The optimization of conventional PID controllers and use of adaptive PID controllers still remain the front runners across industry today for position control as their robustness and simplicity are seen as a worthy trade-off with minor improvements in performance that could be obtained by switching to a more complex and costly design[104], [107], [114], [115]. However, with this being said, if the level of accuracy required proves not to be obtainable through optimization of PID control and system design, a more complex control technique will need to be incorporated. It is expected that with the recent successes of conventional PID control in some high performing 3D-printers and CNC machines this is not expected to occur.

The most adaptable controller design in relation to the multi-axis Cartesian robot is both the use of artificial intelligence or artificial neural network. These solutions require a great deal of computational power and thus have only recently began to attract the interest for smaller scale projects[65], [116]. While there is evidence of their use in the accurate control of stepper motors the level of understanding and development for this method to be implemented does not seem to be rewarded with an increase in relevant performance to warrant inclusion in this project[65], [94]. These options are the best suited to an ever changing system being the most self-adaptable but they do require a long period of time to train to the system and build up data to respond off, seeing as the system proposed does not have many intense non-linearity, this approach may be excessive and unnecessary given its extra cost both in time to implement and financially for the required hardware[116].

The final method of control for the stepper motor reviewed was the Kalman Filter(KF) and Extended Kalman Filter(EKF) [65], [116]. Its proposal for use with stepper motors is seen as a method to reduce the need for physical sensors and compared with the likes of Artificial Intelligence(AI) and Artificial neural networks(ANN) is low cost and not as computationally demanding[117], [118]. However, it is still significantly more complex and demanding to include than the other previously mentioned control options. Both KF and EKF are also used in conjunction with sensors susceptible to noise and interference for example GPS tracking, it is both here and in sensorless systems where they are most successfully implemented[119], [120]. Given the development of motor sensors since the turn of the century and the ability to have a low disturbance sensor in the proposed system, this method seems to be an overly complex solution and thus will not be investigated further unless the more cost-effective and lower complexity level solutions fail to deliver the precision required in the project[121], [122].

To summarise there are various control techniques on offer, which provide a wide range of options. While some papers deem the lower level approaches as outdated and insufficient, they do so to create a requirement for their alternatively proposed system.

Given the level of accuracy required in this project's system, and the limited change in conditions on top of the reducing cost of sensors, the robust and Industry prevalent PID feedback control will be implemented with the use of a high resolution rotary sensor. This will mean that careful design and optimization of the system will be needed to ensure that error in the system due to mechanical non-linearities is minimised to allow the system to stay within the threshold of tolerance given to this project.

2.7 Microscope design for cell observation

The optical requirements for the microscope for this project are relatively straightforward, however, the challenge arises with the need to minimise the physical size of the system and to accommodate it as the end-effector of a multi-axis robotic system. Given the

task is to image cells with approximately 10 times magnification, a simple light microscope is a good starting point for this review. The simplest light microscope uses a lens to increase the size of an image as it appears on our retina. The distance the lens is away from our eye affects the level of magnification. As the area of interest to view gets smaller, as is the case with microscopes, the light required to see the specimens increases, and hence a light source is required [123].

For the microscope shown in Figure 14, light from the light source is focused using a condenser lens and then an aperture is used to only allow a narrow beam of this light to penetrate the sample under investigation. The light then passes through the objective lens and on up the tubing to the eyepiece lens. Microscopes typically have extra lenses for various reasons, for example, a tube lens is used to flip an image to be correctly orientated on the backplane as each time an image passes through a lens its orientation is flipped. They also sometimes have lens pairs for obtaining various magnification and resolution[123]. The various components needed to create a camera microscope are researched and reviewed to try to identify where cost and size can be reduced to fit the needs of this project while also delivering the required images of cells to determine cell health and the confluency of cells within the cell chambers.

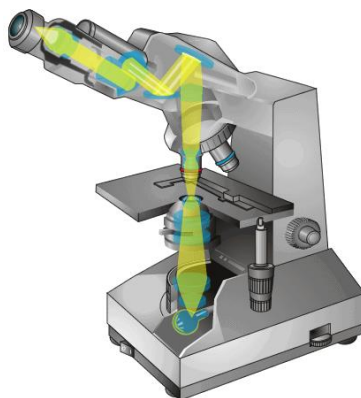


Figure 14: Light path experienced in a common benchtop light microscope [124]

2.7.1 Digital backplane

There are two options in terms of types of Imaging sensors for the microscope these are Charge Coupled Device (CCD) and Complementary metal-oxide-semiconductor(CMOS). Both have their Specific pros and cons for use, depending on the application opinion can be mixed about which is the best equipped to satisfy requirements. CCD technology, for which the inventor(s) received a Nobel prize in 1969 (117) is the older of the two and is the market leader in multiple imaging technologies. However, in more recent history the demand for high volume, inexpensive and smaller image sensors drove the investment and interest in CMOS style sensors.

Both types of sensors operate under that same principle where elements, referred to as pixels, are used to detect light. When a photon of light strikes the pixel it energises an electron into a higher energy state known as a photoelectron which can be detected. The difference between CCD and CMOS sensors is how this information is relayed back to whatever main computing unit is used to build the image from the collected information[125]–[127]. A common analogy used to describe the differences in CCD and CMOS sensors is the Rain Bucket example shown in Figure 15.

For CCD sensors there is a readout at the corner of the sensor. The photoelectrons(rain) are sequentially shuffled through the pixels(buckets) until they reach the readout transistor (measuring device). Whereas in the case of CMOS sensors, each pixel(bucket) has its transistor (measuring device) resulting in a more complex sensor but speeding up image capture. For this reason, the pixel array in a CCD sensor is said to be passive, while the array in a CMOS sensor is said to be active as the conversion from electron to voltage is made locally [128], [129].

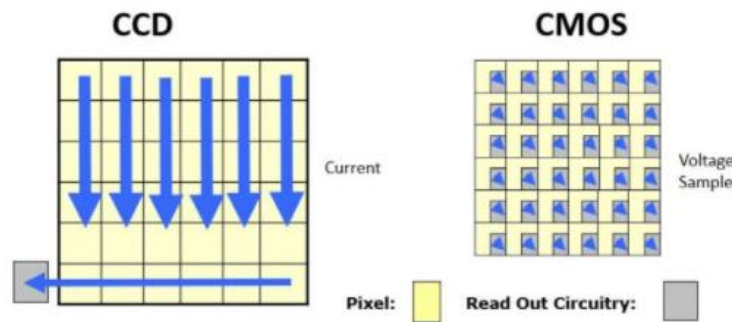


Figure 15: CCD vs CMOS output measuring design [130]

Having explained the basic difference between the two sensors and how they operate, what this effectively means for their suitability is outlined below.

For a long time, CCD sensors were preferred to CMOS sensors as they were more developed and hence performed better across most aspects. However, with the demand driven by mobile phones for more compact sensors with lower power consumption, CMOS sensors are now the preferred option across many industries for numerous reasons. With that said, CCD sensors still have their advantages. With the majority of CCD sensor circuitry being off board, there is less noise. Also, pixel to pixel reproducibility is higher than in CMOS sensors as multiple pixels in CCDs use the same measuring point, therefore the potential error or difference from multiple measuring points which is in the CMOS is not present for CCDs. CCD sensors also have a higher quality analogue to digital conversion(ADC) due to the nature of their design while CMOS sensors tend to be limited to 12-bit ADC[127].

CCD sensors are typically more expensive than their CMOS counterparts, and also have slower readout speeds, this is due to the design of the readout circuitry for both options shown above in Figure 15. Based on the afore mentioned, CMOS sensors were considered as the better solution for this project in terms of expense, size, and power consumption[131].

2.7.2 Magnification and Lens Selection

Having selected the imaging sensor for the microscope attention turns next to the requirements of obtaining the desired magnification. As stated previously an approximate magnification of 10x was desired by project consortium partners to obtain images that could provide the required data for the project. Linear magnification is the relationship between the object size and the image size. When the image is larger the magnification is said to be positive[132]. Linear magnification also known as transverse magnification is derived from the lens equation which explains the relationship between the focal length of a lens and the distance the lens has to both the image and the object. This is captured in the diagram shown in Figure 16 where O is the object distance, I represents the Image distance and F indicates the focal length of the lens in use[123], [132].

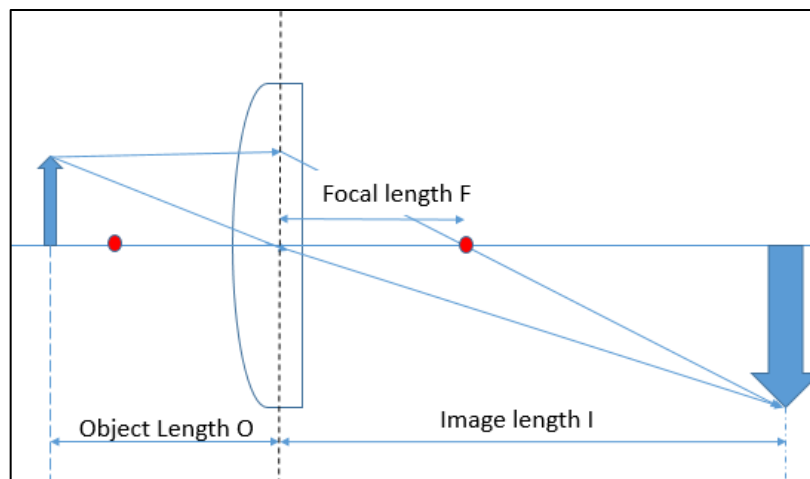


Figure 16: Lens Equation

$$\text{The lens equation is } \frac{1}{O} + \frac{1}{I} = \frac{1}{F}$$

Equation 2

From this, the Transverse magnification can be derived to give the magnification (M) as

$$M = \frac{I}{O}$$

Equation 3

With years of research and development into lens technology and performance, many different coatings and filters have been applied to lenses, as well as multi-lens configuration to act as the objective lens for specific tasks. This part of the literature review looks at the different standard options for the objective lens.

2.7.3 Objective Lens

The objective lens belongs to either the refractive or reflective type. As their names suggest refractive lenses bend or refract the light through either a single or multiple lenses. Reflective lenses use a series of mirrors to reflect the light in a pattern to alter how it is conceived by either the eye or a camera sensor. Reflective objectives are much less common, and while they do have advantages in specific scenarios for example in both ultraviolet and infrared regions of light, the work being done in this project is better suited to the refractive type [133], [134]. This is the case as the task is to obtain an image showing the outline and area coverage of cells at relatively low magnification. Thus, using the more commonly accepted approach gives a wider selection of component providers and so, in turn, means the design can be more cost-effective.

Refractive lenses may be categorised as finite conjugate or infinite conjugate, see Figure 16. A finite conjugate objective lens creates a converging beam pattern requiring an eyepiece to create a viewable image. The distance between the objective and the eyepiece determines the magnification. The infinite conjugate objective lens creates a parallel beam which can then be focussed onto a camera backplane using a tube lens. The distance between the objective and the tube lens does not affect the magnification because of the nature of the parallel beam between the two. Using infinite conjugate lenses is particularly useful if other additional filters need to be added to the objective as it allows for more space for this to be integrated along the light path[133], [135].

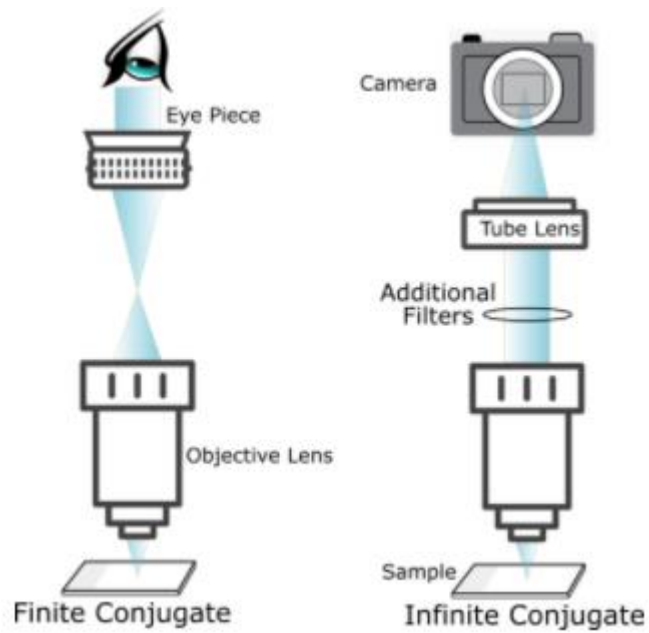


Figure 17: Finite vs Infinite lenses[136]

Refractive lenses can vary from a simple achromatic design where two lenses are used or the apochromatic type, using up to 15 lenses. It becomes apparent that the infinite conjugate set up would be required to accommodate the spatial size of the lenses involved in the apochromatic lens. With cost being a factor in the design of the microscope as well as size the use of a high-level apochromatic objective is ruled out. Thus, attention now turns to the optimum choice of a simple achromatic lens to meet the needs of the project [123], [134], [137].

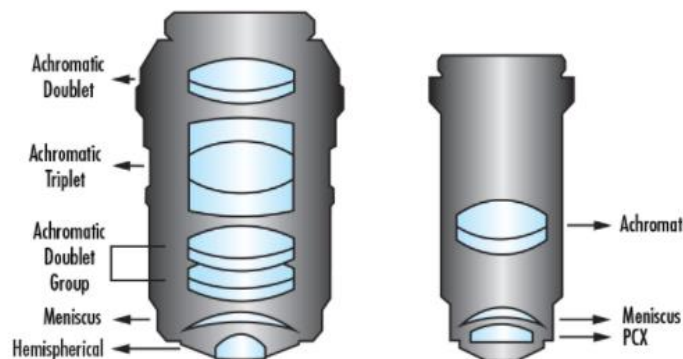


Figure 18: A apochromatic (left) vs. achromatic (right) objective design [133]

As well as a 10x magnification, the working distance, that is the distance between the objective and the object to be viewed must be considered (129). For example, if the working distance is less than that of the cell chamber thickness, the system would be useless. Similarly, if it was too large it will become difficult to integrate lighting into the system. Hence selecting a lens that provided a suitable working distance was an important factor. To achieve a suitable range for the working distance, it is necessary to consider the numerical aperture (NA) of the lens.

A numerical aperture measures the ability of a lens to gather light. This is also an indication of the lens's ability to show details of a specimen or in other words the resolution it can obtain. The larger the NA normally indicates the higher the magnification as the smaller something is of interest the higher a resolution is needed to obtain it in focus thus as NA increases so does the resolution of the images it produces[123], [134]. Depth of focus is inversely proportional to NA as is the brightness of an image, hence the intensity of lighting in microscopes tends to be increased for higher NA lenses. With this all taken into consideration, a low-cost solution with suitable focal length and numerical aperture would be sourced to give the desired resulting magnification and image quality.

2.7.4 Lighting opinions

In microscopy, a large image is created by diverging the light beams from a small object. The consequence of this is that the intensity of the light in the image is weaker than that of the object. Strong lighting is therefore necessary and can be achieved in a number of ways.

Tungsten Lamps are a common inclusion in most light microscopes as they are a reliable light source that can be controlled with a variable resistor to increase and decrease the light intensity to suit the need of the user. However, these bulbs do have their downfalls. Since they produce light by passing large volumes of electricity through a thin metal wire they also produce

large amounts of heat and so can be a safety concern when used over extended periods [138]. Their lifespan is also limited as with these high temperatures thermal stresses fatigue the element leading to a failure[139]. Over time these bulbs do not produce a constant light source and can become discoloured as well as less bright[123]. These issues called for research into other methods of obtaining the desired light source.

Fading is less prevalent with Halogen bulbs due to the introduction of a layer of quartz to protect the glass and bromine gas to surround and protect the filament[139], [140]. The reasoning for these additions is apparent when one looks at the lower wattage that halogen lamps can operate at compared to Tungsten lamps and also their life span as it is almost double that of standard incandescent bulbs[141].

Another lighting option for microscopes is to integrate the use of an arc lamp, unlike bulb options, arc lamps do not create light by passing electricity through a thin metal wire[138], [139]. Instead, light is produced by an electric arc between two electrodes. This method has shown to be particularly useful in specific settings where alternative lighting options could not deliver the desired output. Arc lamps have seen their inclusion particularly in fluorescence microscopes, this is due to the intensity of white light they can produce when the correct materials are used in the construction of the electrodes. However, arc lamps are quite sensitive to changes in a system and experience difficulties remaining constant for a variety of reasons, for example, even a change in the surrounding magnetic field can lead to a change in the light produced[123], [141].

Light Emitting Diodes (LEDs) are relatively a new method of providing a high intensity artificial light source to microscopes. LEDs have both advantages and disadvantages, but for less complex microscopes, they are a cost effective solution. LEDs consume little energy and as a result, do not heat up to the same extent as the solutions outlined earlier. This in conjunction with the significantly longer lifespan makes for a great solution for lower level microscopy[139],

[142], [143]. Some potential disadvantages to the use of an LED based lighting system are that with certain sample types the white light produced leads to the loss of some information due to how it interacts with the sample, however, this is normally overcome with the integration of a filter[143]. The next section considers the configuration of the light pattern as commonly used in different applications, considering the requirements of this project the different options are explored for the most suitable solution.

2.7.5 Lighting Techniques

2.7.5.1 *Brightfield illumination*

Brightfield illumination is the most straight forward lighting technique used for illumination of samples with a microscope, consisting of a light source directly beneath the sample and a method of focusing the light such as a condenser lens. The light then passes through the sample and interacts with the objective lens and the image reaches the sensor. By using this arrangement, the image that is produced is on a bright background where the cells observed are darker in colour[144]. The thicker the cell the more of the light it absorbs and thus the darker it appears. This type of illumination is the most common in light microscopes as it is the easiest to setup and work with. However, depending on the level of detail desired, it does sometimes leave the system limited in terms of the images it can produce[123]. This can be the case when viewing certain animal cells under high magnification, when this happens it is often required that staining of the cells is undertaken, which mostly results in the cells dying. With that said, brightfield illumination is still the most commonly used option used in light microscopy[145].

2.7.5.2 *Darkfield illumination*

Darkfield illumination is another well-known and commonly used illumination technique where the image produced has a dark background while the specimen of interest is bright[145]–[147]. This method is preferred in circumstances where it is not suitable for stained

specimens or higher contrast in the system output is required[145]. To achieve this lighting technique an obstructing disk is added to the light path described previously for the brightfield illumination, see Figure 19. The light from only the outer edges can continue to pass to the condenser lens where it is focused on the sample. From this point the light travels in the same method as brightfield illumination. Given the desired outcome for this project, darkfield illumination is particularly interesting as an alternative method seeing as the addition to the system is minimal and also the extra space required is not limiting the system[146].

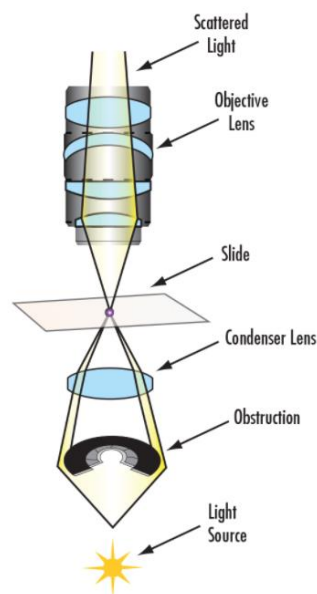


Figure 19: Optical Path for Darkfield Illumination [148]

2.7.5.3 Rheinberg Illumination

Rheinberg Illumination is similar to that of the dark field illumination however instead of adding a disk to obstruct the light Rheinberg's technique allows for two or more colours to be used to create an image that highlights particular areas of interest[138], [145]. This works by inserting a Rheinberg filter between the light source and the condenser lens as seen in the example in Figure 20. The red and green filter is made of a translucent material that will produce an image, the features of which will be impacted by the combination of the filtered light[149], [150].

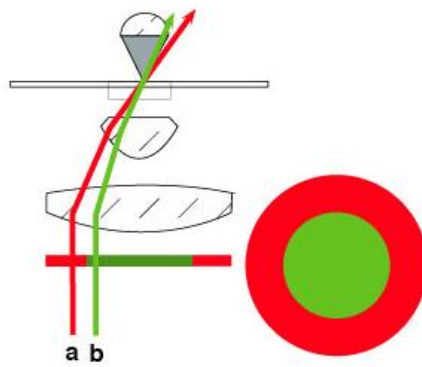


Figure 20: Rheinberg illumination [151]

Below in Figure 21 is a comparison of the different illumination techniques described, the addition of the obstruction disk for darkfield illumination and the Rheinberg filter for Rheinberg illumination is very apparent when the output images are compared[152], [153]. While brightfield is the most straight forward the other options may be useful if the cells under observation as part of this project prove to be too translucent leading to issues with the image processing.

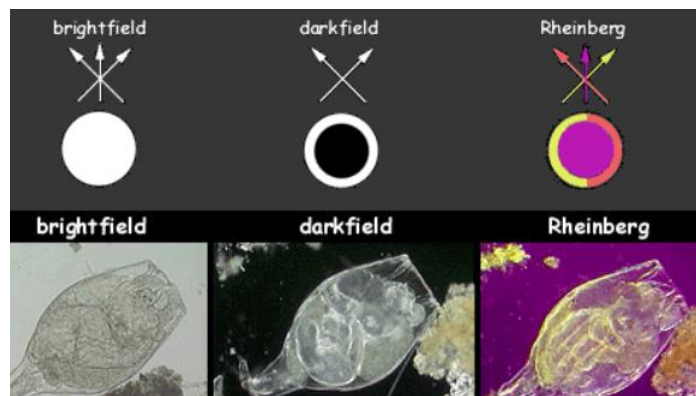


Figure 21: Comparison of illumination techniques [153]

2.7.5.4 Other methods of Illumination

Although the following are mostly used at higher magnifications, fluorescence illumination, phase contrast illumination, and finally differential interference contrast(DIC) were reviewed.

Fluorescence illumination works by identifying what wavelengths of light are being absorbed by the sample from the light source based on what light is reemitted by the sample[154]. The light source is passed through a beam splitter and a filter to redirect the light to the sample in a parallel light path. An emission filter is also present in the system before the light reaches the camera[155]. The success of this type of illumination is often determined by the probes or dyes which are used to make specific parts of cells appear highlighted. Although there is a diverse range of probes, this can be a limiting factor for the use of fluorescence illumination. Also, given that the testing in this project is to observe a change in the cells as they react with specific biomaterials this method would not be suitable if any additional probes or dye were required as it would compromise data from the test.

High contrast in an image is possibly the most important feature universally for maximising the image output in light microscopy darkfield illumination is a simple method of increasing the contrast in a light microscope. A more complex approach which depending on the requirements of the system can provide very adequate results is Phase Contrast Illumination[152], [156]. Phase Contrast Illumination works by using a hollow cone of light. However, unlike Darkfield illumination, additional components are required. A condenser annulus, seen in Figure 22, which creates a ring-like light source before the condenser lens, is added to the brightfield optical train and a phase plate is inserted just before the image plane providing higher contrast[157]. This plate has a ring-shaped slit which allows the light to pass through to the image plane while the rest of the plate is opaque. A diagram of a phase plate example illustrates this in Figure 23 below.



Figure 22: Condenser Annulus [158]

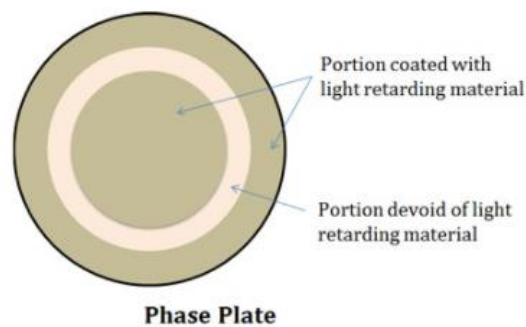


Figure 23:Phase Plate [158]

The last of the illumination techniques considered was differential interference contrast(DIC). DIC works by the addition of several extra components to a simple brightfield optical train, see Figure 23. Light is polarised split into two beams to ensure the beams do not cause mutual interference[152]. The light then continues through the regular path until after the objective there is another prism that recombines the two light beams into one[159], [160]. The analyser which is another prism then removes the polarisation. Finally, the light passes to the camera plane, and a DIC image with high contrast is obtained. DIC illumination is very costly when compared to brightfield or darkfield illumination. Thus, it only tends to be introduced to a system when extremely low levels of contrast are present if using the previously mentioned methods[123], [152], [161]. For 10x magnification, it is very unlikely that this method will be needed or justifiable for inclusion in the proposed system.

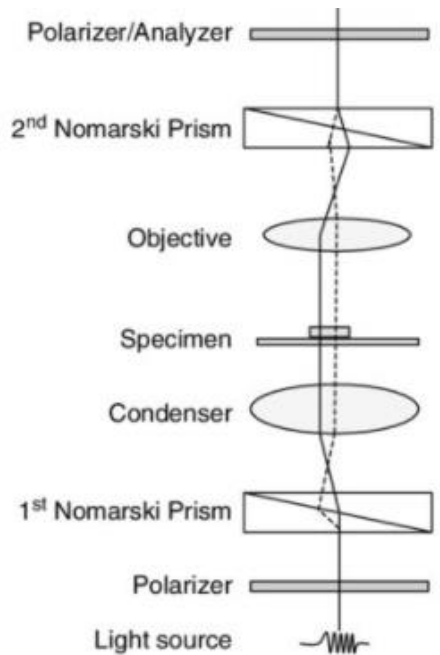


Figure 24: DIC Illumination Path [162]

2.7.6 Autofocusing on an image.

Before discussing the different algorithms that could potentially be used for autofocusing on the cells, it is worthwhile clarifying how focus is achieved. The microscope position on the Z-axis is adjusted so that the cells of interest are at the correct distance from the objective lens. This distance is referred to in microscopy as the working distance (WD) at which point the image is in focus, see Figure 25. Autofocusing is required as any changes in the height of the cells relative to the microscope will change the focus of the image obtained and thus refocusing at every testing point is required.

Positional tolerance of the cell slide or chamber or thermal expansion of a cell holder could be enough to cause the image to lose focus and thus render the system useless if it could not adjust along the Z-axis. Therefore, autofocusing the microscope requires two main factors, the ability to adjust the Z-axis, and the ability to use the information collected from the camera sensor to determine at what height the microscope acquires a focused image.

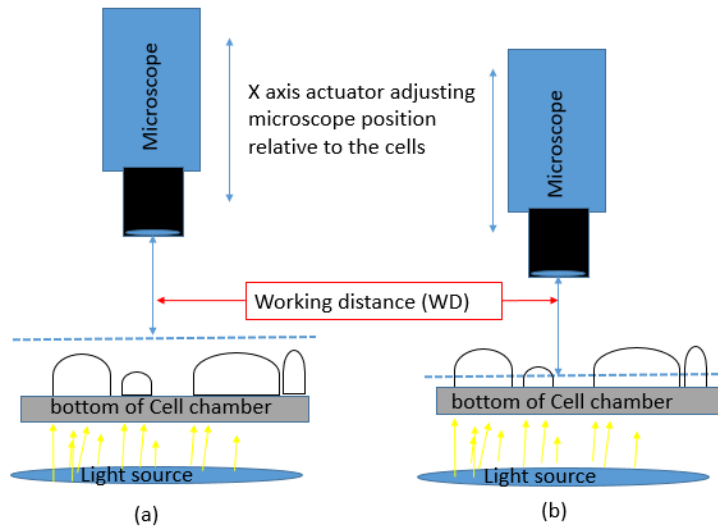


Figure 25: Focusing microscope on cells

2.7.7 Focusing algorithms and techniques

Focus measure functions (FMFs) are used to determine the focus of an image. When comparing the various approaches to FMFs, computational complexity and processing time are relevant[163]. In terms of the demands of this project, the microscope will be required to focus in ten positions across the two chambers, meaning that if imaging needs to occur at regular intervals of twenty minutes the FMFs must be able to autofocus in under two minutes per position to allow for the repositioning of the microscope for each desired location. It is with these factors in mind that the following FMFs are reviewed.

2.7.7.1 Gradient based FMFs

These functions work on the assumption that a well-focused image has more high-frequency content. A larger gradient means sharper edges in the image. These FMFs use the gradient or first-order derivative of the image to obtain the best-focused version of the image[163]. Examples of gradient based FMFs considered for this project include energy of gradient, gaussian derivative, and both the threshold gradient and squared gradient[164]. From reviewing literature around the performance of these FMFs the squared gradient seemed to be the most suitable as it was robust and fast[165]. The use of FMF's for autofocusing is a well-

reviewed area with many studies comparing the various techniques using raw images and processed images.

2.7.7.2 Statistical Based FMFs

The next type of FMFs considered for autofocusing are statistical based FMFs. Suggested by their category these FMFs uses statistical values from the image obtained to determine the level of focus[164], [166]. One of the advantages the statistically based approach has over gradient based approaches, in general, is they are less susceptible to noise. The statistically based options that were of particular interest for inclusion in this project were grey-level variance, standard deviation, and histogram range[163], [167].

2.7.7.3 Alternative FMFS

Other FMFs or algorithms considered that did not fit into either of the previous groups were Laplacian-based FMFs which use the second-order derivative of an image to measure the number of sharp edges in an image[167]. This concept tended to be more complex and time consuming for an improvement that was difficult to identify and therefore considered of limited merit when compared with the likes of both statistical and gradient based approaches[166]. Similar can be said for wavelet-based FMFs and given the type of magnification and illumination used as part of this project its inclusion would be difficult to justify over some of the less complex and more time effective options already mentioned[163], [167].

3. System Development, Testing, and Optimization

3.1 Robotic Brief

As previously stated, the design brief for the robotic system is to move a microscope camera to several locations on the test platform to focus on cells and capture images. To provide suitable positioning over cells, project partners stipulated that an accuracy of $100\mu\text{m}$ is required in the X-Y plane. While no value for Z position accuracy is set, the camera must be capable of autofocussing on the cells. This is achieved by moving the camera along the Z-axis and therefore implies a requirement of the order of $10\mu\text{m}$ accuracy for Z position.

Given the tolerance levels for the system, careful selection of components and drive mechanisms was critical to obtain such accuracy and repeatability of movement. Thus, the options considered for various components are discussed here, and the final selection is explained later in the chapter. Following on from this, testing of the system is undertaken and results are presented showing the required performance of the system as a whole. With the system being run autonomously, ensuring that the system repeatedly produces the required output is essential as the manual adjustment is not a possibility. It was also stated in the brief that while obtaining the stated performance is a necessity, it was also desired to retain a balance between complexity, accuracy, and cost when designing the system.

While position accuracy is a design constraint, there are no requirements placed on trajectory. This means that a simple cartesian robot geometry suited to point-to-point movement is an ideal solution. Thus, by designing a mechanically optimal system, one can take advantage of a less complex solution in terms of control. This chapter documents the design phase for a robotic system and the reasoning behind the part selection, then discusses how the system was tested to provide results showing accuracy. Figure 26 below shows the final prototype used for testing. The design can easily be miniaturized for inclusion inside the

enclosure designed as part of the H2020 project. Currently, however, having the system oversized helps for testing as those interacting with the system have more space to make changes to various parts of the system as required.

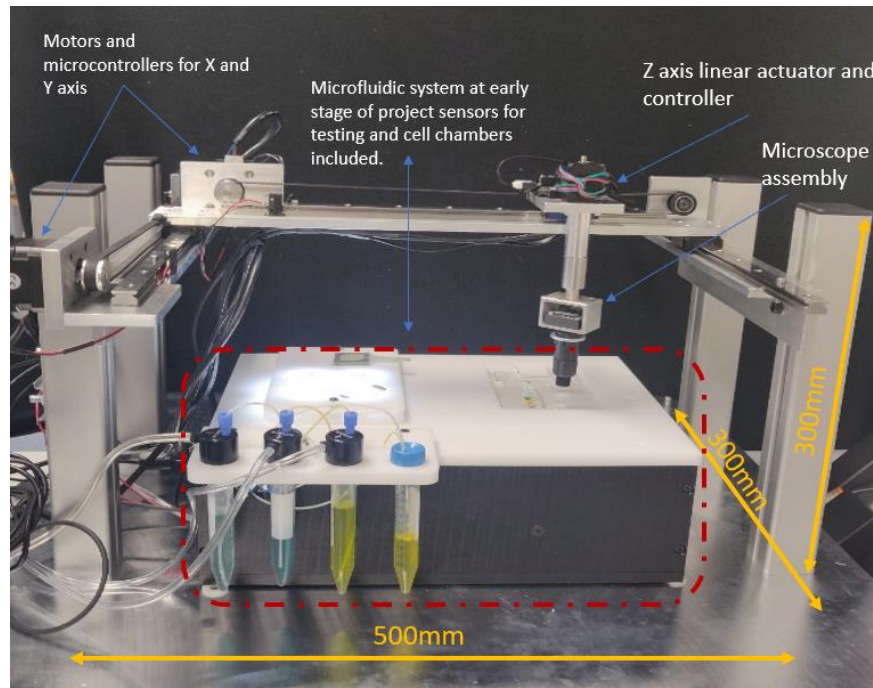


Figure 26: Image of XY robotics

3.2 XY Robotics Design

3.2.1.1 Power transmission selection

As discussed in the literature review, there were multiple options when it came to selecting a driving mechanism for the XY robotics of this system. Those found commonly in machines which require a high level of accuracy over a considerable range were lead screw and ball screw mechanisms both of which incorporate a motor turning a threaded bar which causes a stage connected to the bar to move along an axis. These mechanisms are commonly found in CNC machines as well as precision XY tables. The other power transmission mechanism

considered was a belt drive to move the respective stages for both X and Y axes. This option was preferred for a number of reasons, although traditionally a screw mechanism was credited with having a higher level of accuracy the recent growth in 3D printing showed that belt drives are more than capable of supplying the level of accuracy required for this project.

The advantages of belt drives over either ball screw or lead screw systems are as follows. Firstly they are substantially cheaper, had this project been made with the intention of the machine being a once off this would not have as much significance but seeing as the true goal of the overall H2020 project was to design a functional prototype that could then go on to be a viable commercial product cost reduction was an ever present consideration. Secondly, the speed at which belt drives can operate is significantly higher than a lead screw system. Even though high-speed movements are not an explicit requirement for this project, it was noted that by using a belt-drive, speed limitations would not become an issue when recording cell images at regular intervals during testing. Another reason to prefer the belt drive design to a lead screw design was the overall size of the robotics system if using the latter would be more difficult to scale down when it comes to integrating the final prototype into an enclosure.

Having selected the belt drive as the transmission system a motor was needed to provide the power to the system. Stepper motors were the obvious choice for this project as is evidenced by their use in a wide array of similar applications. As discussed in the Literature Review previously, stepper motors use a high number of poles to the effect that good accuracy can be obtained, this then coupled with using micro-stepping means that one revolution of a motor can be divided into 3200 steps which gives a high level of control in terms of small incremental movements. As well as good position control, stepper motors have the advantage of having a high torque at low speeds meaning that initial slipping does not have as much of an impact as with other motor types. Another advantage to using a stepper motor is that it has zero speed torque which allows the motor to lock into position and hold its desired position

without the need for an external break or mechanical locking mechanism required for other motor types.

Thus the combination of a NEMA 17 motor, a toothed gear, and a smooth idler gear along with a toothed belt was used as a means of powering the system. The belt was toothed as this gave the best results for this type of application. With the belt properly tensioned it meshed with the gear faces adequately to prevent slippage occurring.

3.2.1.2 Slideway selection

The next components for selection were the stages and slideways. Given the level of accuracy required an initial attempt to provide a low-cost solution to this part of the project was unsuitable as, despite the reported specifications, the level of accuracy and precision was not sufficient for the project. Figure 27 shows the T-shaped frame which consisted of aluminium rails and rubber wheels attached to a stage with the use of lock nuts and low-level bearings. Instead of this, high precision slide rails with recirculating ball bearing cartridges were used to allow for a smooth, even movement of each stage for the respective axis. With these slideways, a new H frame structure was implemented with the X-axis being mounted to the two cartridges on the Y-axis slideways.

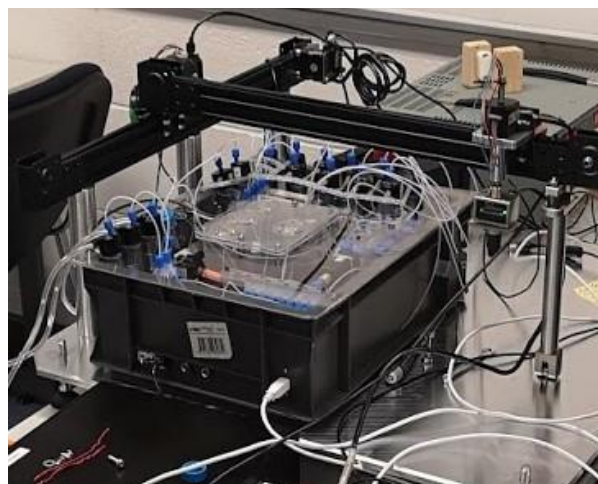


Figure 27: T-frame XY Robotics

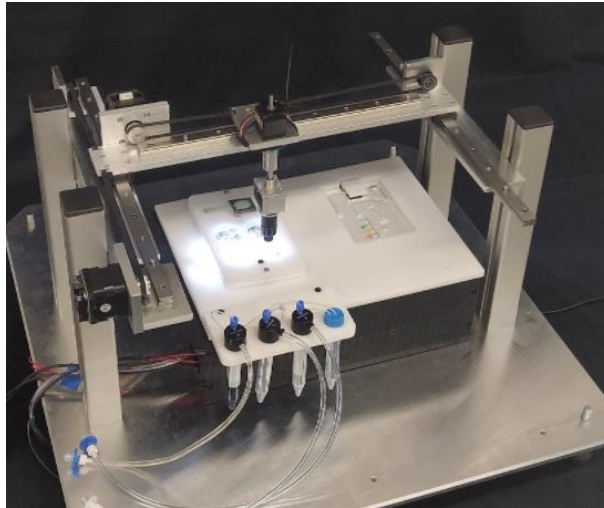


Figure 28: H-frame XY Robotics

This design provided more precise and accurate movements and increased the overall robustness of the system. Even though there are two parallel slideways for the Y-axis, a single motor was adequate given the low loads involved. The play in the carriages and slideways was also insignificant and therefore ensured adequate linear motion. In Figure 28, the H framed XY robotic system can be seen. This design made it possible to obtain the desired levels of accuracy and precision from the system from a mechanical point of view.

3.2.1.3 Microcontroller and encoder selection

A controller for the motors was then selected that could drive the stepper motors and provide the accuracy and precision needed for position control. When the Ustepper S-lite was inspected, it matched the requirements of the project and incorporated a rotary encoder that worked on the basic principle of a Hall effect sensor. This board had a compact design where each controller board could fit on the back of the motor with magnets placed on the motor shaft and the encoder chip located in close proximity to it.

The AS5600 encoder from AMS was a 12-bit contactless encoder that translated to 0.088 degrees' resolution. The encoder chip was already integrated into the board and seen as a

suitable compact dual solution for this project. Figure 29 shows the Ustepper product and just how compactly it fits onto the back of a NEMA 17 motor. With the magnet being placed on the back of the motor shaft. This encoding however used relative position encoding which meant that to ensure accuracy, a constant reference point was necessary. If there was any deviation in this reference point the error would be mirrored to that of the robot end effector position. The reason for using relative encoding, which tracks the movement of the motor from a defined point as opposed to absolute encoding, is a mixture of cost comparison, bulk, and also ease of integration.

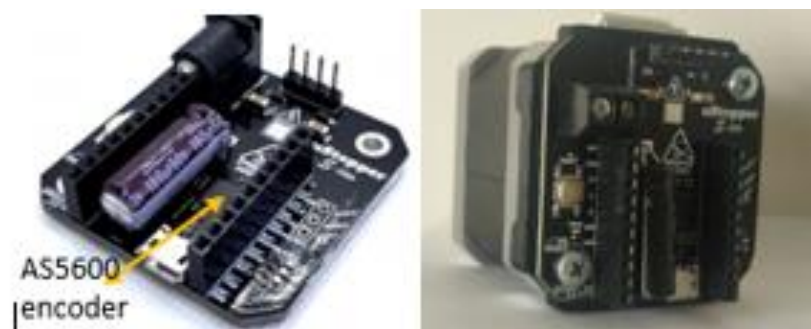


Figure 29: Ustepper S-lite with encoder

Having selected relative encoding the need for a known constant home position was key to achieving accurate positioning. The option that setting a stall torque and just cutting the power to the motor when it encountered a hard stop at the end of the rail was not desirable as although it was the cheapest option the vibrations and rebound from the collision with the hard endstop would not provide the accuracy needed. It was also suspected that over time this method would cause other issues to develop and that parts like stage carriages would need to be replaced more frequently.

Consequently, a series of sensors and switches were investigated to use as endstops for the system. These sensors and switches can be broken into two categories, contact and non-

contact. Contact switches and micro switches with different contact options like levers, plungers, and rollers, designed to suit various applications. Contactless options include infrared sensors, optical sensors, inductive proximity sensors, and Hall effect sensors. All these sensor types were previously discussed, and it was decided based on cost, both a micro switch and Hall effect sensor would be tested for use as an endstop in this system. It was also considered that perhaps by including both in a hybrid system, a performance improvement could be achieved should an individual switch not meet requirements.

Following initial testing of the system small modifications were made to improve the system. Notably, the original toothed gear was replaced with a smaller toothed gear to increase the resolution of linear movement. This change allowed for one step of the motor to translate into $9.5\mu\text{m}$ linear movements instead of the previous $20.3\mu\text{m}$. It should be noted that this did not affect sensor resolution which is 0.088 degrees.

3.2.2 Control design

Having designed the physical XY robotic system with the required accuracy from a physical standpoint, the next step to consider was control of the device. As this system incorporates a relative encoder to track movement the system can only correct an error that enters the system from the motor and not an error from physical nonlinearities like backlash. The first step in terms of control that was taken for this project was to set the motors to take a simple input and run in an open loop at specific speeds. Although it was very likely that open-loop control would not be suitable for the project it was worthwhile seeing the errors that entered the system without the encoder as it would indicate to us if there was an issue with the torque produced by the motor. It also justified the inclusion of encoders and Closed-loop Control to the other partners in the consortium.

Following testing from open-loop control it was apparent that there were errors that exceed the tolerances given and even when the current used by the motor was at a maximum and speed and acceleration set to minimise torque, the desired accuracy and precision were not obtained. This result vindicated the use of encoders in a closed-loop system.

After reviewing the literature in similar application a proportional-integral (PI) control was selected. The principal concern is the accuracy of the end position rather than trajectory tracking and so it was felt that a simple PI architecture would suffice. Since speed was not of prime importance there was no need for derivative control which is very sensitive to noise from sensors and which could have been an issue given the number of systems that comprise the overall system. By contrast, the integral element was necessary to ensure that steady-state error was removed.

Following the introduction of the PI control, the error in position accuracy in the XY axes was reduced immediately concerning the open-loop control however, it was felt improvements could still be made. It was noticed that when the input command was given through an angle command the error was more significant than with a step command. With a step being the single smallest command that the motor could take, the command was now given in steps to bypass the rounding effect that was seen when the command was given in degrees and not steps. Thus from this point tuning the K_p and K_i values to minimise the error was undertaken.

3.2.3 XY axis testing

3.2.3.1 Homing

Having explained the design and inclusion of specific parts of the XY robotic system, this section is used to display the results from testing motor operation modes for error and tolerance levels. Tests were undertaken in relation to the homing sequence. These were

performed using the lever operated microswitch at the end stop. All the results were verified using the coordinate measurement machine in DCU which has an accuracy of 3 μ m.

The purpose of the first test was to try to establish if the braking condition of the motor had an impact on the system accuracy and if so which was the better method to use going forward. Figure 30 shows the home position for when the motor is set to break softly with a range of 400 μ m referring to the stopping position of the system. The test was repeated with the brake mode being set to hard, thus locking the motor in place when reaching the endstop. These results are displayed in Figure 31 and have a smaller range of 85 μ m. Therefore, given that it was desired to lock into each final position anyways and the performance in terms of accuracy is positively impacted by the hard braking inclusion, only tests using the hard stop braking method will be included from this point onwards.

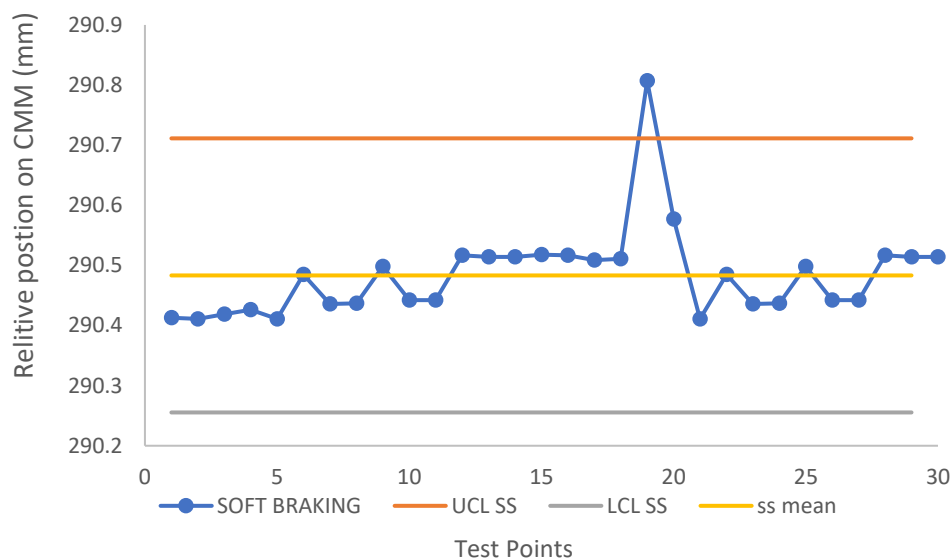


Figure 30: Control Chart for Soft Stop Test

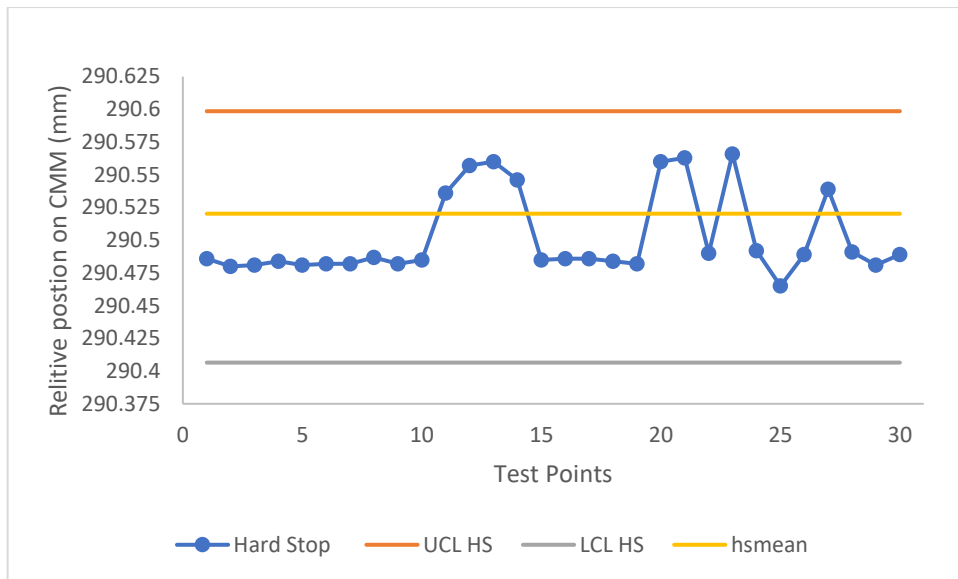


Figure 31: Control Chart for Hard Stop Test

The results plotted below in Figure 32 shows the results of homing using a mid-speed approach, which was being used for general movements. Here is the range of values obtained is evaluated with the aim being reducing that range to be as small as possible. Under these conditions using the micro switch a range of 114µm for homing was experienced, and given the overall tolerance for these axes is 100µm this potential error incurred from a changing reference point is not acceptable thus further work was required.

Above in Figure 31 as part of testing the homing, a slow speed approach was investigated to see if by lowering the speed of the motor, if the error in the homing position is reduced. When compared with the mid-speed approach an improvement in the error is clear due to the reduction in the range of values obtained, with the slower speed the range of results is reduced by 30µm.

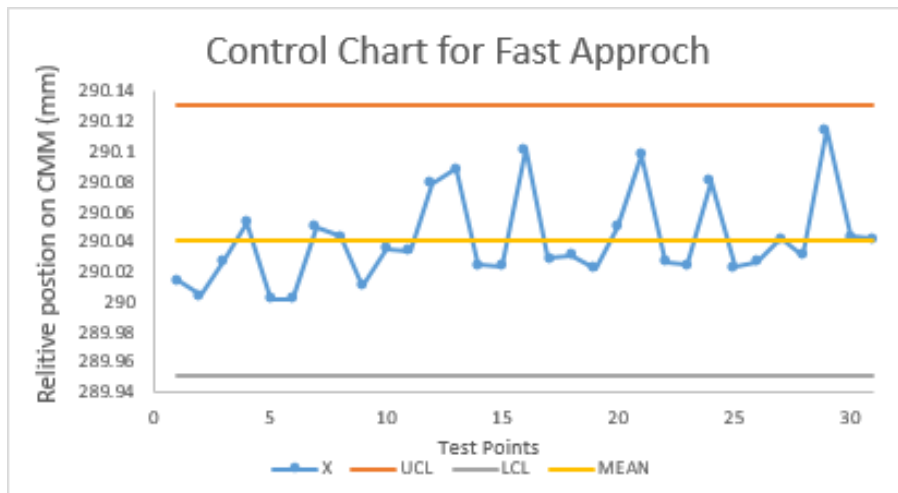


Figure 32: Homing Test Fast Approach

However, even with this, the micro switch was not adequate in terms of providing an accurate home position for the XY system. Therefore, a Hall effect sensor was then mounted to the system as an endstop, and magnets were mounted to the stage on the respective axes. When the distance between the sensor and the magnet reduces below a threshold, the magnetic field will cause the sensor to change its state and thus feedback this information to the microcontroller causing the motor to lock its position. Given that this option is non-contact it was expected that the speed of approach would not have as big an impact compared to the micro switch, however, depending on the time taken for the message to be relayed from sensor to controller and then motor this could still have an impact. And so below are the results for both the full-speed approach in Figure 33 and the slow approach in Figure 34.

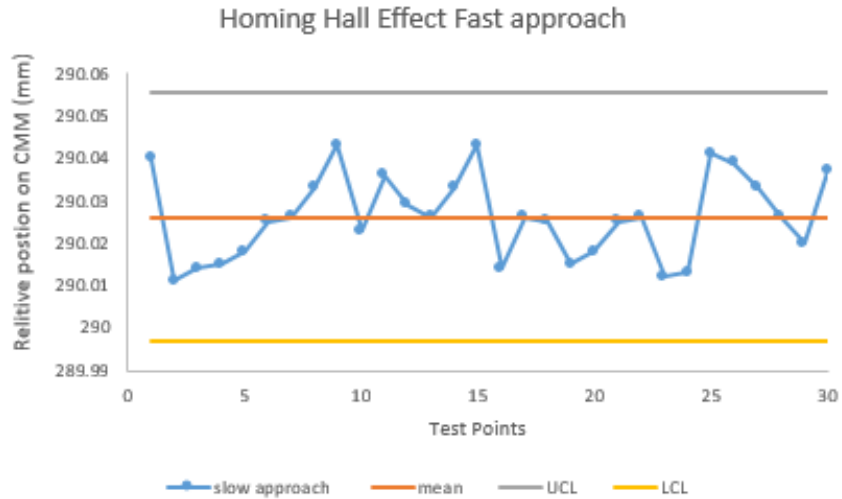


Figure 33: Homing Hall Effect Fast approach

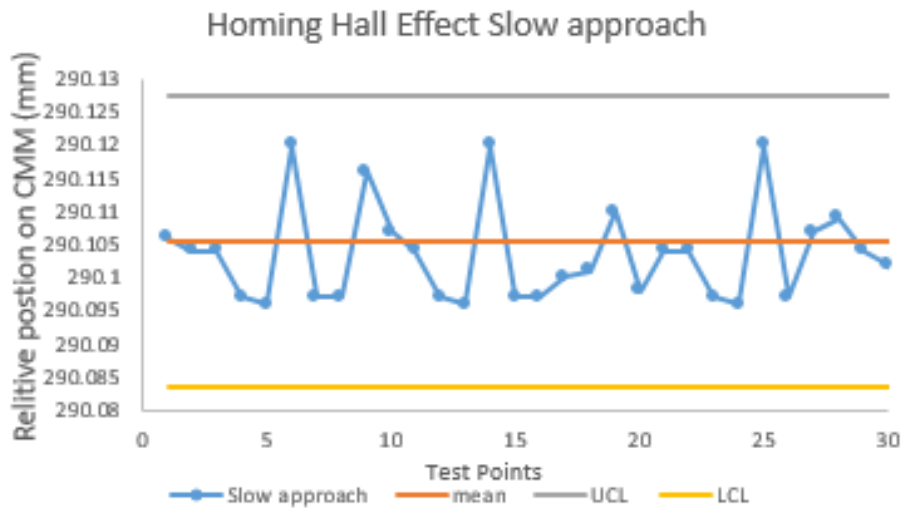


Figure 34: Homing Hall Effect Slow approach

From the above Figures, it is clear that the hall sensor out performs the micro switch. Therefore, the best option of the tested options is the hall effect sensor, and although the slow approach with this setup obtained more repeatable results, both slow and fast were satisfactory in their range for homing. With the standard deviation for the fast approach $9.7\mu\text{m}$ and with the slow approach of $7.3\mu\text{m}$ the system was considered to be approaching its physical limits given one step was the equivalent to $9.5\mu\text{m}$. Nonetheless, this minor level of variation in the

system homing would be sustainable should the relative movement of the axis lie within the tolerances set by the project consortium. Thus, the hall effect sensor with a fast return would be used. If required a dual return option could be implemented to put into use the slow approaches added accuracy.

Next, the relative error for both the X and Y-axis was tested. These tests were taken over a range of distances and in both directions to ensure that any potential abnormalities would be identified and addressed.

3.2.4 Relative movement control

3.2.4.1 Open Loop

Following the work with the open-loop testing, some of which can be seen below in Figure 35, errors of over 1000 μm were apparent which is 10 times more than the target accuracy. From this, it was clear that closed-loop control would be required for this system to reliably obtain the level of accuracy required.

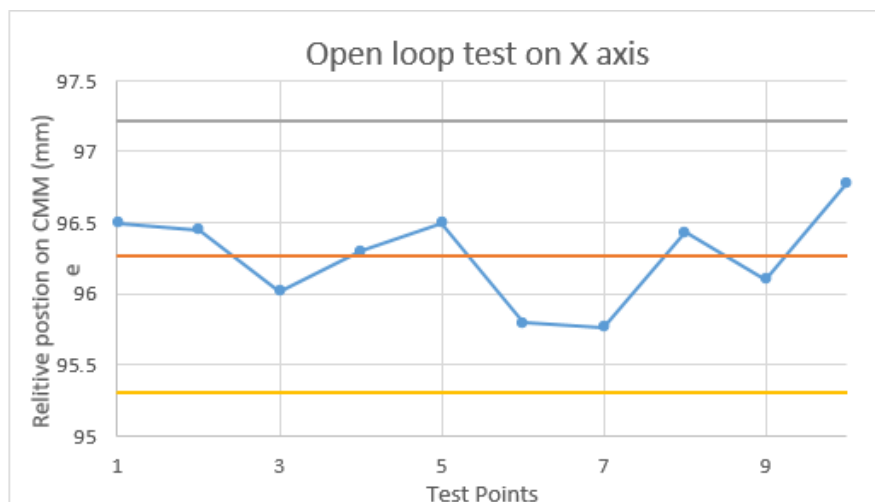


Figure 35: Open-loop test

3.2.4.2 Closed Loop

Initially, the system was run with medium gain proportional control. Below in Figure 36 and Figure 37 show the position of the stage following a set command of steps with the mean

value marked as is the upper and lower limits for a 99.7% confidence interval. The targeted value for this test was 93.75mm which shows us that there is a steady-state error in the system. As can be seen, the range of resulting positions would not in this setup satisfy the brief. In Figure 37 the accuracy is shown for a range of movements with the X-axis of this graph indicating the number of steps with an exception in the last data point being for 5000 steps but has been plotted at 275 for an easier to read graph, this is the case for all calculated vs error style graphs below.

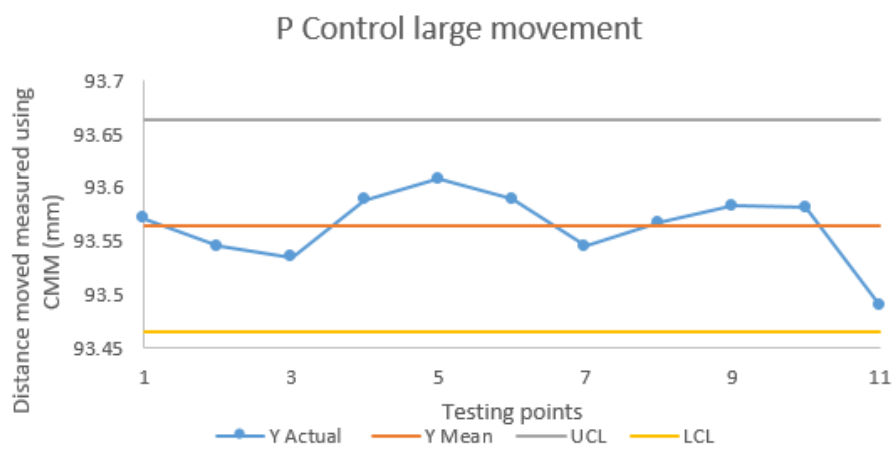


Figure 36: Proportional control large movement

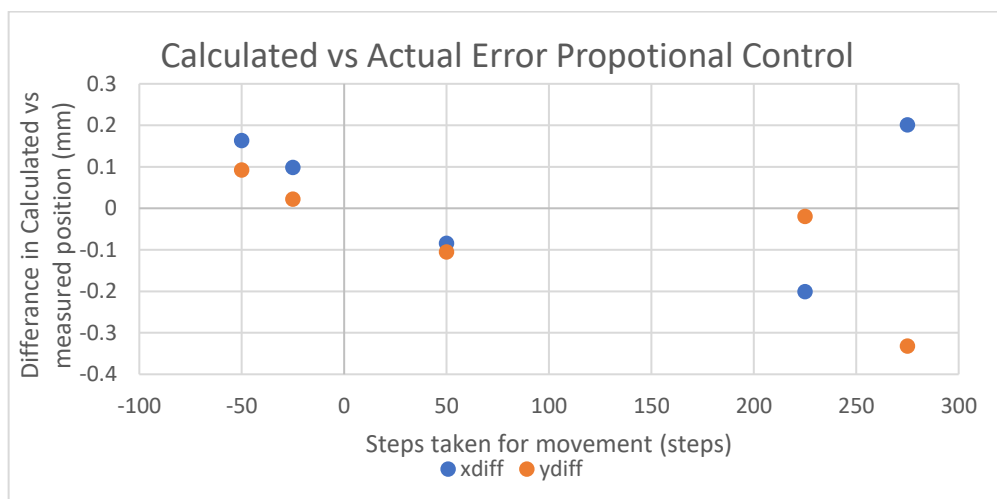


Figure 37: Accuracy for proportional control

Integral control was then added to the system to remove the steady-state error. Below in Figure 38 are similar movements to those shown above however notice that the range for the 99.7% confidence limits is smaller as for P the spread between upper and lower control limits is $210\mu\text{m}$ whereas for PI it is $107\mu\text{m}$. Thus at a glance showing us that the error is reduced. Following this more tests were carried out using this setup to check the system for error over various sized movements in both directions. The average error of each of these tests can be seen in Figure 39 which includes both the Y and X-axis.

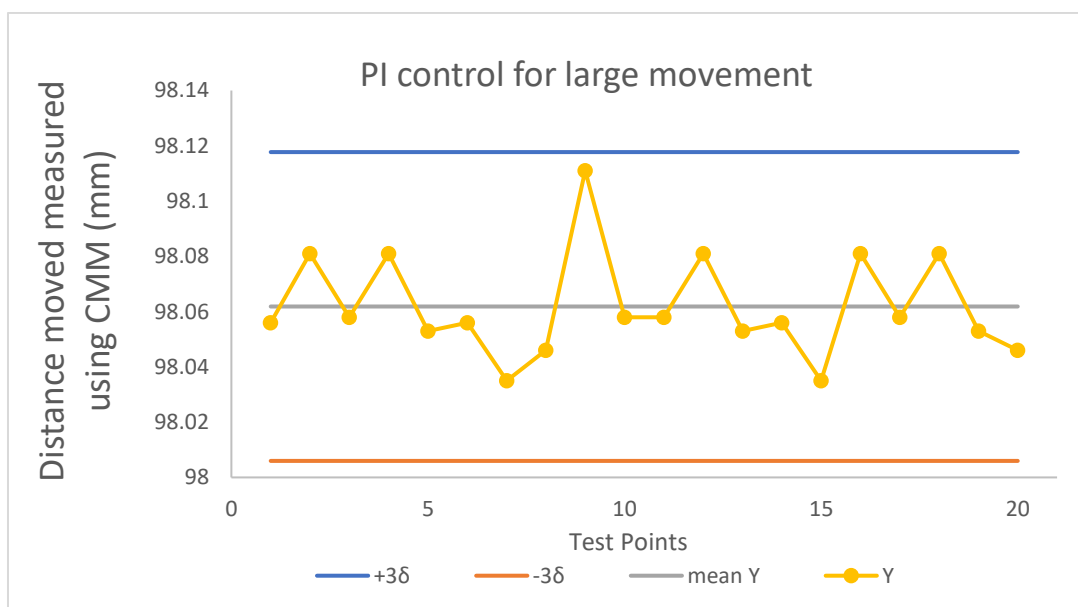


Figure 38:PI control chart for large movement

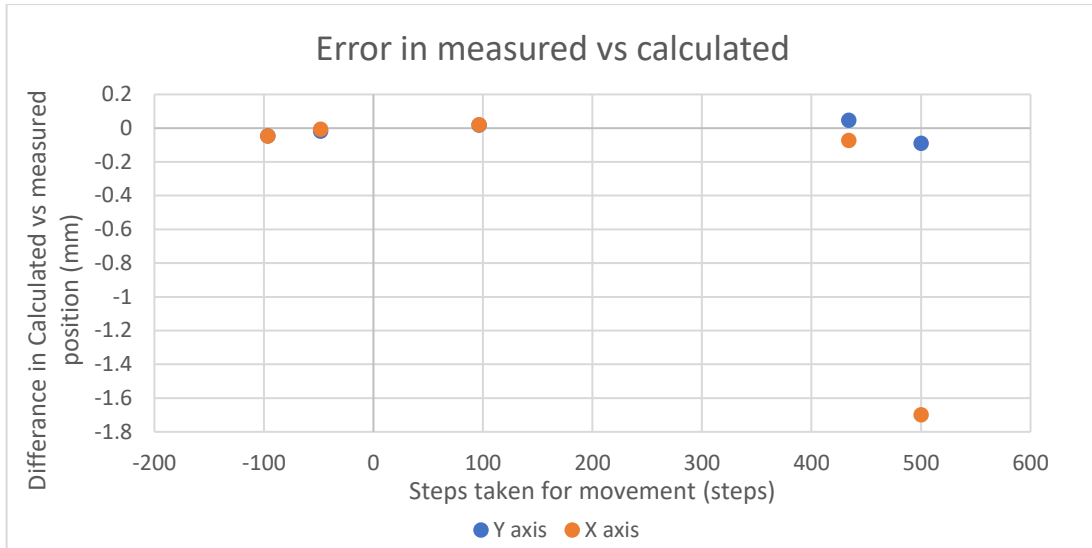


Figure 39: Error in measured vs calculated performance PI control

The results using PI control were all within specification other than one value for long range movement on the Y-axis. This was so far in excess of the others that a systematic fault was suspected. On closer inspection of the system, it was noted that one end of the Y-axis slideway was not securely fastened. During long range motion, the pull from power supply lines etc. on the system induced movement in the Y-axis. This was remedied by simply securing all the bolts on the system so that the results in Figure XYZ were obtained. With this level of error in the system as it is below the tolerances specified for a range of movements in both directions for each axis.

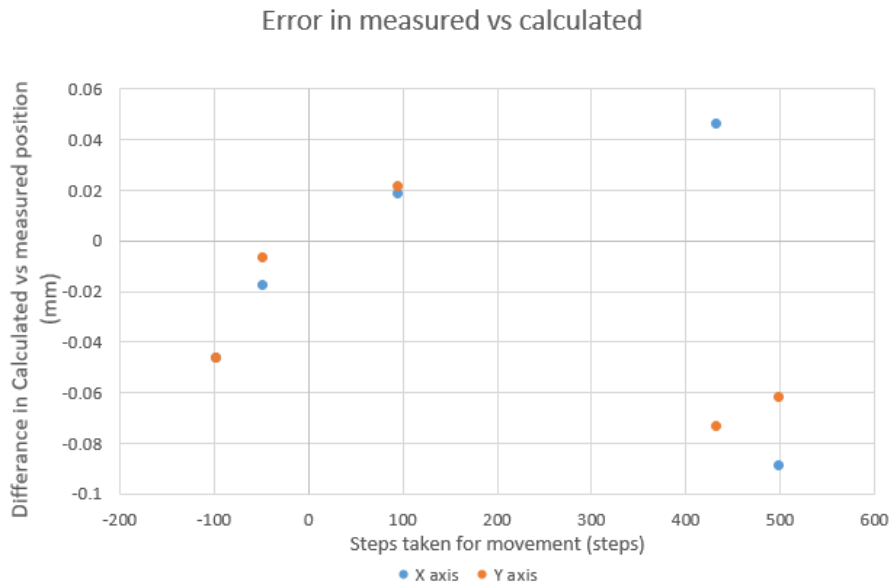


Figure 40: Accuracy for PI control following system adjustments and realignments

3.2.5 Designing a path for testing and testing that the operation is successful

Having tested the XY system with the CMM machine and obtaining the desired accuracy for the 97th percentile, the next stage of testing was to plan the path that the microscope would take to acquire images of conformity level in the two cell chambers in the system.

The standard 5-point approach is adopted where the images are recorded at the four corners of the cell chamber and one central point. To do this the microscope records images at either end of the first side of the chamber repeats this on the second side, and finally captures the central image. At each location, the camera performs autofocus, captures the image, and then stores it for further processing. The camera trajectory is organised to minimize the number of movements (15 in total) and thereby minimising the overall process time. It was also noted that by minimizing the number of movements during a run the cumulative position error is reduced and thus ensuring the total error at any given point is within the 100 μ m tolerance.

3.2.6 Z-axis design, testing, and control

Position resolution on the Z-axis must allow for sharp image focus and as a consequence more demanding than the 100 μ m tolerance required for the XY axes. In light of this, a lead screw type actuator was deemed appropriate

To minimize the space occupied by the power transmission method and avail of the smallest minimum movement possible, integrated motor options were investigated. In addition to high resolution, a working range of 10mm was needed to allow for general positioning.

A solution was found in the form of a self-contained captive linear actuator using a lead screw that rotated as part of a NEMA 11 motor to cause a separate shaft to extend without any turning motion which suited this application. The actuator had a stroke length of 38.1mm, minimal axial play, and a step resolution of 3.2 μ m. The nanotech motor was capable of performing adequately in terms of z-axis resolution in full-step mode, however, with micro-stepping a step size of 0.2 μ m is achievable. The actuator is shown in Figure 41. Given the style of motor, mounting an encoder similar to X and Y axis to the back of the shaft would not be possible. However, this was not required as the feedback control was dictated by image focus derived from the camera.

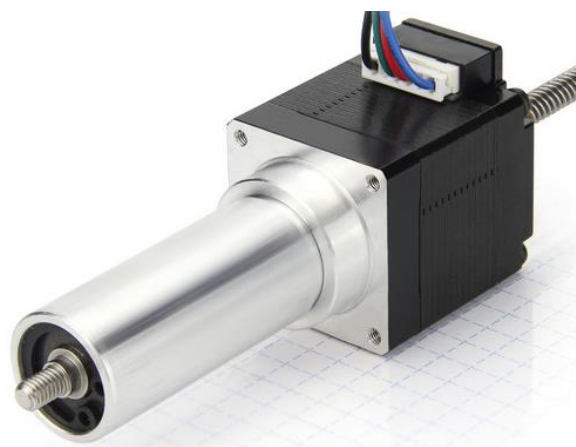


Figure 41: Nanotec actuator [168]

The operational model for the Z-axis was therefore as follows:

- home the Z-axis by retracting the lead screw to a hard stop.
- extend the camera to a known position to place the camera near the focus point above the cells. (this was done to speed up the process)
- run the autofocus algorithm to obtain a final position.

Having mentioned that the repeatability of the homing position for the Z-axis is not as critical, it uses the stall torque technique with a low current set on the motor when given the command to return home. However, a homing sensor using a hall effect sensor similar to the other axis' could be easily integrated if deemed necessary following testing over a long period of time to increase motor lifespan.

4. Microscope Design and Testing

Given the requirements of the project, a microscope capable of imaging cells with approximately x10 magnification was designed. The task of the microscope is to be able to detect changes in cell health by detecting the changes in cell shape following the introduction of a biomaterial and also to determine cell confluency in the cell chambers. The microscope is integrated into the XYZ robotics as the end effector with the Z-axis being used solely to move the microscope into focus. With this in mind, the following section looks at the design and development of such a microscope and the testing to ensure its performance and capabilities are adequate for the project.

The first selection made is to use a CMOS style sensor and not a CCD sensor as the microscope backplane this is based on the findings from the comparison of the two sensor types as described in the literature review. A Basler dart camera, seen with housing in Figure 42, that is capable of communicating over USB 3.0 was selected. The resolution of the backplane is 1280pixels X 960pixels and can operate at 14 frames per second. The camera was selected with

the goal of designing a compact, easily integrated microscope with a magnification of X10. Given that the microscope would be placed as the end effector of a Cartesian frame robot, the field of view of the microscope was not a primary concern as multiple images could be superimposed to give a larger image if required.

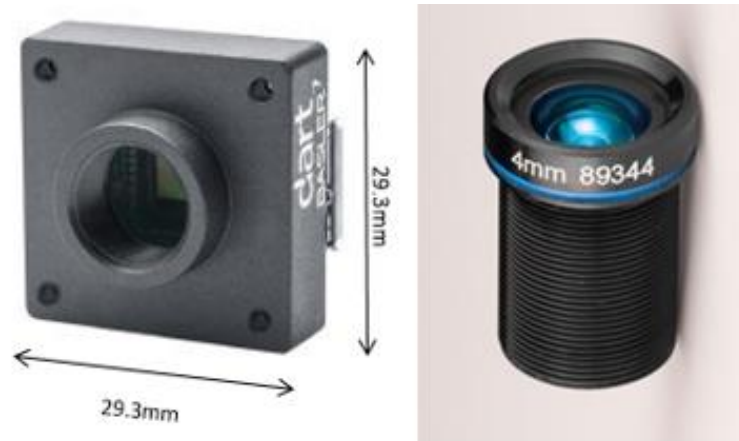


Figure 42: CMOS housing and objective lens

Following camera selection, the required magnification was addressed by selecting an objective lens for the microscope. A cost-effective approach was to take a simple thin lens, like one commonly found in wide-angle lenses for webcams. The concept was to invert the wide-angle lens so that with the correct spacing a compact microscope could be created with a magnification of 10x. This works as the wide-angle lens when inverted now takes the light from a small space and magnifies it onto the CMOS sensor which therefore causes the magnification.

Having selected an objective lens shown in Figure 42 with a focal length of 4mm in the Techspec 4mm FL f/4.0, Blue Series M12 Imaging Lens, the length of the spacer tube is determined to obtain suitable magnification using lens maker's equation and treating the objective as a thin lens. Below in Figure 43, a simple diagram showing the relationship between object distance, image distance, and focal point is shown. From this, one can calculate the magnification.

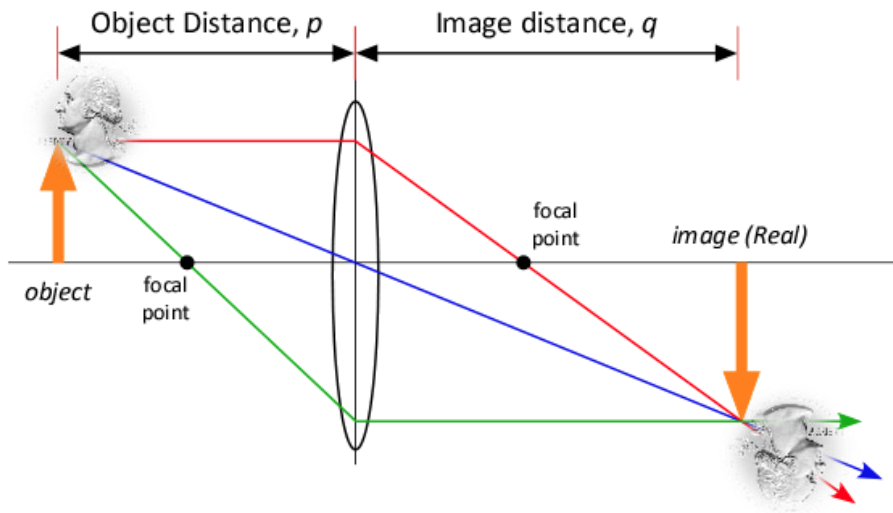


Figure 43: Magnification to lens relationship

The relationship above can be expressed as the following

$$\frac{1}{F} = \frac{1}{p} + \frac{1}{q}$$

Equation 4

Where F is the focal length, following from this linear magnification can be expressed as $M = \frac{q}{p}$

Using these equations, one can determine the value for q to obtain suitable magnification with the use of this objective lens. Setting q=45mm then first calculate u and following on from that M.

If the lens maker's equation is rearranged to isolate p , thus one can write it as

$$p = \frac{fq}{q - f}$$

Equation 5

Thus, finding That p = 4.4mm and thus, M= 10.25 giving us the desired approximate magnification.

Given the thin lens approach for the microscope, the image will be inverted on the camera sensor as shown in Figure 43 by the rotation of the coin. The orientation of the cells is not something of concern for the project and therefore, there is no need to increase the cost and complexity of the microscope by adding an additional lens to allow the image to be correctly orientated. Knowing the correct distance necessary between the objective and CMOS sensor determined, a tube spacer with the required features is designed and machined from Delron. The spacer tube includes a fine tread to attach to the CMOS sensor housing which also allowed for minor adjustments in the length of image distance q should it be required. This spacer tube also is designed to correctly seal the tube with the objective lens being the only viable path that light can follow to arrive at the CMOS sensor.

A small dc fan was also included in the design for the compact microscope as it was decided that with the system being maintained at 37 degrees, the sensor chip may require cooling when operating over longer periods of time. The fan was mounted so that it could supply direct airflow over the back of the camera to maintain a suitable temperature, this camera has an operational temperature range of 0-50°C. The fan was selected based on it being designed for cooling raspberry pi microcontrollers, it was lightweight, had an adequate flowrate, and could be powered from the microcontroller for the z-axis.

To determine if temperature variation had a sufficient impact on our system and to determine would a more extensive cooling system for the Cmos sensor would be required, the following test was carried out. While the z-axis was fixed, the only changing parameter affecting images was the temperature change. These images are shown in Figure 44 and Figure 45.

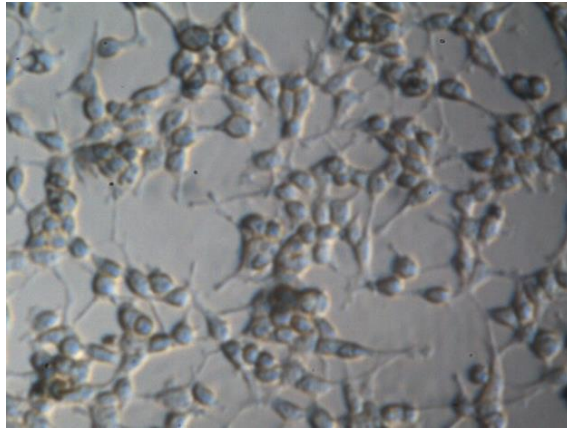


Figure 44: Image at 22°C (room temperature)

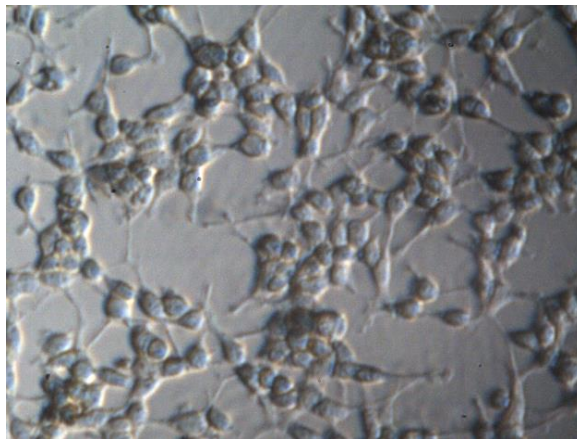


Figure 45: Image at 37°C human body temperature

Figure 44 shows how the camera behaves at cooler temperatures which due to the requirements of maintaining a temperature of 37°C would be more complex to obtain around the microscope. The next image, Figure 45 however shows the resulting image when the system is at the desired 37°C this image is more than satisfactory and the difference between both are minor and difficult to present.

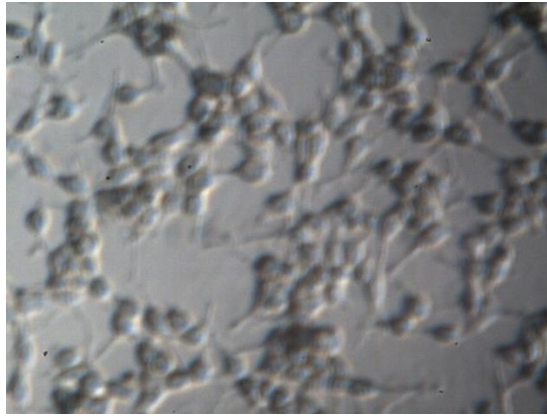


Figure 46: Image at 50°C

Next, the issue of overheating of the chip is investigated, it's recommended operational temperature is 0-50 degrees and so testing the effect of the CMOS sensor reaching this upper limit and the effects on the image output. From Figure 46 you will see that the resolution of the image deteriorates as the temperature rises.

Also incorporated is a base bracket that would connect to the shaft of the linear captive actuator discussed in the previous chapter. This design feature allows for no strain to be placed on the CMOS sensor which is important as its housing does not support load-bearing it also has been specifically designed for a compact solution. Below in Figure 47, this bracket is shown, it is a bespoke part to suit specifically this project.

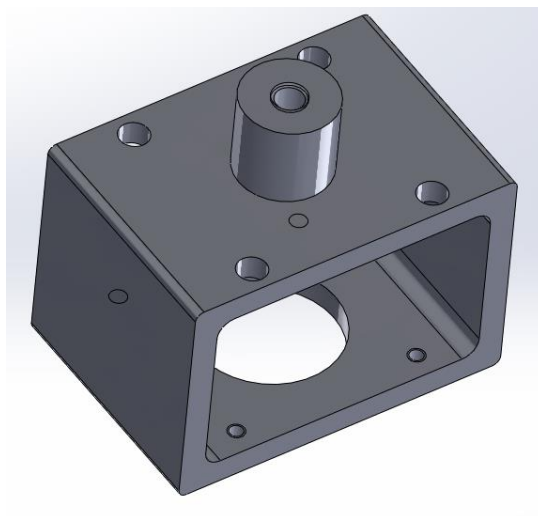


Figure 47: CMOS base bracket

When this assembly was first tested, diffracted rays of light caused an uninterpretable image to appear on the sensor backplane. Following a series of investigations, it was discovered that the reflective surface of the internal faces in the objective tube structure was causing light to bounce and distort the image collected. Thus, the issue was resolved by using a matte non-reflective surface to line the internal walls of the tube spacer. More complex solutions were discussed such as integrating a honeycomb structure which would stop the light that bounces against the tube wall to continue to travel to the CMOS sensor.

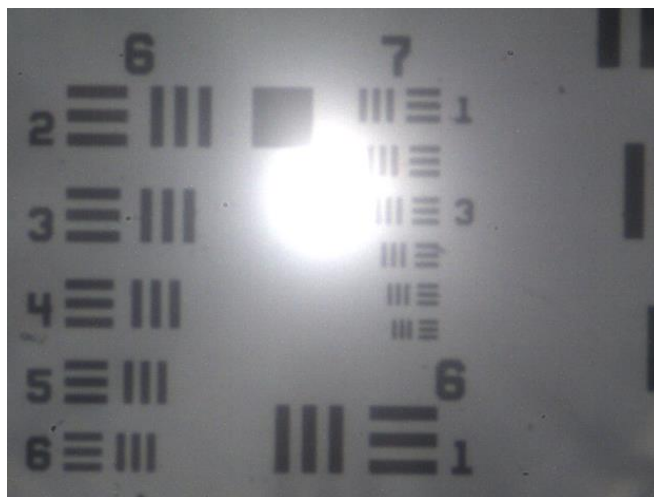


Figure 48: Image obtained without tubing lining

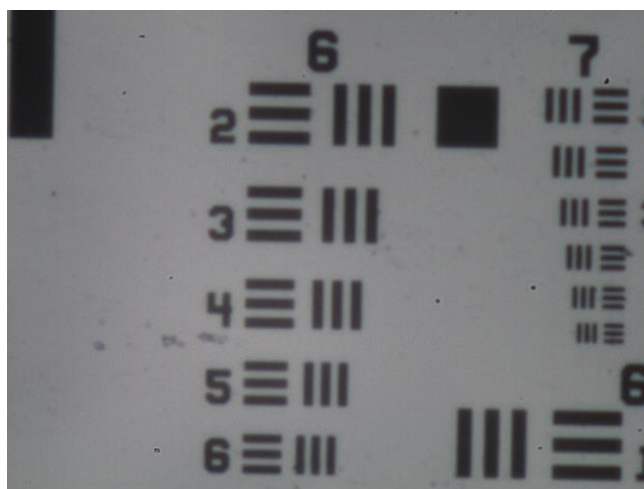


Figure 49: Image obtained with lining

However, as seen in Figure 48 and Figure 49 which compares the system before and after the introduction of the tube lining it is clear that the new lining now allows for satisfying images to be obtained. Thus, the simple solution was deemed a success and the attention of the project turned to the design of the lighting design which was crucial in optimizing the images produced by the microscope. Below is an image of the microscope explained up to this point.

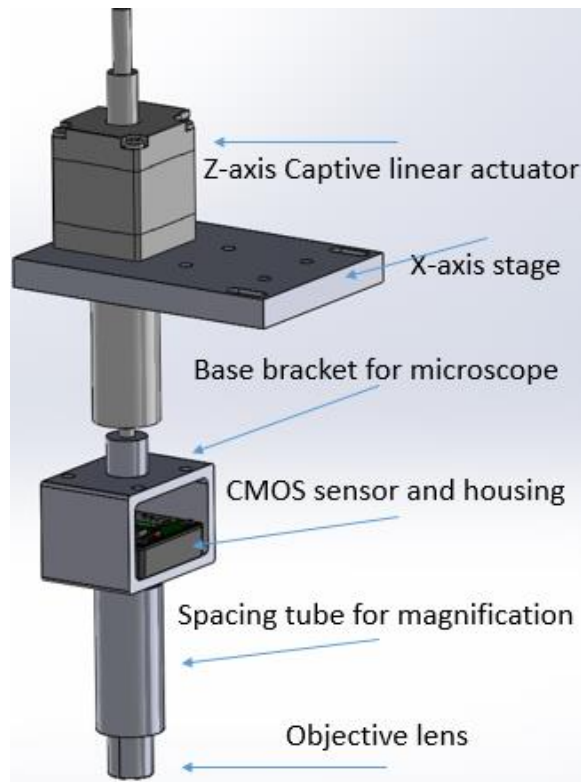


Figure 50: Microscope design with actuator

4.1 Lighting design

As previously discussed in the literature review there are multiple light sources and techniques used in microscopy to obtain images of the desired object regardless of it being cells or otherwise. When designing the lighting solution for a microscope, first it is important to highlight the specific demands of the microscope. As previously stated, these are to image cells under 10x magnification for determining confluency in the cell chambers, and also to determine the changes to cell shape after the cells have been insulted with the chosen biomaterial over a 48-hour period of testing.

With this in mind and following the investigation into the potential options in the literature review, bright field illumination was the method of illumination chosen. Ultra-bright LEDs were selected as the light source for a collection of factors. LEDs are compact compared to other lamp techniques that are employed by large bright field microscopes. LEDs also come in low heat production options which give them a significant advantage in our project since a localised heat source such as a lamp would compromise cell temperature which is to be maintained at 37°C. LEDs also do not require the same level of filtering as tungsten and halogen lamps and will not produce spurious images on the CMOS backplane caused by the shape and vibration of a filament. Also, LEDs tend to maintain their colour over time whereas the other options mentioned do not and feature a colour temperature drift as they age. As a result, LEDs do not need colour filtering as they tend to supply the specified conditions for the duration of the lifespan of the product. Beyond the advantages mentioned, LEDs are easily sourced and can be selected to have a high lumen flux output which is critical for optimising the images produced by the system. Therefore, an ultra-white bright LED was selected as it can supply suitable light for the task of the project under the magnification present. The LEDs selected have a beam angle of 120° and operate off 12Vdc while emitting 550-lumen flux.

Once the LED was selected an array was created to act as the light source to increase the light intensity and provide a light source for the entire area of the multiple cell chambers. When this array was centred underneath the sample it quickly became clear that the direct light from the bare LEDs would not provide a sufficient lighting solution. Figure 51 below shows the LED array mounted to an aluminium backplate with heat resistant epoxy to act as a cooling feature with the provision for the addition of a heat sink if deemed necessary later. Next to it in Figure 53 is an image obtained by the microscope with just the bare LED array as the light source. It is clear this is not suitable and that light from multiple angles is distorting the image.

The final image Figure 52 is one supplied from a project partner and although this image was produced by an expensive high-end microscope with a much larger FOV than our system, it serves to show the type of image the project is aiming to produce. One of the reasons for our poor image is the lack of uniformity in the light source as multiple points in the array will have higher flux densities in comparison to others. It is thus apparent then that creating a uniform light source is desirable.

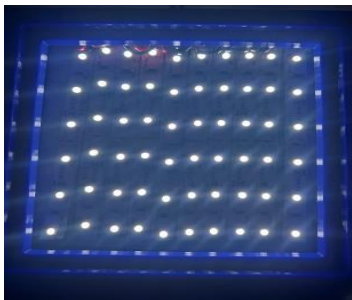


Figure 51: Led array

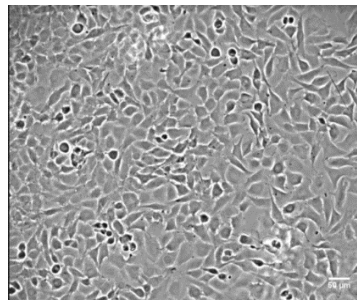


Figure 52: cell image from Celine

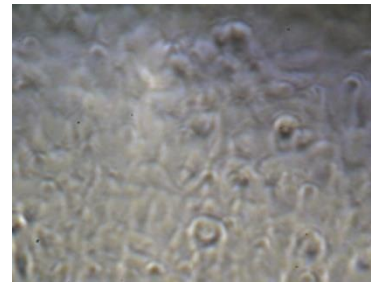


Figure 53: Image with bare array as the light source

As a result, in designing for a compact, inexpensive microscope, attention turned to selecting a diffuser. The purpose of a diffuser is to create an evenly dispersed light source from the LED array. With light intensity so paramount, a sample of diffusers with high light transmission and high diffusivity properties was selected for testing. The reason for this was to identify the combination of conditions that would best minimise the amount of light lost, but create an even light source to allow for better imaging. The distance between the diffuser and LED was determined by using a testing unit which was designed to allow the distance between the diffuser and the LED array to vary for the given diffuser under inspection. The various diffusers were tested at different heights and then based on the best image obtained, the diffuser was selected. The testing setup was designed and manufactured, and its model is shown below in Figure 54. The sample sits on top of the testing rig with the area of interest positioned over the window slot. This allows the full diffuser and LED array to impact the sample in terms of light. The diffuser and led array are suspended from the top of the rig with fine thread bolts which were used to set them at various heights throughout testing, see table 1 .

Four diffusers are tested and the resulting images along with the diffuser positions of is recorded.

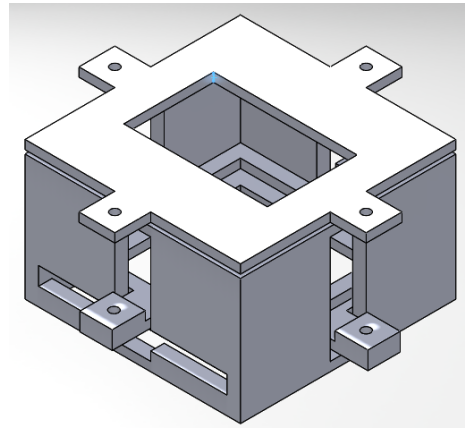


Figure 54: Diffuser Testing rig

	LED Array	Diffuser	Sample
Position 1	35mm	45mm	50mm
Position 2	5mm	45mm	50mm
Position 3	5mm	25mm	50mm
Position 4	5mm	15mm	50mm


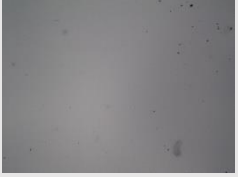
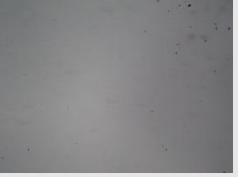



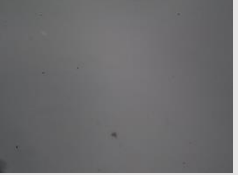
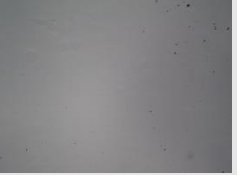

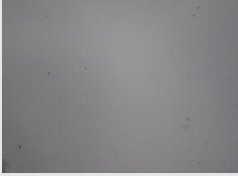






Table 1: Testing for diffuser arrangement

For position 1, the distance between the diffuser and LED array is at a minimum of 10 mm, and the distance of diffuser to sample was 5 mm. For the second position, the LED to diffuser distance is set to 40 mm. Here one would expect the light to be diffused more however the consequence is a loss in light transmission and intensity. For position 3 the LED to diffuser distance is set to 10 mm LED remains in its lowest position relative to the sample and the diffuser moves down towards the LED array with the distance between the two being 20mm. The final position then has both LEDs and diffuser at their furthest point from the sample but

closest to one another so that the distance from the sample to the light source is 40mm but the distance similar to in position one between the LEDs and diffusers is 10mm.

The results shown in Table 2 indicate that samples 1 and 4 over the four different positions have the best results in obtaining a suitable light source by a combination of LEDs and diffuser. For these samples, positions 1 and 4 are the most successful, indicating that the distance between LEDs and diffuser at 10 mm is preferable. The fact that the reduction in the distance between sample and light source improves results is most likely due to the increased intensity of light experienced by the sample before passing to the CMOS sensor through the microscope. From these results, it was sufficiently evident that Sample 1 produced the best results arising from a combination of high light transmission (LT) coupled with good diffusivity. Therefore Sample 1 will be used as the diffuser lighting system.

Table 2: Diffuser table

	Position 1	Position 2	Position 3	Position 4
Sample 1 Matte/gloss; LT% 90 Dif % 57;				
Sample 2 Satin/Satin; LT%81 Dif % 56;				
Sample 3 Matte/Satin; LT%71 Dif%56;				
Sample 4 Matte/Gloss; LT%81 Dif %67;				

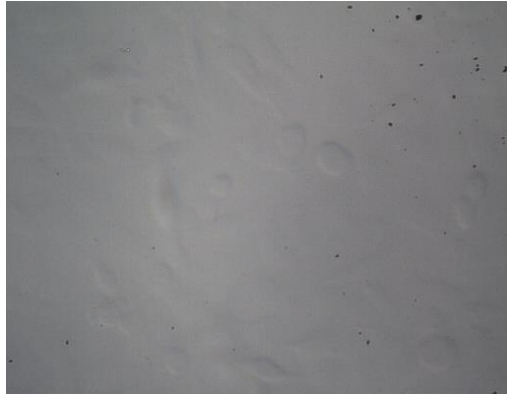


Figure 55: Chosen Diffuser

Figure 55 shows the highest level of detail and where the diffuser has a LT% of 90% and a diffusivity level of 57%. One can consider the LED-diffuser combination as the light source with the remainder of the lighting design referred to as the light conditioning used to optimise the light passing through the sample to the image plane, i.e the CMOS sensor.

Next, to minimise the angle of incidence the light beam makes with the specimen, is the introduction of an aperture diaphragm between the light source and the specimen. By reducing the diameter of the aperture one can increase the contrast of the image and regulate resolution, it also changes the depth of view of the system. In this project having high contrast is desired as it will allow the image processing to determine the cell health based on a change in the curvature of a cell. Using a variable aperture, one can optimize the trade-off between resolution and contrast. Below Figure 56-Figure 58. Shows the progressive improvement in image resolution starting on the left with a bare LED array, in the centre with LED array and aperture, and finally on the right with LED array, aperture, and diffuser where cells can be clearly identified using the compact microscope.

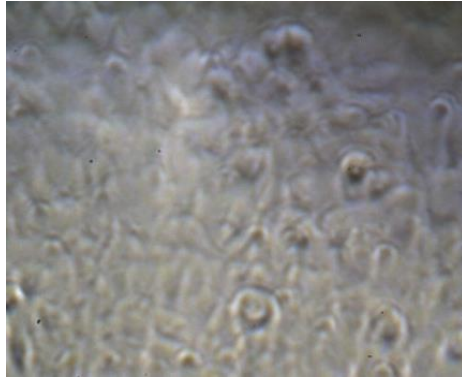


Figure 56: Bare Led Array

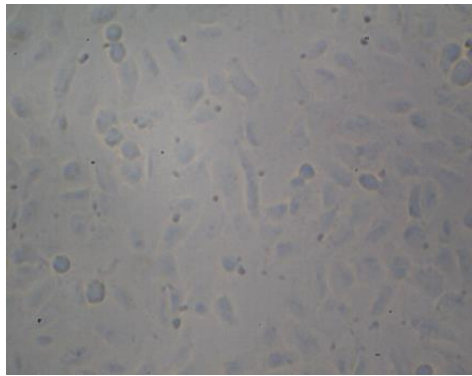


Figure 57: Led Array + Aperture Diaphragm

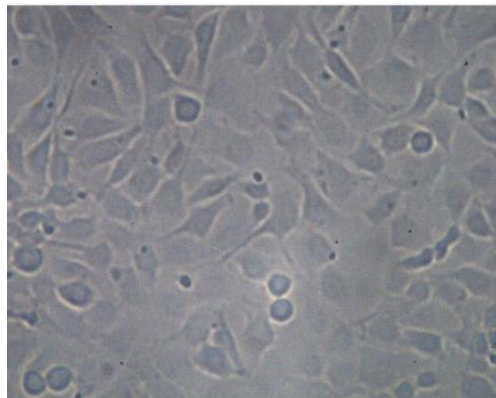


Figure 58: Led array + Aperture diaphragm + Diffuser

Having justified the inclusion of the aperture in the above comparison, the next step was testing various sized apertures to distinguish the optimal diameter. Having purchased a variable diaphragm aperture to ensure no unaccounted for effects occurred, instead of using

set pinholes machined within DCU it was first sought to image either end range of the diaphragm. Following this, the pinhole was set to have a diameter of 4mm this was because literature commonly suggests that the optimum aperture for the resolution of an image is to match the aperture of the light source with that of the objective lens. These images can be seen below in Figure 60-Figure 62.

When comparing these images to an image captured when removing the aperture entirely in Figure 59, a distinct change in the quality of the image obtained can be observed, and hence therefore the inclusion of this microscope part is amply justified.



Figure 59: No aperture present when imaging

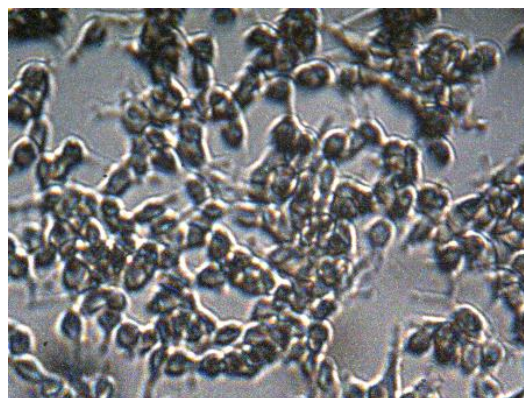


Figure 60: aperture fully closed 0.5mm

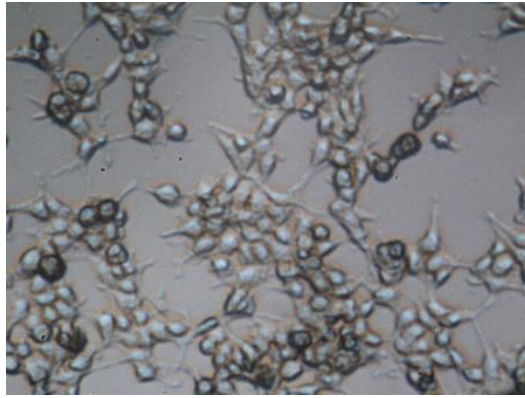


Figure 61: aperture set at 4mm

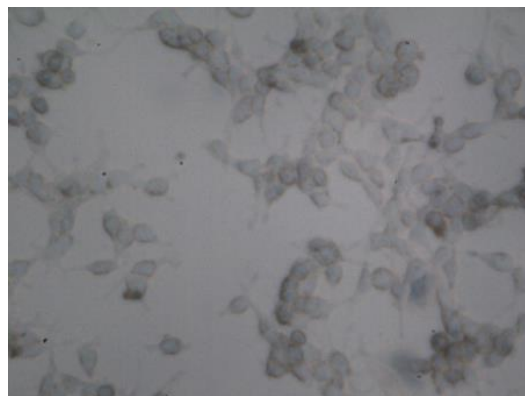


Figure 62: aperture fully open 7mm

The best image obtained as suggested was that where a match was made with the objective lens of 4mm. Small variations to the aperture were then made around this value to optimise the system for the needs of the project. Reducing the diameter produces images with higher contrast while expanding the diameter increases brightness. Results indicated that the most suitable image for the output of this project was obtained by having the light source aperture slightly smaller (3.5mm) than the aperture of the objective lens. This is apparent below.

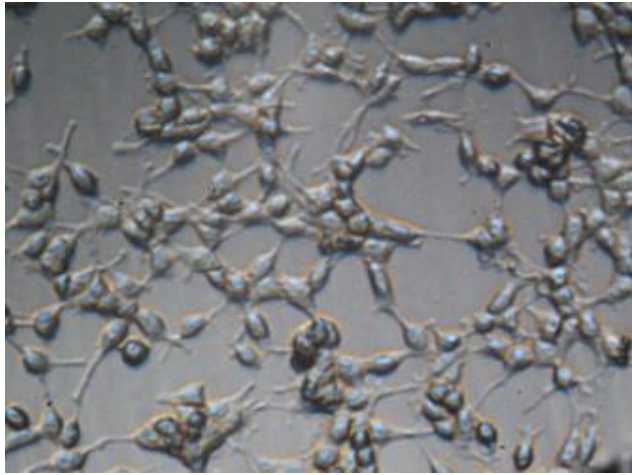


Figure 63:2.5mm Aperture

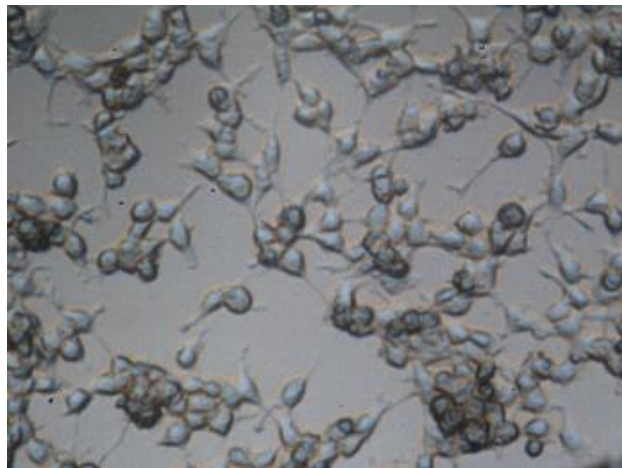


Figure 64:3.5mm aperture

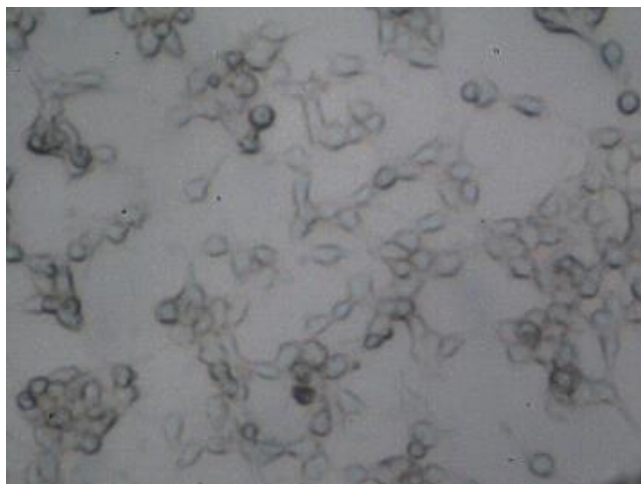


Figure 65:4.5mm aperture

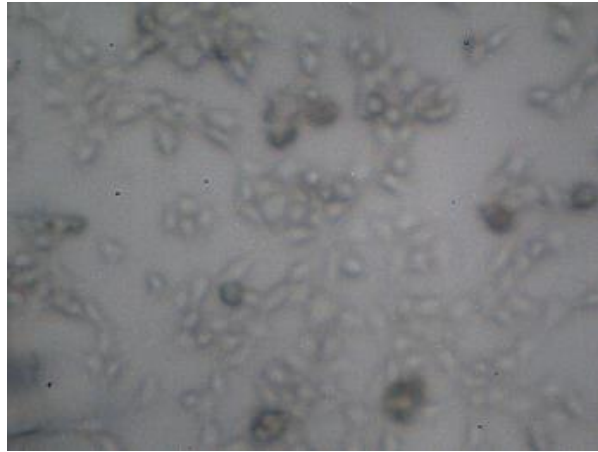


Figure 66:5.5mm aperture

With the aim of minimum cost and a compact design, minimizing the number of lenses in the design was investigated. Testing was carried out both with and without a condenser lens and the testing setup shown below in Figure 67. In addition, a range of condenser lenses was evaluated to explore the utility of including such a lens. For this, uncoated moulded aspheric condenser lenses were selected as they were the most cost-effective option readily available with a selection of focal lengths close to that of our objective lens.

Due to the nature of the project and microscope setup focal lengths of 4mm, 6mm, and 7.5mm were tested. In theory, the 4mm lens should give the best results as it matches the focal length of the objective lens. However, with other effects in this system such as the multiple mediums in the cell chamber and the fact that the objective lens is inverted. These imperfections in the system may cause slight differences in how the lens and that the lens chosen are noted bespoke objective lenses machined for microscopy prompted further investigation.

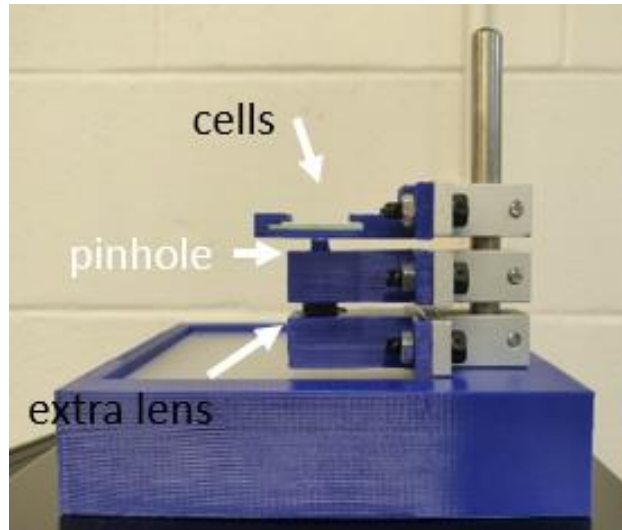


Figure 67: Lighting testing Rig

Figure 67 shows the testing rig used for both aperture analysis and condenser lens testing. The cells on a slide are positioned uppermost with the pinhole, condenser lens and light source below. Through a series of tests, the following Figure 68 show the optimum images obtained by the CMOS sensor when each respective lens was used as a condenser.

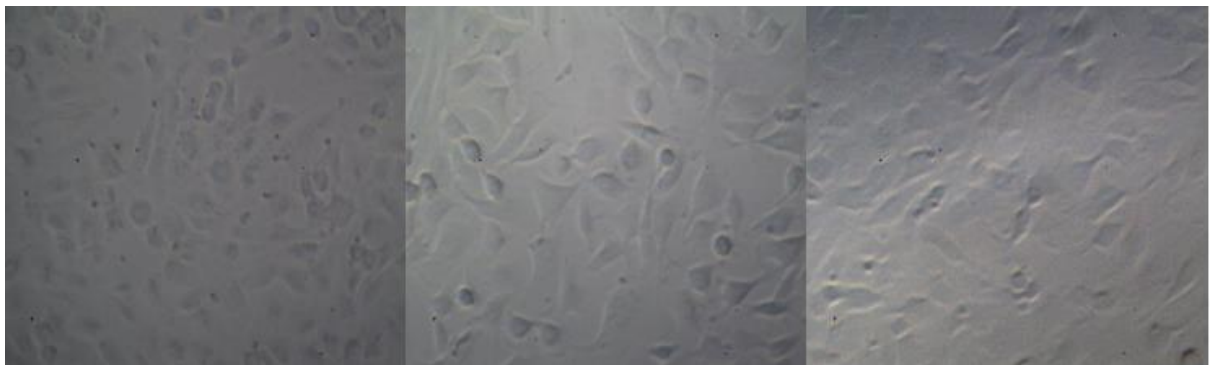


Figure 68: shows from left to right images obtained with lenses of focal length 3.1mm, 6mm, 7.5mm respectively



Figure 69: No condenser lens present

When the above images are compared with the image obtained without a condenser lens present in Figure 69, the increase in image quality is negligible. In terms of the tasks that the microscope will undertake, increasing the contrast of the image solely with the introduction of the aperture provides an inexpensive microscope solution suitable for the project at hand. With this, the microscope design is complete from a component standpoint with just small adjustments being made during testing to fine-tune for optimal imaging. When simplified the microscope is focusing light with a magnification onto a camera sensor to image cells which are approximately $10\mu\text{m}$ in diameter, therefore alignment of the components of the system is critical and taken into consideration in the manufacturing process.

At this point, the method of positioning the cell chambers was considered to achieve good image quality for all cells in the chamber over an area of 2.5cm^2 . To do so requires a parallel relationship between the CMOS sensor and the cell chamber. Deviation in this relationship would contribute to the deformation of cells in the images. The centre plane of all components in the microscope assembly should be parallel also to optimize the image created. However, as these components are fixed in position any error incurred to the system due to misalignments in the microscope components will be constant in all images collected and

therefore all images can be compared to each other fairly. In contrast, the cell chambers will not be permanent fixtures as they will be removed and replaced between testing cycles.

Figure 70 shows the design of the holder for the cell chambers. This design allows for precise positioning of the chambers, ease of positioning of the microscope, and simple mounting of the chambers using spring clips.

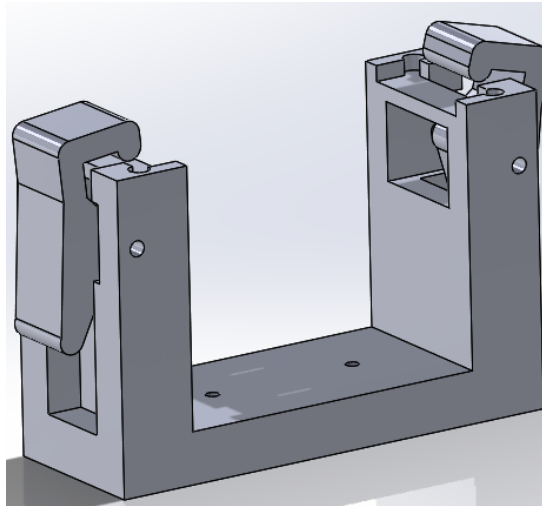


Figure 70: Cell Chamber Precision Holder

Initial testing of the various components for the microscopes light source was done with LEDs to provide a large illuminated area beneath the cell chamber. However, as the project advanced and the cell chambers changed due to project requirements, it was clear that a more suitable approach was to integrate the light source into the microscope. Advantages to this new approach included reducing cost and ensuring the light source remained constant regardless of the area observed. It was also suspected that by reducing the level of ambient and unconditioned light surrounding the system that the image resolution would improve.

It is important to note that the original findings for the optical system of the microscope when using the LED array are still applicable for that of the integrated light source. Instead of an array, a single LED is positioned at the bottom of the optical axis ensuring constant lighting that moves with the microscope as it scans over the cell chamber.

When designing the new lighting arrangement, the geometry of the configuration and overall mass of the system were considered. The support mechanism for the cell chamber shown in Figure 70 meant that the microscope would need to approach from the side of the chamber and then move to various viewpoints over the chamber. Figure 71 shows the chosen design which allows for incorporation of the LED source, the diffuser, the aperture, the microscope lens, the CMOS camera, and the stepper motor. The C-shaped design is compact with low mass allowing for rapid movement without incurring large inertial loads.



Figure 71: Microscope model including a light source

Having finalised the microscope configuration with its bespoke light source, that concludes the work on the design element of this chapter however to validate some of the presumptions and calculations made, testing was undertaken using a resolution target.

4.1.1 Resolution slide testing

After the design was manufactured and assembled in the workshop, the system underwent testing to confirm the required parameters were satisfied by the system. Using a USAF 1951 glass slide resolution target the microscope was focused on line pair segments of the slide with the targeted line pairs positioned in the centre of the image. This is important because the resolution is typically highest at the centre of the image and by creating this standard testing protocol ensures a fair test for each line pair on the slide. The reasoning behind this target being selected over other potential options is that it allows one to calculate resolution and magnification with little adaptation to the system setup. Also by using a glass slide the light refraction will be close to that of the cell chamber.

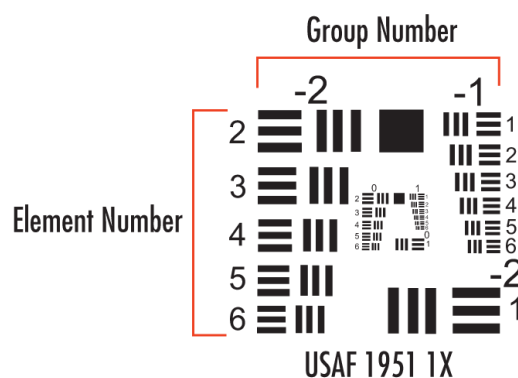


Figure 72: USAF 1951 Target [169]

The USAF 1951 was developed by the US army in 1951, it consists of line pairs which are notated by groups and elements with groups numbered from -2 to 7 and elements from 1-6. Three horizontal bars of equal width and length are located beside the same sized three bars with vertical orientation. As the group and element numbers get larger the target lines get smaller and thus are used to indicate a higher resolution. This type of resolution target became very popular for optical developments as both microscopes and cameras started to use them as a method of specification validation given their simplicity and advantages. The main advantage is due to groups having sets of horizontal and vertical lines so that the resolution can be tested for both simultaneously. This is done by only recognising a group in focus if both sets

of lines are not distorted and the line width appears the same width as the spaces in between the lines.

With regards to reduction of resolution in the corners of the obtained images, it was not expected to be at a level that would affect this system when performing tasks, however, it would be tested to ensure that no unexpected resolution drop-off was experienced due to an unaccounted for abnormality. By comparing the length in pixels of a line to the overall size of the image one could then calculate the magnitude of magnification. This could then be used to compare the originally calculated magnification and verify the difference between the calculated and measured values. Similarly, the field of view can be calculated by using the actual line length and comparing it to the line length on the image by applying a simple ratio.

Before using the slide to measure the field of view and magnification, the resolution was determined by focusing on the slide and making minor adjustments to maximize resolution. It was determined that the lines were not distorted after minor adjustments until group 7,2 and thus group 7,1 was therefore chosen to determine the resolution of the slide Figure 73 captured below illustrates this for the system under its current setup.

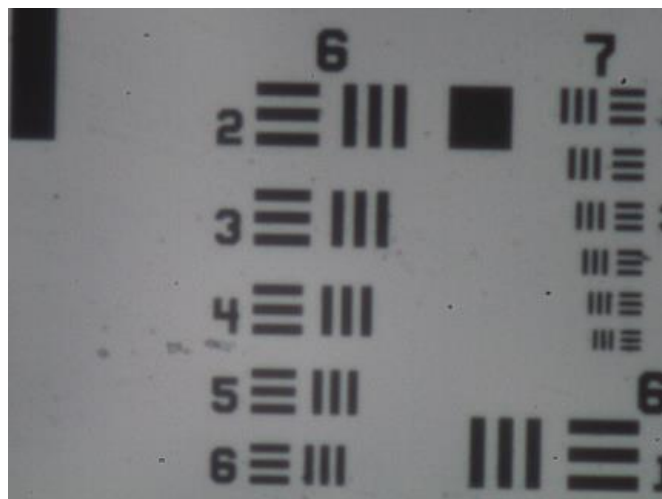


Figure 73: Resolution image of USAF 1951 Slide

The resolution for the setup is determined by the following equation with the resolution given in line pairs per millimeter or lp/mm.

$$Resolution = 2 \left(Group\ Number + \frac{Element\ number - 1}{6} \right)$$

Equation 6

If desired this value can be converted to microns instead by applying the simple steps taken in the given equation below.

$$Resolution\ (\mu m) = \frac{1000}{Resolution\ \left(\frac{lp}{mm}\right)}$$

Equation 7

Using the above two equations one can determine that the resolution of this system is 128lp/mm or when converted to microns 7.8125 μ m. Following this and having inspected the larger groups and their elements under the microscope the following image was used to determine the full field of view of the camera system. The reason behind calculating FOV and magnification on the basis of a larger line pair is to minimise and potential error in the calculation and obtain the best approximation possible.



Figure 74: Image used to determine FOV

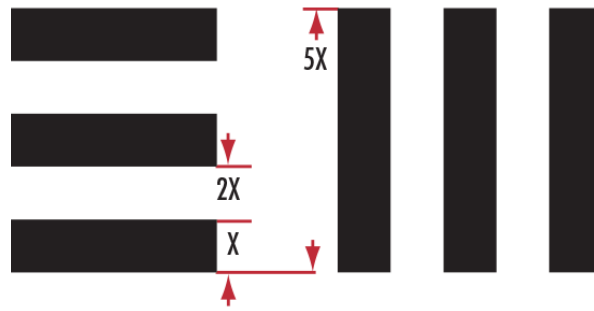


Figure 75: Dimensions Relationship of Line Pairs on USAF 1951 Slide [170]

Therefore, the width of the line for the group 4 element 2 marked X Figure 74 in Figure 75 taken to be $27.8\mu\text{m}$ meaning the length of the line as illustrated by Figure 74 would be $139.2\mu\text{m}$, which when measured took up 487 out of 1280 possible pixels. The measuring element of the image was marked in Figure 74 with a red line. From this one can calculate that one pixel is the equivalent to $0.3\mu\text{m}$, thus the field of view of the sensor 1280×960 had a field of view of approximately $365\mu\text{m}$ by $275\mu\text{m}$ which given that the cells under investigation are approximately $10\text{-}20\mu\text{m}$ in diameter both the FOV and resolution are satisfactory for the project to move forward.

The length of the line marked in Figure 74 occupies 487 pixels, each of which is $3.75\mu\text{m}$ long. The image length is thus $1826\mu\text{m}$ which when compared to the actual line length of $139.2\mu\text{m}$ gives a magnification of 13.1. While this longer than the original calculation, the difference does not have an impact on the task and therefore is not of major concern. The most likely cause for the difference is that the ratio from object distance to the image distance in the manufactured and fully assembled microscope is slightly different from that of the proposed lengths.

4.1.2 Cost Analysis of Microscope

Given the results of the testing documented in this chapter, the microscope system designed has now been verified and will fulfil the operational requirements for the project. Throughout this project having a cost-effective approach, as well as maximising operational

performance was also an important factor. Thus, to document the advantages of developing the system in-house compared to purchasing a finished commercial option and attempting to alter it to satisfy the project requirements the following section is included. It comprises of the identification as a possible commercial alternative as well as describing the extra work that would be required to make it suitable for the overall project. To highlight the main requirements once more for the microscope for it to be capable to perform the tasks required. The microscope required to have a magnification of approximately 10X, move as the end effector of an XYZ robotic system, manoeuvre about the cell chambers and focus on the cells inside the system. The following table, Table 3 documents the parts involved in constructing the microscope, the costs of parts are also listed to construct one complete unit. The reasoning for the inclusion for each given part is then summarised in the table.

Table 3: Cost Breakdown of Microscope

Supplier	Part name	Summary	Cost per unit (€)	notes
Basler	Camera	CMOS sensor	159	
Basler	Camera housing	Required housing & high-speed cable	40	
DCU	Base bracket	Designed and manufactured in DCU	10	Machined out of aluminium
Edmund optics	Objective lens	Inverted wide-angle lens	95	
DCU	Tube spacer	Custom design for project minimising space occupied	5	lightweight and inexpensive
Makerfire	Cooling fan	5/3.3V DC fan for cooling	4	
DCU	Tubing lining	Thin matte surface to stop internal reflection	1	20+ units worth
DCU	Condenser aperture	Simple thin machined piece with a set diameter	5	Once off cost
Prasied Xtreme Acrylic	Diffuser	High light transmission and diffusivity %	5	20 units worth of diffusers
Radionics	LED strip	White light LED used each strip containing 3 LEDs	17	For 1m strip only 50cm per microscope

DCU	Lighting housing	Designed and produced in house	5	Potential to reduce cost as design finalised
Total Cost			346	
Development	once off only			
Edmund optics	Condenser lenses	3 lenses	82	Used for testing the effects of inclusion
thorlabs	Variable aperture	high precision variable aperture	125	Not essential but great to have for development
Thorlabs	USAF 1951 slide	1-inch diameter testing slide	125	Used for verification of microscope
Total including development			678	

From Table 3, excluding the one-off expenses incurred for equipment needed for testing, the microscope's once-off cost was €346. This figure could be reduced further should it be desired to produce multiple units. Comparing then this compact design with potential commercial options which range in values from €1000 to €10,000 in cost. For example, Otpo a German manufacture priced a microscope system at €4022 while the Echo Rebel equivalent would cost approximately €4600 and finally, Zeiss quoted €6000 for a suitable product from their range. Even at these prices, the Microscopes would have to be adapted to suit the system

and potentially add complexity to the Z-axis of the robot which would most likely entail just as much work as building a custom microscope as done in this project. Having clearly shown the cost benefits of developing the system over commercial options it should be noted that the image quality and different magnification options offered by commercial options are often superior to the self-assembled microscope however they were deemed unnecessary features for the deliverable of this project.

To include one of the commercial microscopes would require a redesign of the system to accommodate their appreciably larger size. To give a simple comparison, the developed system discussed in this thesis would fit in a box less than 312cm^3 compared to $20,000\text{cm}^3$ to fit the Otpo alternative and $12,600\text{cm}^3$ for the Lecia Paula. In summary, the development of the compact lightweight microscope has proven to be a worthwhile undertaking with a significant reduction in size, mass, and cost when compared to the commercial alternatives available.

System operational requirements could at this point be finalised as all components have been selected, a single 12vdc power supply was required for the 3 motors that made up the cartesian robot and their respective controller boards. Also, the LEDs would be supplied from this source. The maximum output of which is 2A which satisfied the needs of this project. There was also the need for a USB port extender for the various communications back to the main PC. This would supply the power required to the microscope's sensor.

5. Autofocusing of the microscope

This section looks at how the autofocus technique was selected and designed for the microscope. Autofocusing is required in this project as once the test begins, the microscope is required to focus on several cell chambers and at multiple locations within these chambers. This occurs multiple times over the course of a 48-hour testing period and during this period the system runs autonomously, hence the system must be able to autofocus on cells. A set height for the microscope would not be a viable approach, as even the slightest variance in chamber thickness or changes due to surrounding conditions would cause the cells to appear out of focus on the CMOS sensor. Thus, by including the Z-axis actuator discussed in the robotics chapter and using the output of the microscope, the image, as feedback the hardware for a closed-loop control system for positioning the microscope was developed. At this point, it is worthwhile explaining that when adjusting the Z-axis height of the microscope, the purpose is to adjust the working distance of the microscope and thus the focus.

The cells used for testing in this project were mainly Mouse BalbC 3T3 fibroblasts as these would be the first cells used to test cytotoxicity in trials of the device. These cells were prepared on both standard microscope glass slides and then in the cell chambers that would be used for the microfluidic system to ensure that the change in the method of containing the cells did not impact the performance of the microscope. The cells chambers consisted of an inlet and outlet port with a channel running between to allow for cells to seed to the lower surface of the chamber allowing the microscope to determine cell health. The microscope would also, during the time in which the cells were initially incubated, regularly check, for a conformal layer of cells a large percentage of the total chamber area.

Having the physical system in place to adjust the microscope system in increments as small as $0.2\mu\text{m}$, multiple focusing techniques were considered to focus the system. When it

came to this project both statistical based and gradient-based focus measure functions (FMF) were researched, for more detail see the literature review. Following this review, the search narrowed, and the following options were investigated. The squared gradient FMF is a concept that has been explored and is commonly used for focusing images and could potentially be used in the current setup. Similarly using grey level variants as a function to focus an image is another example where researchers have had success in locating the highest point of focus in an image. Another FMF considered for inclusion in this project was the standard deviation of an image to determine its sharpness and thus, using this information to locate the focus point of that image. Different factors that must be considered while developing a method to focus the microscope in terms of this project are primarily the run time of the method for autofocusing to occur. The system designed as part of this project requires that multiple cell chambers undergo focusing at 5 locations in each chamber per testing round. It is possible that these testing rounds are as often as every 10 minutes, thus developing an autofocusing system that can meet these requirements is required. After considering the speed of operation and accuracy, the standard deviation technique was selected over the other techniques.

5.1 Development of LabVIEW program

As LabVIEW was chosen to be used as the main software package for the integration of the overall PanBioRa project it was decided to design the autofocusing method using this platform. Initially, the method contained inputs of step size and the number of iterations to run. From this, the VI or virtual instrument, which is essentially the name given to a subroutine in LabVIEW, goes through several steps to obtain the best focused image. A Virtual Instrument (VI) has a front panel and a block diagram, the front panel provides the graphical user interface (GUI) and the block diagram contains the code for the VI. Once initialised, the Z actuator is driven to a fixed location, from this point the Z actuator moves one step and captures an image. The standard deviation of this image is calculated and stored in an array and presented on the

GUI. This process is repeated for the number of iterations specified, and once completed the point at which the highest standard deviation is selected and the Z actuator returns the microscope to this position and retakes the image.

Following initial testing with this setup, adjustments were made to the VI to improve performance and increase reliability. The first change made was to add a pre-sampling phase to the initialization of the camera, this effectively disregarded the first images obtained by the camera when switched on. The reasoning for this was that as the camera would not have adjusted its exposure time before the first images were collected, outliers could be added to the standard deviation curve and thereby causing issues with the autofocusing. To reduce computational time and also the complexity of the system, the image obtained was first converted to grayscale before the standard deviation of this image was obtained. For each pixel a single value now indicating its luminance would be recorded as opposed to 3 values relating to levels of red green and blue for the RGB image originally obtained. The original image is still displayed to the user on the GUI. With these changes in place, the autofocusing VI was run on the USAF 1951 test slide, to test the autofocusing method. To compare the images obtained by the autofocusing VI, images with the microscope at various heights were collected manually. These images are shown below in Figure 76 and indicate what can be expected as the microscope takes images of the test slide through the range of heights for the microscope. From left to right examples of what image is collected by the CMOS as the microscope moves downward to focus is shown.



Figure 76: Range of Images focus using USAF 1951

The autofocus algorithm was assessed by comparing the result of the algorithm to a manually focused image when viewing the slide. The results are shown in Figure 77 and Figure 78 where it is apparent that the autofocus technique is comparable to the manual image. To obtain this result however the smallest step size was used, therefore the largest number of iterations were required to cover the desired range of positions for the microscope, thus increasing the total runtime of the VI. In an attempt to reduce runtime without compromising runtime, a two-step approach was designed. This approach was inspired by the focus arrangement of a simple standalone bench microscope, these simple microscopes have two focus knobs one for coarse focusing and a second for fine adjustments. By applying this concept to the autofocusing, the time taken to cover the desired range of heights for the microscope is reduced but the performance which is obtained by the smaller increments of movement is maintained.

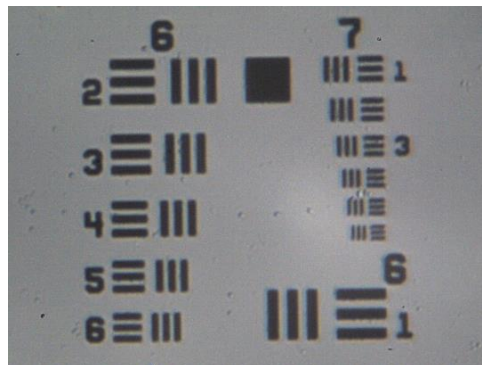


Figure 77: Manually obtained in focus image

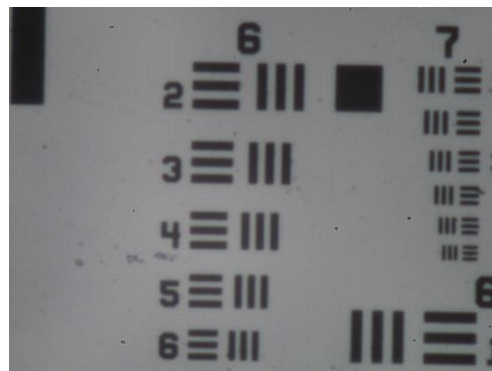


Figure 78: Image obtained from autofocusing VI

5.2 Dual focus technique

To instigate the dual approach, the original auto-focusing VI is essentially running twice, the first time being a coarse focus which locates a rough position for focus after which the system moves back to a set distance above the rough focus point followed by the fine focus stage to obtain the fine focus image. Initially, the addition of coarse focus could introduce abnormalities to disrupt the shape of the standard deviation graph. For example, if the focusing procedure starts too far away from the cells it could instead focus on the dust or debris that may settle on top of the cell chamber, this has the potential to be the highest point on the standard deviation curve and thus the technique may then fail. Similarly, the coarse focus could go too far past the cells and focus again on some other material or object which is not of interest. To prevent such occurrences, a trial and error technique was employed to establish a suitable range of operation within which the microscope stage operates to ensure the capture of appropriate cell images.

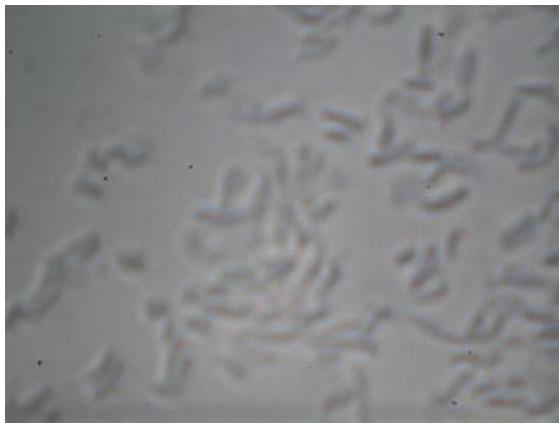


Figure 79: Coarse focus of cells

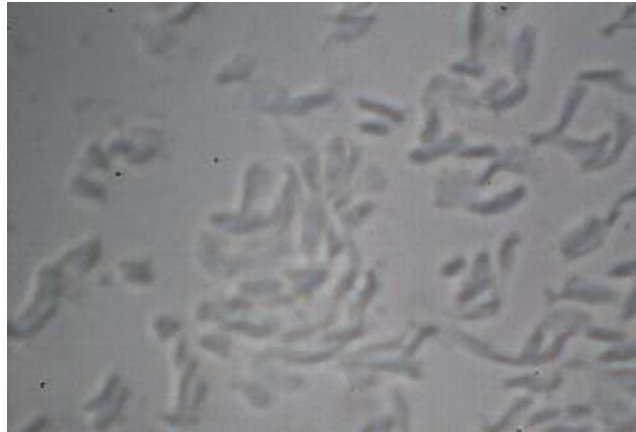


Figure 80: Fine focus of cells

In Figure 79 and Figure 80 the level of focus between fine and coarse can clearly be distinguished indicating that using just a coarse adjustment alone would not be a viable option to obtain optimal focus. The dual focus approach was tested on cells supplied on slides from project partners and further adjustments were made to increase the repeatability of the autofocusing algorithm. As the camera captures the image immediately after the motor movement ceases, it was noticed sporadically that the fine focus image obtained was blurred. This blurring, even though the microscope was at the desired height to obtain optimum focus was investigated and the cause of the issue was identified to be slight vibrations in the XYZ robotics, which occurred momentarily when the actuators stopped. With this discovery, a minor time delay was entered into the VI to allow for this vibrating of the system to cease before the image grab occurs. Figure 81 shows how the usually in focus image blurs and why this addition is necessary. Although this was also present when testing with the USAF 1951 slide it was not as noticeable and hence addressed when focusing began with cells.

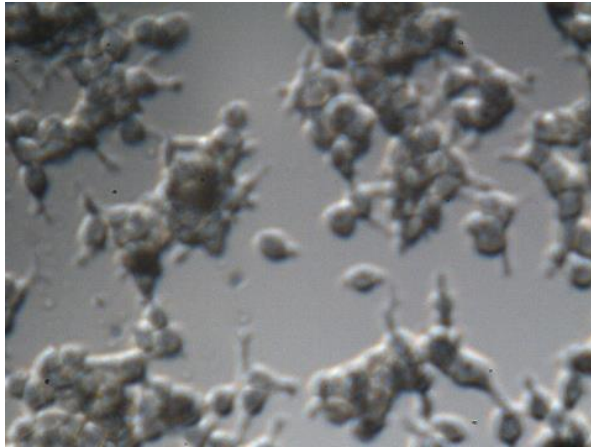


Figure 81: A blurred image of cells due to vibrations

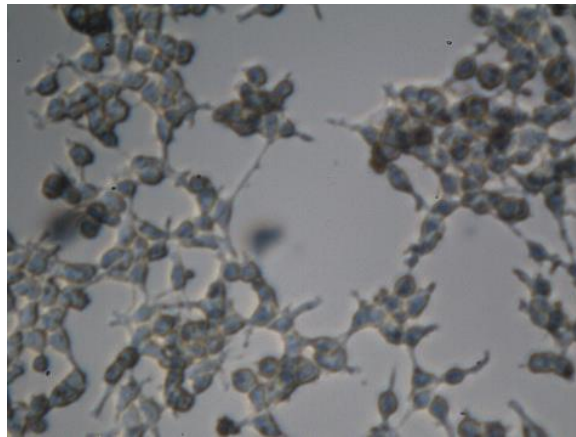


Figure 82: Image obtained without vibrations present

The autofocus was tested on the cell chambers which will be used in live tests. The chambers used were pre-seeded with cells similar to those which will be used in future tests. This is the most important test for the autofocus, as it is the closest to a live test scenario, with the medium used to transport the cells also filling the cell chamber. Figure 83 shows an example of the image captured from the autofocus which can be compared that to the manually focused image in Figure 84.

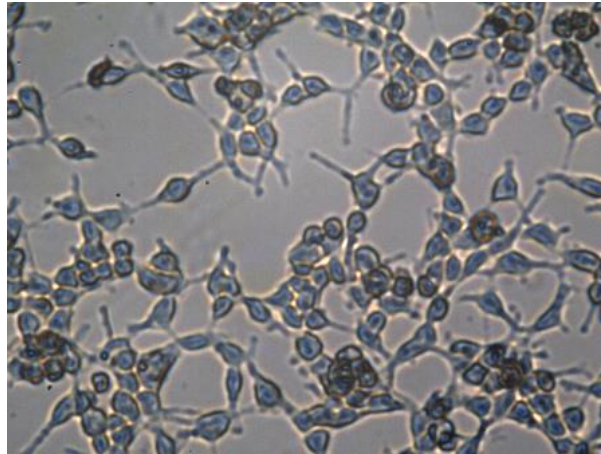


Figure 83: Manually focused

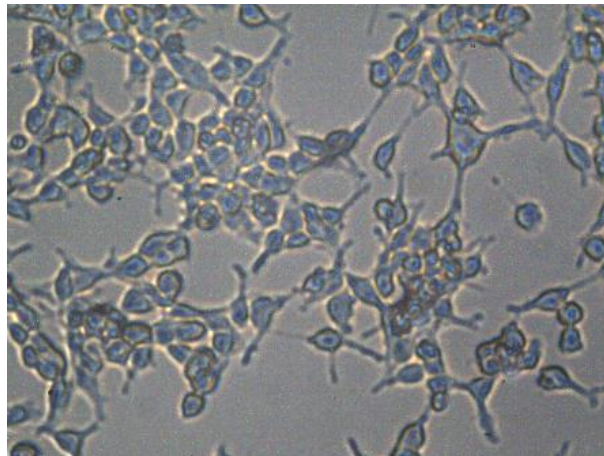


Figure 84: Autofocused image

However, with continued testing of the autofocus algorithm, an anomaly arose when looking at cell images. It became apparent that it was possible to obtain two different views of the same image both of which appeared to be in focus. Associated with this phenomenon, a double peak in the standard deviation curve was present when focusing on the cells.

When inspecting the plot generated for the USAF 1951 slide, shown in Figure 85, a single maximum of the standard deviation is obtained. However, in Figure 86 and finally Figure 87 the graphs for the seeded cell chamber and the cell chamber respectively show a new feature not seen in the USAF test slide. Instead of showing a single maximum, the cell slide and cell chamber

have double maxima. The plots show the standard deviation values as the microscope lowers towards the cell with the horizontal axis referring to the microscope vertical position.

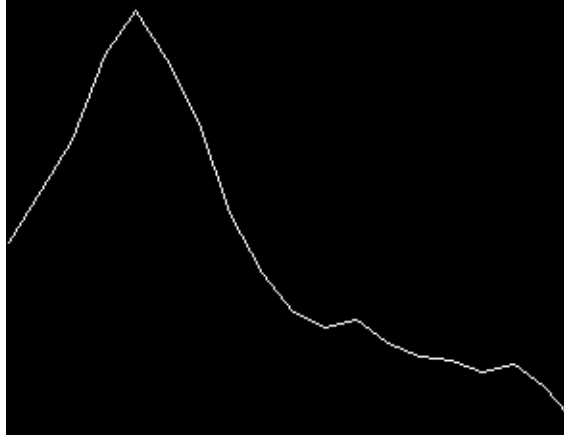


Figure 85: USAF 1951 SD curve for autofocus

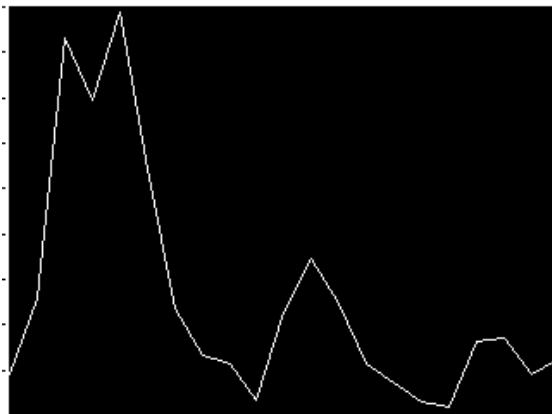


Figure 86: Test cell slide SD curve for autofocus

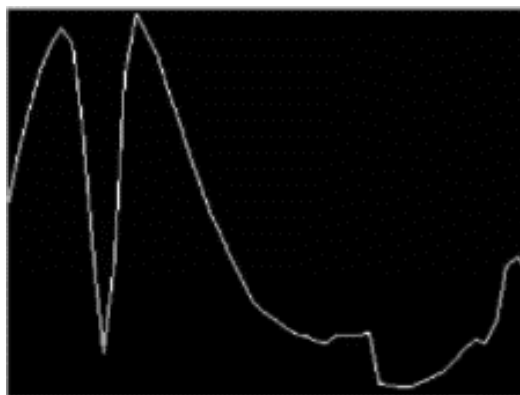


Figure 87: Cell chamber SD curve for autofocus

5.3 Investigation of Double peak in SD curve

To suitably adapt the autofocusing to deal with this phenomenon, it is important to firstly identify the cause of the double peak occurring with the standard deviation curve. By properly identifying the cause of the issue it can be determined if the issue is removable or if it is something that is a consequence of the setup that is not possible or cost effective to remove. If it is the case that the issue remains in the system, then focus turns to how to adapt the system to deal with the abnormality and continue to perform adequately in its presence.

Corresponding to the two maxima on the standard deviation plot, two in-focus images were obtained. The first in-focus image that appeared as the microscope moved towards the cells is shown in Figure 88. Here it is apparent that the cells appear brighter than the background. It should be remembered that the cells are backlight in all images. The second image corresponding to the second maximum is shown in Figure 89 where the cells appear darker than the background. Figure 90 shows the standard deviation curve associated with the two images.

To establish whether this phenomenon is unique to the prototype system as developed here, the same cell slides were viewed on a standard laboratory microscope. Manual focusing was applied and it was noted that cell images similar to those in Figure 88 and Figure 89 could also be seen. The phenomenon is therefore not unique to the prototype system but despite this little is available in the literature documenting this effect.

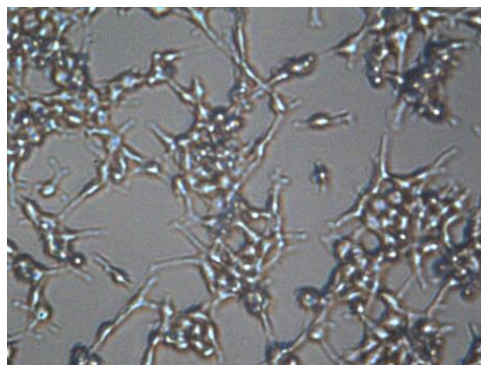


Figure 88: Bright cell image

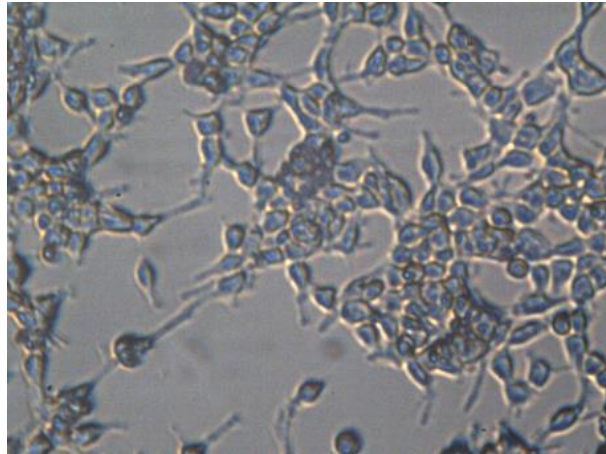


Figure 89:Dark cell image

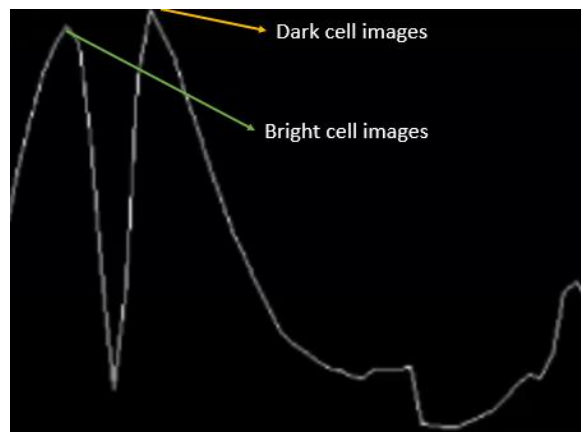


Figure 90:Standard deviation curve for cell chamber

The question remained as to why was there a double peak present in the standard deviation curve, and how was it possible to obtain two similar in focus images at different heights. Given the type of illumination being employed in this project was a version of bright field illumination, the image of interest is the highest focus of dark cells available to us. This relates to the second of the SD peaks when the microscope performs the focusing algorithm. It was also confirmed by other project partners that the desired image to be obtained was the image where the cells appeared dark on a bright background, this is because the brighter cells would not be suitable for the different image processing algorithms required to determine cell health and to determine whether a conformal layer of cells is present in the chamber.

One concept was that the production of the second focused image of bright cells was due to some sort of internal reflection of the cell chamber due to the different materials. However, when comparing the two different methods of housing the cells, one was a standard microscope glass slide with a coverslip and some agent to fix the cells, the second had the glass slide, polymer material, and the medium used to transport live cells. Two very different arrangements would suggest that if the internal reflection was the issue due to the housing, the position of the maxima on the standard deviation curve would be different for each. However, it was noted that the distance between the two maxima for the peaks did not vary to any great degree thus discounting the internal reflection explanation.

An ideal imaging system is modelled as a camera that uses a pinhole to focus rays onto the backplane. In reality, one cannot use a pinhole because the amount of light transmitted is too small to create a bright image. Instead, a lens of a finite size is employed to focus the image which will refract light rays to different extents depending on how they pass through the lens. This can lead to spurious effects which can be mitigated by reducing the range of angles of incidence of the light source to the lens. For this work, this amounts to changing the light source from an array of LEDs to a single LED.

Using a single LED placed on the axis of the optical system, the standard deviation plot showed only one peak, see Figure 91. Corresponding to this peak, the image obtained in Figure 92 was that of dark cells on a bright background. The net result is that the first peak seen previously no longer appears. From this, it is thought that when using the larger light source, the cells themselves were acting as a lens refracting incident light rays from multiple angles to create bright spots.

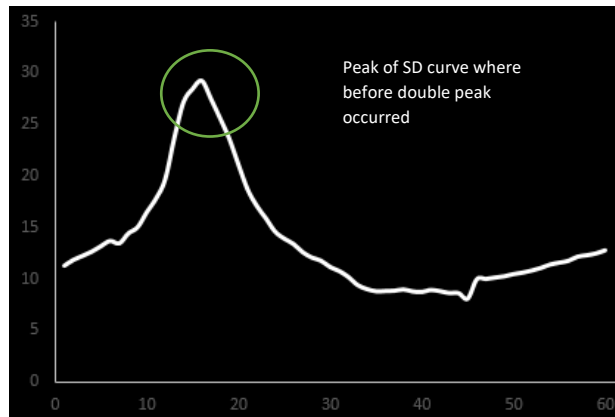


Figure 91:SD curve of finalised autofocus output

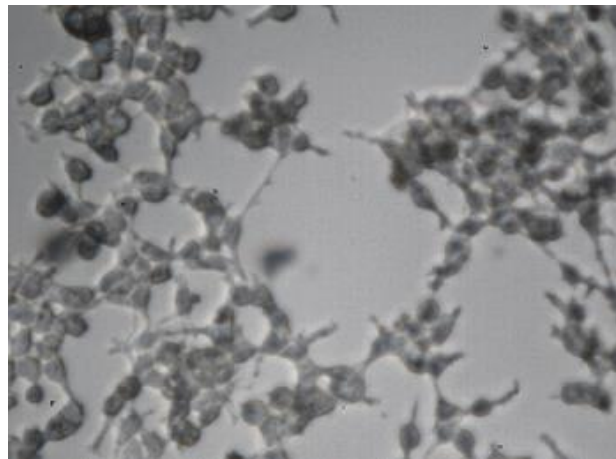


Figure 92: Example of the output image of autofocus algorithm following adjustments

The new images produced were accepted by the project partners as suitable for any image processing they wished to carry out to identify conformal layers and cell health. With the autofocusing algorithm now running robustly and consistently capturing in-focus images of dark cells, this concludes the work undertaken concerning this particular challenge as part of the project.

6. Conclusions

On designing building and testing a multi-axis robotic device that was capable of accurately positioning its end effector. The success of these objectives was investigated. Having designed a system that was suitable to the brief supplied by the project consortium, the system was tested to ensure it could produce the accuracy of $100\mu\text{m}$ in both the X and Y axis. Similarly, in order to test that the desired performance was obtained from the Z axis images that were captured manually were compared to those captured via the autofocus algorithm and deemed successful. Given this axis was solely used for focusing the microscope it was more practical to verify the performance using the microscopes output. The Z-axis also had a minimum movement resolution of $0.2\mu\text{m}$ almost two orders of magnitude greater than the accuracy described in the project brief.

Following this the microscope was designed and assembled to allow for the required movement around the cell chambers. Integrating a lighting system was key to allowing for a constant light source in all the various points at which the microscope focused and took images of the cells. Having calculated the desired tube lengths to give the required magnification the system was tested for several performance indicators. The magnification was determined by using a test slide to calculate the actual magnification and field of view as well as calculate the resolution of the system.

For the microscope, to autofocus, a program was designed to use the standard deviation of the image collected following its conversion to grayscale this system worked effectively to robustly select the correct height to allow for the image of the highest focus to be captured. The above was achieved while retaining a key focus on applying the most cost-effective approach suitable and also while assisting the overall project with various integration tasks. Thus, all objectives set for this project had been satisfied and the work was deemed as successful.

7. Future Work

Following the completion of this project in terms of the work undertaken as part of the research project, there continue to be areas where both improvements can be made with the current functional prototype and also the PANBioRa project as a viable commercialised product. When focusing on the current system the current system could be altered to give each cell imaging position a set location and the robotic system is commanded to go to that location rather than its current set up of obtaining specific movement commands to move set distances to go from one location to the next.

This would add another element of control and potentially help minimise errors building up in the system. With regards to potential work with the microscope given its function in this project and how it satisfies the needs of the project to collect suitable images of high contrast while being lightweight small and inexpensive to build, there was no further work at this time seen as a priority in terms of future work. Finally, from an overall project perspective having designed a functional prototype and integrated the various project partners components. The next stage was to work closely with the team at Dolmen a project partner designing the overall enclosure for the modular style benchtop device, and begin minimizing the system and undertaking any redesign required to transfer the many components inside the enclosure. This would allow for the work completed to date to be forwarded to a commercialization stage.

8. References

- [1] N. G. Hockstein, C G Gourin, R. A. Faust, and D J Terris, "A history of robots: from science fiction to surgical robotics," vol. 1, pp. 113–118, 2007, doi: 10.1007/s11701-007-0021-2.
- [2] H. Melkote, F. Khorrami, and J. Ish-Shalom, "Closed-loop control of a three degree-of-freedom ultra accurate linear stepper motor," in *Proceedings of the 1997 IEEE International Conference on Control Applications*, 1997, pp. 639–644, doi: 10.1109/CCA.1997.627731.
- [3] A. Hace, K. Jezernik, B. Curk, and M. Terbuc, "Robust motion control of XY table for laser cutting machine," in *IECON '98. Proceedings of the 24th Annual Conference of the IEEE Industrial Electronics Society (Cat. No.98CH36200)*, 1998, vol. 2, pp. 1097–1102 vol.2, doi: 10.1109/IECON.1998.724249.
- [4] J. Quan, C. Shen, C. Li, and X. Zhu, "Research on positioning control strategy for linear belt-driven," in *2011 2nd International Conference on Artificial Intelligence, Management Science and Electronic Commerce, AIMSEC 2011 - Proceedings*, 2011, pp. 4256–4259, doi: 10.1109/AIMSEC.2011.6010105.
- [5] M. Jokinen, S. Saarakkala, M. Niemela, R. Pollanen, and J. Pyrhonen, "Physical drawbacks of linear high-speed tooth belt drives," in *2008 International Symposium on Power Electronics, Electrical Drives, Automation and Motion (SPEEDAM)*, Apr. 2008, pp. 872–877, doi: 10.1109/SPEEDHAM.2008.4581140.
- [6] R. Ramesh, M.A. Mannan, A.N. Poo, "Tracking and contour error control in CNC servo systems." *International Journal of Machine Tools and Manufacture*, Volume 45, Issue 3, p. Pages 301-326, Apr. 07, 2020.
- [7] H. Lim, J.-W. Seo, and C.-H. Choi, "Position control of XY table in CNC machining center with non-rigid ballscrew," in *Proceedings of the 2000 American Control Conference. ACC (IEEE Cat. No.00CH36334)*, 2000, vol. 3, pp. 1542–1546 vol.3, doi: 10.1109/ACC.2000.879458.
- [8] E.-C. Park, H. Lim, and C.-H. Choi, "Position control of X-Y table at velocity reversal using presliding friction characteristics," *IEEE Trans. Control Syst. Technol.*, vol. 11, no. 1, pp. 24–31, 2003, doi: 10.1109/TCST.2002.806436.
- [9] M. Serge, T. Patrick, and F. Duquenoy, "Motion Systems: An Overview of Linear, Air Bearing, and Piezo Stages," in *Three-Dimensional Microfabrication Using Two-photon Polymerization*, Elsevier, 2016, pp. 148–167.
- [10] J. F. Cuttino, T. A. Dow, and B. F. Knight, "Analytical and Experimental Identification of Nonlinearities in a Single-Nut, Preloaded Ball Screw," *J. Mech. Des.*, vol. 119, no. 1, pp. 15–19, Apr. 1997, doi: 10.1115/1.2828782.
- [11] "Stage Components Considerations." <https://www.newport.com/n/stage-components-considerations> (accessed Jun. 23, 2021).
- [12] O. Vahid-Araghi and F. Golnaraghi, *Friction-induced vibration in lead screw drives*. 2011.
- [13] Lim HSeo JChoi C, "Torsional displacement compensation in position control for machining centers." Apr. 07, 2020, doi: [https://dx.doi.org/10.1016/S0967-0661\(00\)00076-9](https://dx.doi.org/10.1016/S0967-0661(00)00076-9).

- [14] T. Takemura and H. Fujimoto, "Simultaneous identification of linear parameters and nonlinear rolling friction for ball screw driven stage," in *IECON 2011 - 37th Annual Conference of the IEEE Industrial Electronics Society*, 2011, pp. 3424–3429, doi: 10.1109/IECON.2011.6119862.
- [15] A. Kamalzadeh, "Precision control of high speed ball screw drives," 2009.
- [16] D. Y. Zheng, X. Y. Guan, X. Chen, and Z. L. Zhang, "Study of Flat Belt Drive Mechanics," *Key Eng. Mater.*, vol. 419–420, pp. 265–268, Apr. 2009, doi: 10.4028/www.scientific.net/KEM.419-420.265.
- [17] E.-W. Chen, H.-H. Lin, and N. Ferguson, "Experimental investigation of the transverse nonlinear vibration of an axially travelling belt." *Journal of Vibroengineering*, Apr. 09, 2016, doi: <http://dx.doi.org/10.21595/jve.2016.17341>.
- [18] M. Jokinen, S. Saarakkala, M. Niemela, R. Pollanen, and J. Pyrhonen, "Physical drawbacks of linear high-speed tooth belt drives," in *Automation and Motion 2008 International Symposium on Power Electronics, Electrical Drives*, 2008, pp. 872–877, doi: 10.1109/SPEEDHAM.2008.4581140.
- [19] K. S. Sollmann, M. K. Jouaneh, and D. Lavender, "Dynamic Modeling of a Two-Axis, Parallel, H-Frame-Type XY Positioning System," *IEEE/ASME Trans. Mechatronics*, vol. 15, no. 2, pp. 280–290, 2010, doi: 10.1109/TMECH.2009.2020823.
- [20] A. S. Kulkarni and M. A. El-Sharkawi, "Intelligent precision position control of elastic drive systems," *IEEE Trans. Energy Convers.*, vol. 16, no. 1, pp. 26–31, 2001, doi: 10.1109/60.911399.
- [21] W. Li and X. Cheng, "Adaptive high-precision control of positioning tables-theory and experiments," *IEEE Trans. Control Syst. Technol.*, vol. 2, no. 3, pp. 265–270, 1994, doi: 10.1109/87.317983.
- [22] J. Quan, C. Shen, C. Li, and X. Zhu, "Research on positioning control strategy for linear belt-driven," in *2011 2nd International Conference on Artificial Intelligence, Management Science and Electronic Commerce (AIMSEC)*, 2011, pp. 4256–4259, doi: 10.1109/AIMSEC.2011.6010105.
- [23] A. Hace, K. Jezernik, and A. Sabanovic, "Improved design of VSS controller for a linear belt-driven servomechanism," *IEEE/ASME Trans. Mechatronics*, vol. 10, no. 4, pp. 385–390, 2005, doi: 10.1109/TMECH.2005.852448.
- [24] W. Li and M. Rehani, "Modeling and control of a belt-drive positioning table," in *22nd International Conference on Industrial Electronics, Control, and Instrumentation Proceedings of the 1996 IEEE IECON*, 1996, vol. 3, pp. 1984–1989 vol.3, doi: 10.1109/IECON.1996.570782.
- [25] B. Drinčić, "Mechanical Models of Friction That Exhibit Hysteresis, Stick-Slip, and the Stribeck Effect," p. 183.
- [26] J. de Marchi, "MODELING OF DYNAMIC FRICTION, IMPACT BACKLASH AND ELASTIC COMPLIANCE NONLINEARITIES IN MACHINE TOOLS, WITH APPLICATIONS TO ASYMMETRIC VISCOUS AND KINETIC FRICTION IDENTIFICATION," *ResearchGate*, Apr. 2020.
- [27] "Chapter 8. Models of Friction." Apr. 22, 2020, [Online]. Available: http://www.mogi.bme.hu/TAMOP/robot_applications/ch07.html#ch-8.4.1.1.

- [28] Z. Jamaludin, H. Van Brussel, G. Pipeleers, J. Swevers, "Accurate motion control of xy high-speed linear drives using friction model feedforward and cutting forces estimation," Apr. 2020, doi: <https://doi.org/10.1016/j.cirp.2008.03.037>.
- [29] Y. F. Liu, J. Li, Z. M. Zhang, X. H. Hu, and W. J. Zhang, "Experimental comparison of five friction models on the same test-bed of the micro stick-slip motion system," *Mech. Sci.*, vol. 6, pp. 15–28, 2015, doi: 10.5194/ms-6-15-2015.
- [30] H. S. Lee and M. Tomizuka, "Robust motion controller design for high-accuracy positioning systems," *IEEE Trans. Ind. Electron.*, vol. 43, no. 1, pp. 48–55, 1996, doi: 10.1109/41.481407.
- [31] P. Hamon, M. Gautier, and P. Garrec, "Dynamic Identification of Robots with a Dry Friction Model Depending on Load and Velocity," Apr. 2010, pp. 6187–6193, doi: 10.1109/IROS.2010.5649189.
- [32] Elhami M Brookfield D, "Sequential identification of coulomb and viscous friction in robot drives," Apr. 1997, doi: [https://dx.doi.org/10.1016/S0005-1098\(96\)00183-5](https://dx.doi.org/10.1016/S0005-1098(96)00183-5).
- [33] B. Armstrong-Helouvry, "Stick-slip arising from Stribeck friction," in *IEEE International Conference on Robotics and Automation Proceedings*, 1990, pp. 1377–1382 vol.2, doi: 10.1109/ROBOT.1990.126194.
- [34] L. Xu and B. Yao, "Adaptive robust precision motion control of linear motors with negligible electrical dynamics: theory and experiments," *IEEE/ASME Trans. Mechatronics*, vol. 6, no. 4, pp. 444–452, 2001, doi: 10.1109/3516.974858.
- [35] C. Canudas, K. J. Åström, and K. Braun, "Adaptive Friction Compensation in DC-Motor Drives," *IEEE J. Robot. Autom.*, vol. 3, no. 6, pp. 681–685, 1987, doi: 10.1109/JRA.1987.1087142.
- [36] J. A. de Marchi, "Modeling of dynamic friction, impact backlash and elastic compliance nonlinearities in machine tools, with applications to asymmetric viscous and kinetic friction identification," 1998.
- [37] I. Dułęba and J. Sasiadek, *Robot Control 2003 (SYROCO '03): A Proceedings Volume from the 7th IFAC Symposium, Wrocław, Poland, 1-3 September 2003*. Elsevier, 2004.
- [38] P.-C. T. Wu, Ruh-Hua, "Studies of Stick-Slip Friction, Presliding Displacement, and Hunting," *Journal-of-Dynamic-Systems-Measurement-and-Control*, Apr. 2002.
- [39] V. van Geffen, I. D. Rijlaarsdam ir PWJM Nuij Supervisor, and dr M. ir Steinbuch, "A study of friction models and friction compensation Traineeship report Coach(es)," 2009.
- [40] B. Bona and M. Indri, "Friction Compensation in Robotics: an Overview," *Decis. Control. 2005 2005 Eur. Control Conf.*, Apr. 2005, [Online]. Available: https://www.researchgate.net/publication/224627455_Friction_Compensation_in_Robotics_an_Overview.
- [41] C.-J. Lin, H.-T. Yau, and Y.-C. Tian, "Identification and Compensation of Nonlinear Friction Characteristics and Precision Control for a Linear Motor Stage," *IEEE/ASME Trans. Mechatronics*, vol. 18, no. 4, pp. 1385–1396, 2013, doi: 10.1109/TMECH.2012.2202679.
- [42] N. Wang, J. Yu, and W. Lin, "Positioning control for a linear actuator with nonlinear friction and input saturation using output-feedback control," *Complexity*, vol. 21, no.

- S2, pp. 191–200, Apr. 2016, doi: 10.1002/cplx.21797.
- [43] D. Chou, “Dahl Friction Modeling ARCHIVES,” 2004.
- [44] M. Nordin and P. O. Gutman, “Controlling mechanical systems with backlash - A survey,” *Automatica*, vol. 38, no. 10, pp. 1633–1649, Oct. 2002, doi: 10.1016/S0005-1098(02)00047-X.
- [45] D. Gouaillier, C. Collette, and C. Kilner, “Omni-directional closed-loop walk for NAO,” in *2010 10th IEEE-RAS International Conference on Humanoid Robots, Humanoids 2010*, 2010, pp. 448–454, doi: 10.1109/ICHR.2010.5686291.
- [46] M. Kagotani and H. Ueda, “Factors affecting transmission error in helical synchronous belt with error on belt side face under bidirectional operation,” *J. Mech. Des. Trans. ASME*, vol. 132, no. 7, pp. 0710051–0710059, Jul. 2010, doi: 10.1115/1.4001667.
- [47] J. Nylén, “Belt drive optimisation-an automotive problem,” Feb. 1988, doi: 10.4271/880414.
- [48] S. K. Kim and J. M. Lee, “Analysis of the non-linear vibration characteristics of a belt-driven system,” *J. Sound Vib.*, vol. 223, no. 5, pp. 723–740, Jun. 1999, doi: 10.1006/jsvi.1998.2159.
- [49] S. Abrate, “Vibrations of belts and belt drives,” *Mech. Mach. Theory*, vol. 27, no. 6, pp. 645–659, Nov. 1992, doi: 10.1016/0094-114X(92)90064-O.
- [50] M. Kagotani and H. Ueda, “Factors affecting transmission error in helical synchronous belt with error on belt side face under bidirectional operation,” in *Proceedings of the ASME Design Engineering Technical Conference*, 2009, vol. 6, pp. 177–186, doi: 10.1115/DETC2009-86132.
- [51] T. Koyama and K. M. Marshek, “Toothed belt drives-Past, present and future,” *Mech. Mach. Theory*, vol. 23, no. 3, pp. 227–241, 1988, doi: 10.1016/0094-114X(88)90108-5.
- [52] A. Thattil, S. Vachhani, D. Raval, P. Patel, P. Sharma, and U. G. Students, “Comparative Study of using Different Electric Motors for EV,” *Int. Res. J. Eng. Technol.*, vol. 9001, 2008, Accessed: Feb. 10, 2021. [Online]. Available: www.irjet.net.
- [53] FAULHABER, “Stepper motor basics What is a stepper motor?,” pp. 1–13.
- [54] S. Derammelaere, M. Haemers, J. De Viaene, F. Verbelen, and K. Stockman, “A quantitative comparison between BLDC, PMSM, brushed DC and stepping motor technologies,” 2017.
- [55] K. Hameyer and R. J. M. Belmans, “Permanent magnet excited brushed DC motors,” *IEEE Trans. Ind. Electron.*, vol. 43, no. 2, pp. 247–255, 1996, doi: 10.1109/41.491348.
- [56] Padmaraja Yedamale, “Brushless DC (BLDC) Motor Fundamentals,” 2003.
- [57] G. C. R. Sincero, J. Cros, and P. Viarouge, “Efficient simulation method for comparison of brush and brushless DC motors for light traction application,” 2009, Accessed: Feb. 11, 2021. [Online]. Available: <https://ieeexplore.ieee.org/stamp/stamp.jsp?tp=&number=5279022>.
- [58] A. Thattil, S. Vachhani, D. Raval, P. Patel, P. Sharma, and U. G. Students, “Comparative Study of using Different Electric Motors for EV,” *Int. Res. J. Eng. Technol.*, vol. 9001, 2008, Accessed: Feb. 11, 2021. [Online]. Available: www.irjet.net.

- [59] Riazollah Firoozian, *Servo Motors and Industrial Control Theory* . 2014.
- [60] Bill Lackey, "Servo Motor vs Stepper Motor: Which is right for your application? - Motion Solutions," *Motion Solution*, 2017. <https://www.motionsolutions.com/servo-motor-vs-stepper-motor-right-application/> (accessed Feb. 11, 2021).
- [61] B. Vinod, G. Gurusamy, and C. Sasikumar, "Design and analysis of power failure detector module for control of axis runaway in CNC machines during unprecedented power failures," *Int. J. Mach. Tools Manuf.*, vol. 46, no. 12–13, pp. 1610–1616, Oct. 2006, doi: 10.1016/j.ijmachtools.2005.09.008.
- [62] "Servo Motor vs Stepper Motor: Differences & Advantages | Arrow.com | Arrow.com." <https://www.arrow.com/en/research-and-events/articles/servo-or-stepper-choosing-the-best-motor-for-the-job> (accessed Feb. 11, 2021).
- [63] H. Gill, "Stepper Motor or Servo Motor : Which should it be ?," pp. 1–8, 2016, Accessed: Feb. 11, 2021. [Online]. Available: https://www.kollmorgen.com/uploadedFiles/kollmorgencom/Service_and_Support/Knowledge_Center/White_Papers/Servo_or_Stepper_08_05_16_WhitePaper_FINAL.pdf.
- [64] T. Shree Roy, H. Kabir, and M. A. Mannan Chowdhury, "Simple Discussion on Stepper Motors for the Development of Electronic Device Textile or Fashion Marketing View project Solar selective surfaces View project Simple Discussion on Stepper Motors for the Development of Electronic Device," *Int. J. Sci. Eng. Res.*, vol. 5, no. 1, 2014, Accessed: Feb. 11, 2021. [Online]. Available: <http://www.ijser.org>.
- [65] T. A. Khan, T. A. Taj, and I. Ijaz, "Hybrid stepper motor and its controlling techniques a survey," in *Proceedings of the 2014 IEEE North West Russia Young Researchers in Electrical and Electronic Engineering Conference, ElConRusNW 2014*, 2014, pp. 79–83, doi: 10.1109/ElConRusNW.2014.6839207.
- [66] FAULHABER, "Stepper motor basics What is a stepper motor?"
- [67] "How to Improve Motion Smoothness and Accuracy of Stepper Motors," 2020. Accessed: Feb. 15, 2021. [Online]. Available: www.ti.com.
- [68] L. Warguła, P. Krawiec, J. M. Adamiec, and K. J. Waluś, "The Investigations of Dynamic Characteristics of a Stepper Motor," in *Procedia Engineering*, 2017, vol. 177, pp. 318–323, doi: 10.1016/j.proeng.2017.02.232.
- [69] "What is Back EMF in a DC Motor? - Circuit Globe." <https://circuitglobe.com/what-is-back-emf-in-dc-motor.html> (accessed Feb. 22, 2021).
- [70] K. Bai and K.-M. Lee, "Research on Intelligent Manufacturing Permanent Magnet Spherical Motors Model and Field Based Approaches for Design, Sensing and Control." Accessed: Feb. 22, 2021. [Online]. Available: <http://www.springer.com/series/15516>.
- [71] L. Zaccarian, "DC motors: dynamic model and control techniques," *Semin. handouts*, pp. 1–23, 2005.
- [72] A. C. Lee, S. Wang, and C. J. Fan, "A Current Index Approach to Compensate Commutation Phase Error for Sensorless Brushless DC Motors with Nonideal Back EMF," *IEEE Trans. Power Electron.*, vol. 31, no. 6, pp. 4389–4399, Jun. 2016, doi: 10.1109/TPEL.2015.2468081.
- [73] R. Ni, K. Lu, F. Blaabjerg, and D. Xu, "A comparative study on pulse sinusoidal high frequency voltage injection and INFORM methods for PMSM position sensorless

- control,” in *IECON Proceedings (Industrial Electronics Conference)*, Dec. 2016, pp. 2600–2605, doi: 10.1109/IECON.2016.7793021.
- [74] Jianwen Shao, D. Nolan, and T. Hopkins, “A novel direct back EMF detection for sensorless brushless DC (BLDC) motor drives,” in *APEC. Seventeenth Annual IEEE Applied Power Electronics Conference and Exposition (Cat. No.02CH37335)*, pp. 33–37, doi: 10.1109/APEC.2002.989224.
- [75] profdrir J. van Amerongen drir JF Broenink ir MA Groothuis AP de Vries, “Endstops for the Mechatronic Demonstrator Albert Post Individual Design Assignment,” 2008.
- [76] M. Claudio De Simone, A. Quatrano, M. C. De Simone, Z. B. Rivera Assistant Professor, and D. Guida Full Professor, “Development and Implementation of a Control System for a Retrofitted CNC Machine by Using Arduino,” doi: 10.5937/fmet1704565Q.
- [77] Heney Paul, “Achieving precision with limit switches,” 2018.
- [78] J. Li, “Design, analysis and experiments on micro-switches for optical applications,” 2003.
- [79] “Sealed Ultra Subminiature Basic Switch.”
- [80] N. Hendrich, F. Wasserfall, and J. Zhang, “3D Printed Low-Cost Force-Torque Sensors,” *IEEE Access*, vol. 8, pp. 140569–140585, 2020, doi: 10.1109/ACCESS.2020.3007565.
- [81] B. Vinod, G. Gurusamy, and C. Sasikumar, “Design and analysis of power failure detector module for control of axis runaway in CNC machines during unprecedented power failures,” *Int. J. Mach. Tools Manuf.*, vol. 46, pp. 1610–1616, 2006, doi: 10.1016/j.ijmachtools.2005.09.008.
- [82] “Exploring optical and magnetic sensors - Embedded.com.” <https://www.embedded.com/exploring-optical-and-magnetic-sensors/> (accessed Jun. 24, 2021).
- [83] K. Koyama, M. Shimojo, T. Senoo, and M. Ishikawa, “High-Speed High-Precision Proximity Sensor for Detection of Tilt, Distance, and Contact,” *IEEE Robot. Autom. Lett.*, vol. 3, no. 4, pp. 3224–3231, Oct. 2018, doi: 10.1109/LRA.2018.2850975.
- [84] M. J. McGrath, C. N. Scanaill, M. J. McGrath, and C. N. Scanaill, “Sensing and Sensor Fundamentals,” in *Sensor Technologies*, Apress, 2013, pp. 15–50.
- [85] Ishikawa, K. Koyama, M. Shimojo, T. Senoo, and Masatoshi, “High-Speed High-Precision Proximity Sensor for Detection of Tilt, Distance, and Contact.”
- [86] “Infrared Sensors or IR Sensors,” Accessed: Mar. 10, 2021. [Online]. Available: https://www.engineersgarage.com/article_page/infrared-sensors-or-ir-sensors/.
- [87] P. Ripka, J. Blažek, M. Mirzaei, P. Lipovský, M. Šmelko, and K. Draganová, “Inductive Position and Speed Sensors,” *Sensors*, vol. 20, no. 1, p. 65, Dec. 2019, doi: 10.3390/s20010065.
- [88] S. Fericean and R. Droxler, “New noncontacting inductive analog proximity and inductive linear displacement sensors for industrial automation,” *IEEE Sens. J.*, vol. 7, no. 11, pp. 1538–1545, 2007, doi: 10.1109/JSEN.2007.908232.
- [89] T. Subhasankari, A. Sharvin Infant, A. Viswasundar, M. Venkatesan, and N. Mithran, “Integration of Hall Sensor in a 3D Printer as a Limit Switch,” Nov. 2018, doi: 10.1109/ICCIC.2017.8524539.

- [90] R. T. Sataloff, M. M. Johns, and K. M. Kost, *Magnetism and Magnetic Materials*. .
- [91] X. Song, J. Fang, and B. Han, "High-Precision Rotor Position Detection for High-Speed Surface PMSM Drive Based on Linear Hall-Effect Sensors," *IEEE Trans. Power Electron.*, vol. 31, no. 7, pp. 4720–4731, Jul. 2016, doi: 10.1109/TPEL.2015.2479642.
- [92] A. Morar, "DC motor speed and position control system," in *IFAC Proceedings Volumes (IFAC-PapersOnline)*, 2007, vol. 1, no. PART 1, pp. 203–208, doi: 10.3182/20070709-3-ro-4910.00034.
- [93] D. Zhang, J. Wang, L. Qian, and J. Yi, "Stepper motor open-loop control system modeling and control strategy optimization," *Arch. Electr. Eng.*, vol. 68, no. 1, pp. 63–75, 2019, doi: 10.24425/ae.2019.125980.
- [94] K. M. Le, H. Van Hoang, and J. W. Jeon, "An Advanced Closed-Loop Control to Improve the Performance of Hybrid Stepper Motors," *IEEE Trans. Power Electron.*, vol. 32, no. 9, pp. 7244–7255, Sep. 2017, doi: 10.1109/TPEL.2016.2623341.
- [95] S. Sayeef, G. Foo, and M. F. Rahman, "Rotor position and speed estimation of a variable structure direct-torque-controlled IPM synchronous motor drive at very low speeds including standstill," *IEEE Trans. Ind. Electron.*, vol. 57, no. 11, pp. 3715–3723, Nov. 2010, doi: 10.1109/TIE.2010.2041730.
- [96] Z. Z. Liu, F. L. Luo, and M. A. Rahman, "Robust and precision motion control system of linear-motor direct drive for high-speed X-Y table positioning mechanism," *IEEE Trans. Ind. Electron.*, vol. 52, no. 5, pp. 1357–1363, 2005, doi: 10.1109/TIE.2005.855661.
- [97] "Programming and wiring of a low-cost tachometer megtekintése." <https://ojs.uni-miskolc.hu/index.php/multi/article/view/556/323> (accessed Mar. 19, 2021).
- [98] M. Hopkins and Sr, "THE STATE OF THE ART IN HALL EFFECT TECHNOLOGY AND ITS IMPLICATIONS FOR APPLIANCE DESIGN AND DEVELOPMENT," 2004.
- [99] W. J. Fleming, "Overview of Automotive Sensors," *IEEE Sens. J.*, vol. 1, no. 4, pp. 296–308, 2001, doi: 10.1109/7361.983469.
- [100] S. Gordon and M. T. Hillery, "Development of a high-speed CNC cutting machine using linear motors," *J. Mater. Process. Technol.*, vol. 166, no. 3, pp. 321–329, Aug. 2005, doi: 10.1016/j.jmatprotec.2003.08.009.
- [101] D. S. Nyce, "Encoders," in *Linear Position Sensors*, Hoboken, NJ, USA: John Wiley & Sons, Inc., 2004, pp. 151–161.
- [102] M. Lacroix, J. Santos, and R. Stiffler, "THE ADVANTAGES OF MAGNETIC ENCODER TECHNOLOGY IN HARSH OPERATING ENVIRONMENTS." Accessed: Mar. 20, 2021. [Online]. Available: www.timken.com.
- [103] "The Hall Effect," in *Linear Position Sensors*, Hoboken, NJ, USA: John Wiley & Sons, Inc., pp. 109–121.
- [104] S. W. Khubalkar, A. S. Chopade, A. S. Junghare, and M. V. Aware, "Design and tuning of fractional order PID controller for speed control of permanent magnet brushless DC motor," in *2016 IEEE 1st International Conference on Control, Measurement and Instrumentation, CMI 2016*, Feb. 2016, pp. 326–330, doi: 10.1109/CMI.2016.7413764.
- [105] M. Z. F. B. M. Zawawi, I. Elamvazuthi, A. B. A. Aziz, and S. A. Daud, "Comparison of PID and fuzzy logic controller for DC servo motor in the development of lower extremity exoskeleton for rehabilitation," in *2017 IEEE 3rd International Symposium in Robotics*

and Manufacturing Automation, ROMA 2017, Dec. 2017, vol. 2017-Decem, pp. 1–6, doi: 10.1109/ROMA.2017.8231822.

- [106] S. A. Bhatti, S. A. Malik, and A. Daraz, "Comparison of P-I and I-P controller by using Ziegler-Nichols tuning method for speed control of DC motor," in *2016 International Conference on Intelligent Systems Engineering, ICISE 2016*, May 2016, pp. 330–334, doi: 10.1109/INTELSE.2016.7475144.
- [107] E. Joseph and O. O. O, "Cohen-coon PID Tuning Method; A Better Option to Ziegler Nichols-PID Tuning Method," *Int. J. Recent Eng. Res. Dev. www.ijrerd.com* //, vol. 02, no. 11, pp. 141–145, 2017, Accessed: Mar. 20, 2021. [Online]. Available: www.ijrerd.com.
- [108] M. Papoutsidakis *et al.*, "Methodology of PID Control-A Case Study for Stepper Motors Control of Pneumatic Positioning Systems View project Methodology of PID Control-A Case Study for Stepper Motors," *Artic. Int. J. Comput. Appl.*, vol. 179, no. 30, pp. 975–8887, 2018, doi: 10.5120/ijca2018916689.
- [109] N. M. Elsodany, S. F. Rezek, and N. A. Maharem, "Adaptive PID control of a stepper motor driving a flexible rotor," *Alexandria Eng. J.*, vol. 50, no. 2, pp. 127–136, 2011, doi: 10.1016/j.aej.2010.08.002.
- [110] B. R. Copeland, "The Design of PID Controllers using Ziegler Nichols Tuning," 2008.
- [111] S. Bennett, "Development of the PID Controller," *IEEE Control Syst.*, vol. 13, no. 6, pp. 58–62, 1993, doi: 10.1109/37.248006.
- [112] R. Goswami and D. Joshi, "Performance Review of Fuzzy Logic Based Controllers Employed in Brushless DC Motor," in *Procedia Computer Science*, Jan. 2018, vol. 132, pp. 623–631, doi: 10.1016/j.procs.2018.05.061.
- [113] M. R. H Mohd Adnan *et al.*, "Fuzzy logic for modeling machining process: a review," *Artif Intell Rev*, vol. 43, pp. 345–379, 2015, doi: 10.1007/s10462-012-9381-8.
- [114] S. Dorin-Mirel, I. Lita, and M. Oproescu, "Comparative analysis of stepper motors in open loop and closed loop used in nuclear engineering," in *2017 IEEE 23rd International Symposium for Design and Technology in Electronic Packaging, SIITME 2017 - Proceedings*, Jul. 2017, vol. 2018-January, pp. 357–360, doi: 10.1109/SIITME.2017.8259924.
- [115] N. M. Elsodany, S. F. Rezek, and N. A. Maharem, "Adaptive PID control of a stepper motor driving a flexible rotor," *Alexandria Eng. J.*, vol. 50, no. 2, pp. 127–136, Jun. 2011, doi: 10.1016/j.aej.2010.08.002.
- [116] S. Sakunthala, R. Kiranmayi, and P. N. Mandadi, "A review on artificial intelligence techniques in electrical drives: Neural networks, fuzzy logic, and genetic algorithm," in *Proceedings of the 2017 International Conference On Smart Technology for Smart Nation, SmartTechCon 2017*, May 2018, pp. 11–16, doi: 10.1109/SmartTechCon.2017.8358335.
- [117] Y. V Parkale, "Comparison of ANN Controller and PID Controller for Industrial Water Bath Temperature Control System using MATLAB Environment," 2012.
- [118] "(16) (PDF) Artificial Neural Network Applications in Control of Induction Machines." https://www.researchgate.net/publication/258286604_Artificial_Neural_Network_Applications_in_Control_of_Induction_Machines (accessed Mar. 21, 2021).

- [119] E. Zerdali and M. Barut, "The Comparisons of Optimized Extended Kalman Filters for Speed-Sensorless Control of Induction Motors," *IEEE Trans. Ind. Electron.*, vol. 64, no. 6, pp. 4340–4351, Jun. 2017, doi: 10.1109/TIE.2017.2674579.
- [120] F. Auger, M. Hilaiet, J. M. Guerrero, E. Monmasson, T. Orłowska-Kowalska, and S. Katsura, "Industrial applications of the kalman filter: A review," *IEEE Trans. Ind. Electron.*, vol. 60, no. 12, pp. 5458–5471, 2013, doi: 10.1109/TIE.2012.2236994.
- [121] S. Y. Chen, "Kalman filter for robot vision: A survey," *IEEE Trans. Ind. Electron.*, vol. 59, no. 11, pp. 4409–4420, Nov. 2012, doi: 10.1109/TIE.2011.2162714.
- [122] Z. Yin, F. Gao, Y. Zhang, C. Du, G. Li, and X. Sun, "A review of nonlinear Kalman filter applying to sensorless control for AC motor drives," *CES Trans. Electr. Mach. Syst.*, vol. 3, no. 4, pp. 351–362, Dec. 2019, doi: 10.30941/cestems.2019.00047.
- [123] "Fundamentals of Light Microscopy and Electronic Imaging - Douglas B. Murphy - Google Books," .
- [124] J. Burrows, "Study Notes: Parts of a Microscope," 2004.
- [125] N. Waltham, "CCD and CMOS sensors," in *Observing Photons in Space*, Springer New York, 2013, pp. 423–442.
- [126] S. Mehta, A. Patel, and J. Mehta, "CCD or CMOS Image sensor for photography," in *2015 International Conference on Communication and Signal Processing, ICCSP 2015*, Nov. 2015, pp. 291–294, doi: 10.1109/ICCSP.2015.7322890.
- [127] J. Joubert and D. Sharma, "Using CMOS Cameras for Light Microscopy," *Micros. Today*, vol. 19, no. 4, pp. 22–28, Jul. 2011, doi: 10.1017/s155192951100054x.
- [128] "CCD versus CMOS: Which is Better? - Astronomy & Scientific Imaging Solutions." <https://diffractionlimited.com/ccd-versus-cmos-better/> (accessed May 26, 2021).
- [129] E. R. Fossum, D. B. Hondongwa, and S. Member, "A Review of the Pinned Photodiode for CCD and CMOS Image Sensors Recommended Citation A Review of the Pinned Photodiode for CCD and CMOS Image Sensors," *IEEE J. ELECTRON DEVICES Soc.*, vol. 2, no. 3, p. 33, 2014, doi: 10.1109/JEDS.2014.2306412.
- [130] "What are the benefits of CMOS based machine vision cameras vs CCD?" <https://www.1stvision.com/machine-vision-solutions/2019/07/benefits-of-cmos-based-machine-vision-cameras-vs-ccd.html> (accessed Jun. 24, 2021).
- [131] L. C. P. Gouveia and B. Choubey, "Advances on CMOS image sensors," *Sens. Rev.*, vol. 36, no. 3, pp. 231–239, Jun. 2016, doi: 10.1108/SR-11-2015-0189.
- [132] "Image Formation by Lenses." <http://hyperphysics.phy-astr.gsu.edu/hbase/geoopt/lensdet.html#c2> (accessed May 28, 2021).
- [133] S. Briggs, "Understanding Microscopes and Objectives," *Edmund Opt. Inc.*, pp. 1–17, 2014, Accessed: May 28, 2021. [Online]. Available: <https://www.edmundoptics.com/knowledge-center/application-notes/microscopy/understanding-microscopes-and-objectives/>.
- [134] N. Aperture, "Chapter 7 Lenses," *Microscopy*, pp. 1–15, 2007.
- [135] "Objective Lenses - Types based on Classification and Specifications." <https://www.microscopemaster.com/objective-lenses.html> (accessed May 28, 2021).

- [136] "Microscopy Basics — Klar Scientific." <http://klarscientific.com/microscopy-basics> (accessed Jun. 24, 2021).
- [137] C. Zeiss Microscopy GmbH and S. Gliem, "How to choose the optimal objective?," 2016.
- [138] "Understanding Light Microscopy - Jeremy Sanderson - Google Books." .
- [139] "Four Common Types of Microscope Light Sources." <https://www.amscope.com/blog/Common-Types-Microscope-Light-Sources/> (accessed Jun. 14, 2021).
- [140] "Halogen vs LED Lighting in Digital Microscopy." <https://bitesizebio.com/30334/halogen-vs-led-digital-microscopy/> (accessed Jun. 14, 2021).
- [141] "Choosing the best light source for your fluorescence experiment," Accessed: Jun. 14, 2021. [Online]. Available: <https://www.scientifica.uk.com/learning-zone/choosing-the-best-light-source-for-your-experiment#>.
- [142] N. Hudallah, Isdiyarto, S. Sukamta, P. K. Nashiroh, M. Harlanu, and S. Purbawanto, "Comparison of CFL lights and led lights reviewed from the side of the price, strong light and heat caused," in *IOP Conference Series: Earth and Environmental Science*, Mar. 2021, vol. 700, no. 1, p. 12014, doi: 10.1088/1755-1315/700/1/012014.
- [143] J. Beacher, "LEDs for fluorescence microscopy," *Biophotonics Int.*, vol. 15, no. 2, pp. 34–37, Feb. 2008, doi: 10.1117/12.525932.
- [144] *Bright-Field Microscopy*. Academic Press. Inc, 2009.
- [145] R. J. Oldfield, "Light Microscopy - Brightfield and Darkfield Illumination," in *Encyclopedia of Life Sciences*, John Wiley & Sons, Ltd, 2010.
- [146] G. Zheng, C. Kolner, and C. Yang, "Microscopy refocusing and dark-field imaging by using a simple LED array," *Opt. Lett.*, vol. 36, no. 20, p. 3987, Oct. 2011, doi: 10.1364/OL.36.003987.
- [147] Z. Liu, L. Tian, S. Liu, and L. Waller, "Real-time brightfield, darkfield, and phase contrast imaging in a light-emitting diode array microscope," *J. Biomed. Opt.*, vol. 19, no. 10, p. 1, 2014, doi: 10.1117/1.JBO.19.10.106002.1.
- [148] "Understanding Microscopes and Objectives | Edmund Optics." <https://www.edmundoptics.eu/knowledge-center/application-notes/microscopy/understanding-microscopes-and-objectives/> (accessed Jun. 24, 2021).
- [149] "Specialized Microscopy Techniques - Rheinberg Illumination | Olympus LS." <https://www.olympus-lifescience.com/en/microscope-resource/primer/techniques/rheinberg/> (accessed Jun. 15, 2021).
- [150] X. Fan, J. J. Healy, K. O'Dwyer, and B. M. Hennelly, "Label-free color staining of quantitative phase images of biological cells by simulated Rheinberg illumination," *Appl. Opt.*, vol. 58, no. 12, p. 3104, Apr. 2019, doi: 10.1364/ao.58.003104.
- [151] "Rheinberg Illumination." <https://microscopy.berkeley.edu/courses/tlm/df/rheinberg.html> (accessed Jun. 24, 2021).
- [152] M. W. Davidson and M. Abramowitz, "Optical Microscopy," in *Encyclopedia of Imaging*

- Science and Technology*, Hoboken, NJ, USA: John Wiley & Sons, Inc., 2002.
- [153] A. A. Havics, "Contrast Methods in Microscopy: Rheinberg Illumination," 2014.
- [154] K. K. Aswani, "Emerging LED Technologies for Fluorescence Microscopy," *Micros. Today*, vol. 24, no. 4, pp. 22–27, Jul. 2016, doi: 10.1017/s1551929516000407.
- [155] G. Koklu, J. Ghaye, R. Beuchat, G. De Micheli, Y. Leblebici, and S. Carrara, "Quantitative comparison of commercial CCD and custom-designed CMOS camera for biological applications," in *ISCAS 2012 - 2012 IEEE International Symposium on Circuits and Systems*, 2012, pp. 2063–2066, doi: 10.1109/ISCAS.2012.6271688.
- [156] "Optical Microscope - an overview | ScienceDirect Topics." <https://www.sciencedirect.com/topics/engineering/optical-microscope> (accessed Jun. 14, 2021).
- [157] Z. Liu, L. Tian, S. Liu, and L. Waller, "Real-time brightfield, darkfield, and phase contrast imaging in a light-emitting diode array microscope," *J. Biomed. Opt.*, vol. 19, no. 10, p. 1, Oct. 2014, doi: 10.1117/1.jbo.19.10.106002.
- [158] "Working Principle of Phase Contrast Microscope | Easy Biology Class." <https://www.easybiologyclass.com/phase-contrast-microscopy-optical-components-working-principle-and-applications-short-notes-with-ppt/> (accessed Jun. 24, 2021).
- [159] R. A. Lugmaier, T. Hugel, M. Benoit, and H. E. Gaub, "Phase contrast and DIC illumination for AFM hybrids," *Ultramicroscopy*, vol. 104, no. 3–4, pp. 255–260, Oct. 2005, doi: 10.1016/j.ultramic.2005.04.008.
- [160] V. Bormuth, J. Howard, and E. Schäffer, "LED illumination for video-enhanced DIC imaging of single microtubules," *J. Microsc.*, vol. 226, no. 1, pp. 1–5, Apr. 2007, doi: 10.1111/j.1365-2818.2007.01756.x.
- [161] D. Fu *et al.*, "Quantitative DIC microscopy using an off-axis self-interference approach," *Opt. Lett.*, vol. 35, no. 14, p. 2370, Jul. 2010, doi: 10.1364/ol.35.002370.
- [162] W. Sun, L. Xiao, and N. Fang, "Imaging Non-fluorescent Nanoparticles in Living Cells with Wavelength-Dependent Differential Interference Contrast Microscopy and Planar Illumination Microscopy," 2012, pp. 169–186.
- [163] M. I. Shah, S. Mishra, M. Sarkar, and C. Rout, "Identification of robust focus measure functions for the automated capturing of focused images from Ziehl–Neelsen stained sputum smear microscopy slide," *Cytom. Part A*, vol. 91, no. 8, pp. 800–809, Aug. 2017, doi: 10.1002/cyto.a.23142.
- [164] C. He, X. Li, Y. Hu, Z. Ye, and H. Kang, "Microscope images automatic focus algorithm based on eight-neighborhood operator and least square planar fitting," *Optik (Stuttg.)*, vol. 206, p. 164232, Mar. 2020, doi: 10.1016/j.ijleo.2020.164232.
- [165] F. C. A. Groen, I. T. Young, and G. Ligthart, "A comparison of different focus functions for use in autofocus algorithms," *Cytometry*, vol. 6, no. 2, pp. 81–91, 1985, doi: 10.1002/cyto.990060202.
- [166] V. V. Bezzubik, S. N. Ustinov, and N. R. Belashenkov, "Optimization of algorithms for autofocusing a digital microscope," *J. Opt. Technol.*, vol. 76, no. 10, p. 603, Oct. 2009, doi: 10.1364/jot.76.000603.
- [167] "Establishment of hybridized focus measure functions as a universal method for autofocusing," *J. Biomed. Opt.*, vol. 22, no. 12, p. 1, Dec. 2017, doi:

10.1117/1.jbo.22.12.126004.

- [168] "LGA281S10-A-UGAQ-019 - Captive linear actuator....."
<https://en.nanotec.com/products/2622-lga281s10-a-ugaq-019/> (accessed Jun. 24, 2021).
- [169] "1951 USAF Resolution Calculator | Edmund Optics."
<https://www.edmundoptics.com/knowledge-center/tech-tools/1951-usaf-resolution/> (accessed Jun. 24, 2021).
- [170] بارانی، س. ن. ع. س. و. ح.، "T-20 USAF 1951 Chart," vol. 148, pp. 148–162.

9. Appendix

Below is a link that gives access to a google drive where all Solidworks designs, firmware code for the motor controllers, and LabVIEW files are copied that were used in the development of this project.

https://drive.google.com/drive/folders/1g4rlh7B38Jx8zNh0Q_duaaL2wbuOlq2?usp=sharing